CHEMICAL
RESEARCH,
DEVELOPMENT &
ENGINEERING
CENTER

CRDEC-CR-86047

# INVESTIGATION OF A TECHNIQUE FOR CLEARING AND/OR MODIFYING A MILITARY SMOKE CLOUD

by Josef Podzimek, Ph. D.
UNIVERSITY OF MISSOURI-ROLLA
Rolla, MO 65401

June 1986





U.S. ARMY
ARMAMENT
MUNITIONS
CHEMICAL COMMAND

Aberdeen Proving Ground, Maryland 21010-5423

## Disclaimer

The findings in this report are not to be construed as an official Department of the Army position unless so designated by other authorizing documents.

## Distribution Statement

Approved for public release; distribution is unlimited.

UNCLASSIFIED
SECURITY CLASSIFICATION OF THIS PAGE

# REPORT DOCUMENTATION PAGE

| | |
|---|---|
| 1a. REPORT SECURITY CLASSIFICATION<br>UNCLASSIFIED | 1b. RESTRICTIVE MARKINGS |
| 2a. SECURITY CLASSIFICATION AUTHORITY | 3. DISTRIBUTION/AVAILABILITY OF REPORT<br>Approved for public release; distribution is unlimited. |
| 2b. DECLASSIFICATION/DOWNGRADING SCHEDULE | |
| 4. PERFORMING ORGANIZATION REPORT NUMBER(S)<br>CRDEC-CR-86047 | 5. MONITORING ORGANIZATION REPORT NUMBER(S)<br>AG-13 |
| 6a. NAME OF PERFORMING ORGANIZATION<br>University of Missouri-Rolla<br>6b. OFFICE SYMBOL (If applicable) | 7a. NAME OF MONITORING ORGANIZATION<br>U.S. Army Research Office |
| 6c. ADDRESS (City, State, and ZIP Code)<br>Rolla, MO 65401 | 7b. ADDRESS (City, State, and ZIP Code)<br>Research Triangle Park, NC 27709-2211 |
| 8a. NAME OF FUNDING/SPONSORING ORGANIZATION<br>CRDEC<br>8b. OFFICE SYMBOL (If applicable)<br>SMCCR-RSP-B | 9. PROCUREMENT INSTRUMENT IDENTIFICATION NUMBER<br>DAAK11-81-C-0075 |
| 8c. ADDRESS (City, State, and ZIP Code)<br>Aberdeen Proving Ground, MD 21010-5423 | 10. SOURCE OF FUNDING NUMBERS<br>PROGRAM ELEMENT NO. / PROJECT NO. 1L161102 / TASK NO. A71AD / WORK UNIT ACCESSION NO. |

11. TITLE (Include Security Classification)
Investigation of a Technique for Clearing and/or Modifying a Military Smoke Cloud

12. PERSONAL AUTHOR(S)
Podzimek, Josef, Ph.D.

| 13a. TYPE OF REPORT | 13b. TIME COVERED | 14. DATE OF REPORT (Year, Month, Day) | 15. PAGE COUNT |
|---|---|---|---|
| Contractor | FROM 81 Jul TO 83 Sep | 1986 June | 96 |

16. SUPPLEMENTARY NOTATION
COR: Glenn Rubel, SMCCR-RSP-B, (301) 671-2326

| 17. COSATI CODES | | | 18. SUBJECT TERMS (Continue on reverse if necessary and identify by block number) |
|---|---|---|---|
| FIELD | GROUP | SUB-GROUP | Scavenging of military smoke particles<br>Deposition of $TiCl_4$ particles on disks, cylinders, and grids |
| 04 | 02 | | |
| | | | |

19. ABSTRACT (Continue on reverse if necessary and identify by block number)

A numerical model is applied to assess the smoke particle ($0.1 < R_p < 5.0$ μm) scavenging by an oblate spheroid in the range of Reynolds numbers $0.1 < Re_c < 30$. The calculated collision efficiency is between 0.3% and 4.0%. The collision efficiency of a charged thin spheroid ($Q_c = 2$ e.s.u./cm$^2$) colliding with smoke particles of $R_p = 0.3$ μm is 14% for $Re_c = 50$.

Experimental study of the smoke particle deposition on disks in the range of $80 < Re_c < 320$ in an aerodynamic wind tunnel leads to the following conclusion:

Collection efficiencies of stationary (or steady settling) disks are between 0.5 and 2.0%. For disks oscillating at a frequency simulating the falling disk in the atmosphere, the collection efficiency is 20% higher. Collection efficiency of electrically charged disks ($0.57 < Q_c < 2.86$ e.s.u./cm$^2$) is between 3% and 14%. Deposition of particulates with

| 20. DISTRIBUTION/AVAILABILITY OF ABSTRACT | 21. ABSTRACT SECURITY CLASSIFICATION |
|---|---|
| ☒ UNCLASSIFIED/UNLIMITED ☐ SAME AS RPT. ☐ DTIC USERS | UNCLASSIFIED |
| 22a. NAME OF RESPONSIBLE INDIVIDUAL<br>TIMOTHY E. HAMPTON | 22b. TELEPHONE (Include Area Code)<br>(301) 671-2914 / 22c. OFFICE SYMBOL<br>SMCCR-SPD-R |

DD FORM 1473, 84 MAR 83 APR edition may be used until exhausted
All other editions are obsolete

SECURITY CLASSIFICATION OF THIS PAGE
UNCLASSIFIED

18. Subject Terms (Continued)

Particle deposition on electrically charged scavengers

19. Abstract (Continued)

$R_p < 0.35$ μm is higher on the disk's back side than on the front side. Charged cylinders are featured by a collection efficiency between 0.3% to 5.0% for $3.5 < Re_c < 26$ and potential differences from 1 kV to 8 kV. High collection efficiencies are found on charged grids (several percent for 1 kV and more than 5% for 5 kV).

The effect of falling scavenger zone is considered to be more important for the scavenger's fall velocity and its collection efficiency than for scavenger dispersion.

## PREFACE

The work described in this report was authorized under Contract No. DAAK11-81-C-0075. This work was started in July 1981 and completed in September 1983.

The use of trade names or manufacturers' names in this report does not constitute an official endorsement of any commercial products. This report may not be cited for purposes of advertisement.



This document has been approved for release to the public.

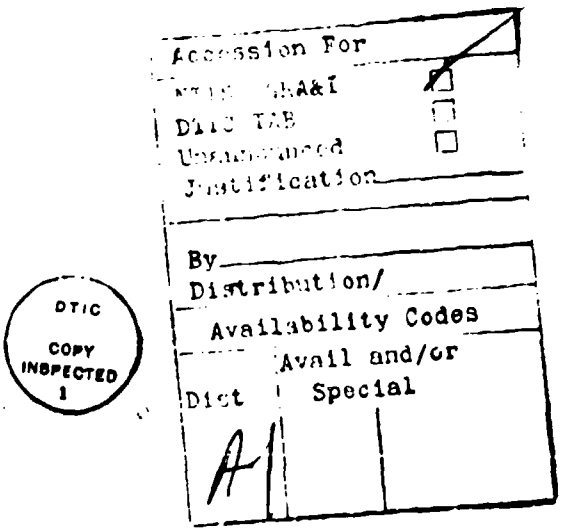


*This work was completed when the U.S. Army Chemical Research, Development and Engineering Center (CRDEC) was known as the U.S. Army Chemical Research and Development Center (CRDC).

Blank

CONTENTS

# INVESTIGATION OF A TECHNIQUE FOR CLEARING AND/OR MODIFYING A MILITARY SMOKE CLOUD

## 1. INTRODUCTION

This Final Report covers the time period between July, 1981 and September 1983. By its nature, it can be considered as the continuation of the two year program supported by the U.S. Army Research Office (DAAG29-79-C-0075). However, unlike the previous exploratory study, it focuses on several specific avenues of research which were found promising during the past investigation.

The numerical model, which justifies the attention paid to nonspherical models, was extended into the domain of high Reynolds numbers ($Re \geq 50$) for a disk. The role of electrostatic charge and of thermo- and diffusiophoretic force in the smoke particle deposition on disks is discussed in detail. Following the same line of research, a systematic experimental investigation was aimed to answer the question of how important is the scavenger oscillatory motion for the particle deposition. Because of the great importance of cylindrical and grid type scavengers their efficiency has been checked in a laboratory wind tunnel and compared with neutral or electrostatically charged disks. Finally, some preliminary calculations and assessment of the nonspherical scavenger hydrodynamic interaction and of the potential effect of the "Scavenger Falling Zone" on the smoke particle settling have been made.

The above outlined research and the results of investigation are described in Chapter 2 (Theoretical Analysis, Materials and Methods) and in Chapter 3 (Experiments with scavenger motion and particle deposition). In Chapter 5 (Discussion of the Results) the results of the investigation are evaluated, correlated and compared with the data known from other studies. Chapter 6 (Conclusion) contains also several suggestions for the future research and practical application of the main results.

This report is a result of the cooperation between two investigators (Dr. J. Podzimek and Dr. J.J. Martin), two graduate students (Miss S. West in 1981 and 1982; Mr. Y. Liu in 1983) and three student research assistants (Mr. V. Wojnar, A. Keshavarz and G. Stowel. Mrs. V. Maples ably helped to prepare the manuscript for printing.

## 2. THEORETICAL ANALYSIS, MATERIALS AND METHODS

### 2.1 Theoretical Investigation of the Smoke Particle Scavenging by Planar Collectors.

Most of the comprehensive studies of the droplet and particle scavenging by planar collectors during fifteen past years have been done by Sood and Jackson (1969), Pitter (1973, 1977), Magono, et al. (1974), Pitter, et al. (1973), Pitter and Pruppacher (1974), Knutson, et al. (1976), Prodi (1976), Martin (1979), Martin, et al. (1980a, 1980b, 1981). For the deposition of aerosol particles on scavengers of utmost importance is the complex contribution of the forces, such as inertial, gravitational, thermo- and diffusiophoretical and electrical. Several studies have been published on the deposition of aerosol particles in diffusio- and thermophoretical force fields (e.g., Podzimek, 1965; Slinn and Hales, 1971; Carstens and Martin, 1982). The general conclusion of these studies supports the experimental evidence of a "Greenfield gap" for particle diameters between 0.1 and 1.0 μm and the more effective scavenging by planar collectors if compared with the approximate same size of droplets. In cloud aerosol scavenging by evaporating or growing elements can be influenced by all forces, however several of them will dominate for specific aerosol size and nature. Brownian diffusion will affect particle sizes below 0.1 μm. Thermophoretic force was found much more important than diffusiophoretic at most of the natural atmospheric conditions for submicron aerosol. However, the submicron particles with $r < 0.1$ μm will suffer a reduction of their Brownian diffusion transport by phoretic drift (Carstens and Martin, 1982). For the goals of this study dealing with clearing of a military smoke cloud (with smoke particle diameters between 0.2 and several μm) by solid planar scavengers, the most important seems to be the electric charge effect on the particle collection--besides the inertial deposition and particle settling.

The method used for calculating the efficiency with which spherical smoke particles are collected by an oblate spheroid is based mainly on the studies by Pitter (1973), Pitter and Pruppacher (1974), Martin, et al. (1980a, 1980b) and described

(without the effect of phoretical forces) in Appendix I (the flow field), II (the numerical technique), and III (the description of particle trajectories and calculation of the collision efficiency). In addition, a technique has been developed to describe the deposition of particles in the size range $0.1 \leq r \leq 10$ μm when inertial effects, Brownian diffusion and electric charges are effective (Martin, 1979; Martin and Podzimek, 1982). All these models are based on the assumption that the collector (scavenger) is steadily falling in a gravitational field and that the tiny smoke particles, homogeneously dispersed in the air, do not affect the orientation of the disk (oblate spheroid) while impacting its surface or flowing around. Further is assumed that the smoke particles do not interact with other particles, even in a polydisperse aerosol. Under these conditions the set of equations from Appendix III (25.A; 26.A and 29.A to 33.A) will be reduced basically to one vector equation describing the trajectory of a smoke particle with radius $R_p \geq 0.1$ μm, the mass $m_p$ and density $\rho_p$

$$m_p \frac{d\vec{V}_p}{dt} = m\vec{g}\left(1-\frac{\rho_{air}}{\rho_p}\right) - \frac{6\pi\mu R_p}{1+\alpha Kn}\left(\vec{V}_p-\vec{U}\right) + \vec{F}_e \qquad (1)$$

where Knudsen-Weber correction, $(1+\alpha Kn)$, with $Kn = \frac{\gamma}{R_p}$ ($\gamma$ is the mean free path of air molecules), and $\alpha = 1.25 + 0.44 \exp(-1.1\, Kn^{-k})$, was added for covering a wide range of aerosol particles. Other symbols are explained in Appendix III.

The outer forces are represented in Eq. (1) only by the electric force which is due to the surface charge on the particle, $Q_p$, and on the collector, $Q_c$. One can write (Martin, et al. 1980c) in oblate spheroidal coordinates (Appendix I)

$$F_e = -\frac{Q_p Q_c \operatorname{sech}\xi \sin^{-1}[1-A_c)^{1/2}]}{R_c^2 \operatorname{sech}\xi_o [1-A_c^2]^{1/2} [\frac{\pi}{2} - \sin^{-1}A_c][\sinh^2\xi+\cos^2\eta]^{1/2}} \qquad (2)$$

From the known flow field around the thin oblate spheroid

(Appendix I and II), the particle trajectory was calculated (by adding to the formulas in Appendix III the electric force term, $\vec{F}_e$). The particle trajectories enable the calculation of collision efficiencies according the formula

$$E = \frac{y_{cr}^2}{(R_c+R_p)^2} \quad . \tag{3}$$

Its validity is limited by several important assumptions which are discussed in Appendix III (formula 40.A). Essential is the determination of the largest offset distance of a particle from the main axis along which the center of collector is settling, $y_{cr}$. It depends, besides other parameters, on the particle radius, $R_p$, which affects the just "touching" particle position at the rim of the collector (for the corresponding, $y_{cr}$).

The model for clearing the smoke cloud (with particle concentration, n) by planar scavengers is deduced from the relationship

$$-\frac{1}{n}\frac{\partial n(R_p,t)}{\partial t} \equiv A(R_p,t) = N_{RC}\int_{R_{p1}}^{R_{p2}} K_i(R_p,R_c)\,n(R_p,t)\,dR_p \tag{4}$$

where $K_i(R_p,R_c)$ is the collision kernel defined with the known collision efficiency E as

$$K_i(R_p,R_c) = E\,(R_c + R_p)^2(V_{R_c} - V_{R_p}) \quad . \tag{5}$$

The eq. (4) and (5) assume that the collectors have the same size (mass accretion and shape change due to the collision with smoke particles is neglected) and that their concentration in the space, $N_{RC}$, is constant. Under these assumptions the clearing of a smoke cloud (removal of aerosol particles) is governed by the equation

$$n(R_p,t) = n(R_p,0)\,\exp\,[-A(R_p)t] \quad . \tag{6}$$

For the sake of making the model of clearing a smoke cloud more universal another complementary model for smoke particle radii, $R_p < 0.1\ \mu m$, was deduced. It is based on the assumption that the deposition of very small particles on scavengers is governed mainly by Brownian diffusion and electrostatic field. Then the particle flux can be derived from the Fick's law (Martin, et al., 1980c)

$$\vec{j} = nB[m\,\vec{g}(1-\frac{\rho_{air}}{\rho_p})+\vec{F}_e] - D_p\nabla n \ , \qquad (7)$$

where, B, is the particle mobility $[B = (1+\alpha Kn)(6\pi R_p\mu)^{-1}]$, n is the smoke particle concentration and $D_p$ is the particle diffusivity in the air. The solution of eq. (7) is in oblate spheroidal coordinates

$$n = n_\infty \frac{\exp\{(-\beta\varepsilon\sin^{-1}\tanh\xi)(\frac{\pi}{2}-\sin^{-1}A_c)^{-1}\}-\exp\{(-\beta\varepsilon\sin^{-1}A_c)(\frac{\pi}{2}-\sin^{-1}A_c)^{-1}\}}{\exp\{(-\frac{\pi}{2}\beta\varepsilon)(\frac{\pi}{2}-\sin^{-1}A_c)^{-1}\}-\exp\{(-\beta\varepsilon\sin^{-1}A_c)(\frac{\pi}{2}-\sin^{-1}A_c^{-1})\}} \ . \qquad (8)$$

$n_\infty$ is the smoke particle ambient concentration, $\varepsilon = |\vec{F}_e|$, and the factor $\beta = Bf_p/D_p$ (where $f_p$ is the ventilation coefficient for the collector) is unimportant in our case. The total flux of particles to the collector's surface, S, is

$$J_p = \int f_p D_p (\nabla n)_{\xi=\xi_o} dS \qquad (9)$$

$\xi = \xi_o$ means that the particle gradient is taken at the surface of the collector. In a similar way like the deduction of eq. (5) for a collision kernel was obtained

$$K_2 \equiv \frac{J_p}{n} = \frac{4\pi BCR_c\,\mathrm{sech}\xi_o}{(\frac{\pi}{2}-\sin^{-1}A_c)}\left[\exp(\frac{BC}{D_p f_p}-1)\right] \ . \qquad (10)$$

The equations described in this paragraph are used later for the calculation of smoke particle deposition on neutral and electrically charged collectors.

## 2.2 Numerical Model. Assumptions, Basic Parameters and Results.

Numerical model requires several strong simplifications for economical reasons and for our not sufficient knowledge of the very complex nature of the mechanism of particle deposition on scavengers. We don't know sufficiently the conditions of particle sticking at the surface, which has an utmost importance for the deposition, of particle continuity in the whole field around the scavengers where, mainly in the case of a polydisperse aerosol, smoke particle trajectories will cross and particle coagulation might be effective. There is no particle interaction assumed due to electrostatic and phoretic forces and no rotation of particles is assumed in the steep velocity gradients close to the rim. The calculation of the potential impact of thermo- and diffusiophoresis on aerosol and droplet deposition has been published by several authors (Martin, et al., 1980; Carstens and Martin, 1982) with the intention to describe the processes inside and around clouds in nature. For our goals, and due to the nature of an artificial scavenger, was assumed that we can neglect these processes--at least in the first approximation.

Both formulas for collision kernel (eqs. 5 and 10) were taken as the basis for the evaluation of the smoke particle deposition on planar scavengers (oblate spheroid with an axis ratio $A_c$ = b/a = 0.05). The final effect was obtained as a formal addition of both processes--the deposition under inertial and electrostatic forces and the effect of Brownian diffusion with electrostatic forces. All the other assumptions (e.g., definition of particle sticking) and the details of the numerical model are mentioned in Appendix III of this report.

A wide range of collector radii was selected ($R_c$ = 50.6; 87.9; 112.8; 146.8; 213.0; 289; 404; 639.2 μm what corresponds to $Re_c$ = 0.1; 0.5; 1.0; 2.0; 5.0; 10; 20; 50). An attempt was also made to extend the upper limit of $Re_c$. There are, however, considerable difficulties with a model for $Re_c$ = 80 due to the numerical solution convergence and instability and the questionable interpretation of the creeping flow equation for such a high $Re_c$.

The particles considered had radii between $0.1 \leq R_p \leq 0.5$ μm and densities, $\rho_p$, 0.75; 0.85; 0.90; and 0.95 g $cm^{-3}$. They might be close to the droplets forming the oil fog or originated on highly hygroscopic nuclei (red phosphorus). For "dry" $TiCl_4$ particles which have polycrystallinic nature (Figs. 13 and 14) and spherical shape, the assumed density is probably too low. Due to the minimum size of smoke (fog) particulates ($r_{min}$ = 0.1 μm), the calculated diffusional particle deposition will be much smaller than the inertial and electrostatic force contribution to the total collision efficiency. The effect of droplet ventilation, is included in the factor $f_p$ (eqs. 9 and 10), following the calculation by Hall and Pruppacher (1976), however, its value is not very significant for our case.

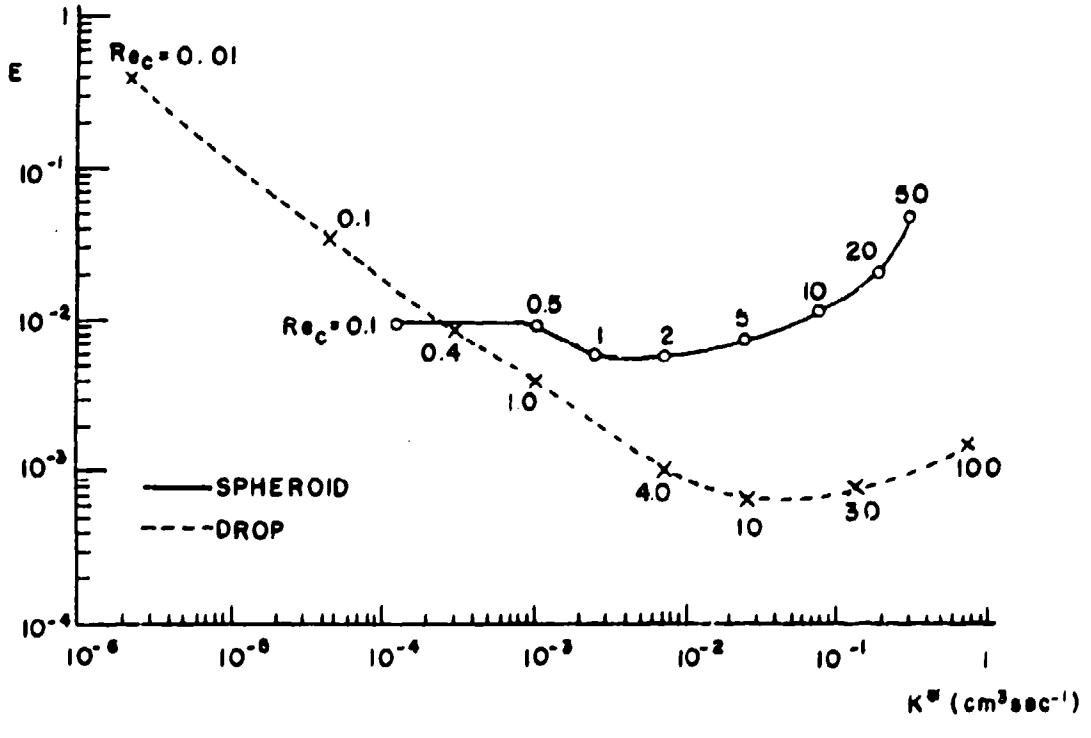


Fig. 1 Calculated collision efficiency of a thin spheroidal (full line) and spherical (dashed line) collectors with spherical water droplets as a function of $K^* = \pi R_c^2 V$ .

The electric charge effect calculation was based on the following assumptions: only the Coulomb forces (or image forces) are considered with the charge on the collector $Q_c = q_c R_c^2 = q_c a_c^2$. That means, the charge of the collector is proportional to its area. The smoke particles bear one, two, three,... elementary charges, what probably simplifies strongly the situation in a real smoke cloud with regard to the size and art of generation of a smoke cloud. Nevertheless, the electric charge seems to be an important factor in the evaluation of a clearing of a smoke cloud.

The results of the numerical calculation (Martin and Podzimek, 1982) are referred to the main tasks of the theoretical study. The first question was perhaps, whether the collision efficiency of a spheroidal (disk) model is greater than that of a spherical collector (liquid drop). In Fig. 1 is clearly shown that differently sized oblate spheroidal collectors will have higher collision efficiency if compared to the spherical collector. The comparability of these measurements prompted the introduction of the so called geometric volume swept out by the scavenger per unit time, $K^* = \pi R_c^2 V_\infty$. This parameter, however, does not include any effect of hydrodynamic (phoretic and electrostatic charge) interaction of scavengers which are supposed to fall as single collector through the aerosol cloud. Under this assumption, thin oblate spheroid ($A_c = 0.05$) is a better scavenger for $K^* \geq 2.5$ cm$^3$sec$^{-1}$ if smoke aerosol of a uniform size, $R_p = 0.6$ μm, and density $\rho_p = 0.95$ g cm$^{-3}$ and scavengers with properties similar to falling plate type crystals or cloud drops were assumed. There is one order of magnitude difference between the collision efficiencies of thin oblate spheroids and drops for $Re_c > 10$, when the inertial deposition of particles prevails. For $Re > 0.2$, on the other hand, the diffusional deposition of particles overrides the other deposition processes and the larger surface of tiny spherical collectors (combined with a small settling velocity) dominates.

Figure 2 represents the dependence of collision efficiencies on the $Re_c$ and the radius of the aerosol particle, $R_p$, with $\rho_p = 0.95$ g cm$^{-3}$. As expected, the collision efficiency is

dramatically increasing with $Re_c > 10$. In this domain the effect of inertial deposition prevails. This is featured by a typical saddle type portion of the collision efficiency curve for particle radii between 0.6 μm and 2.5 μm followed by a steep increase of the collision efficiency for larger particles. For particles with radii $R_p < 0.6$ μm the phoretical and diffusional deposition starts to be effective. In mean, for the smoke particle size range

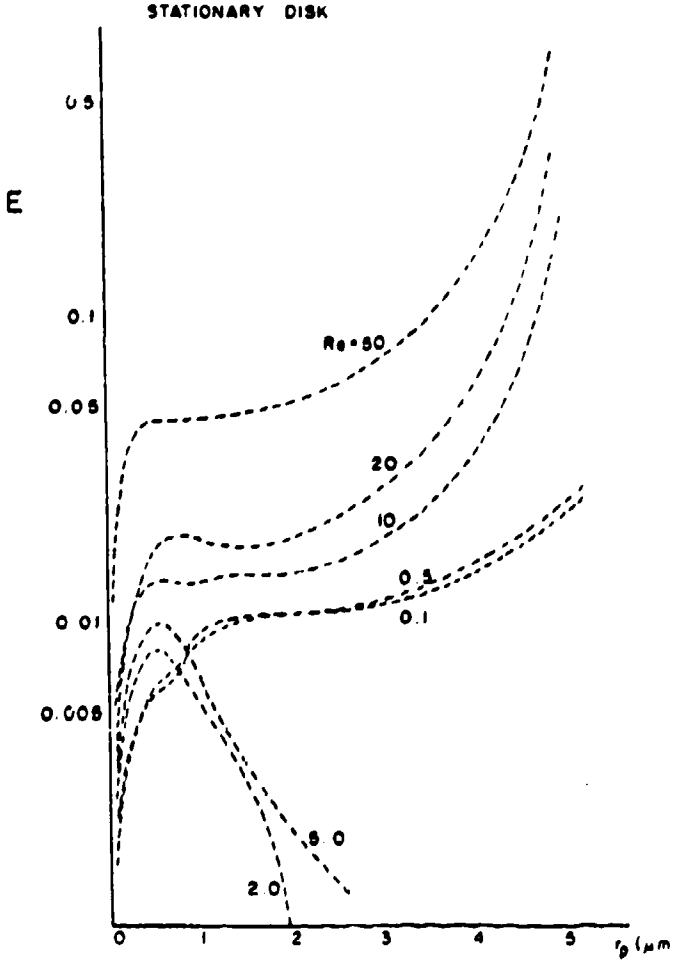


Fig. 2 Calculated collision efficiencies of a spheroid ($A_c$=0.05) with drops of radii, $R_p$, for different Reynolds numbers, $Re_c$.

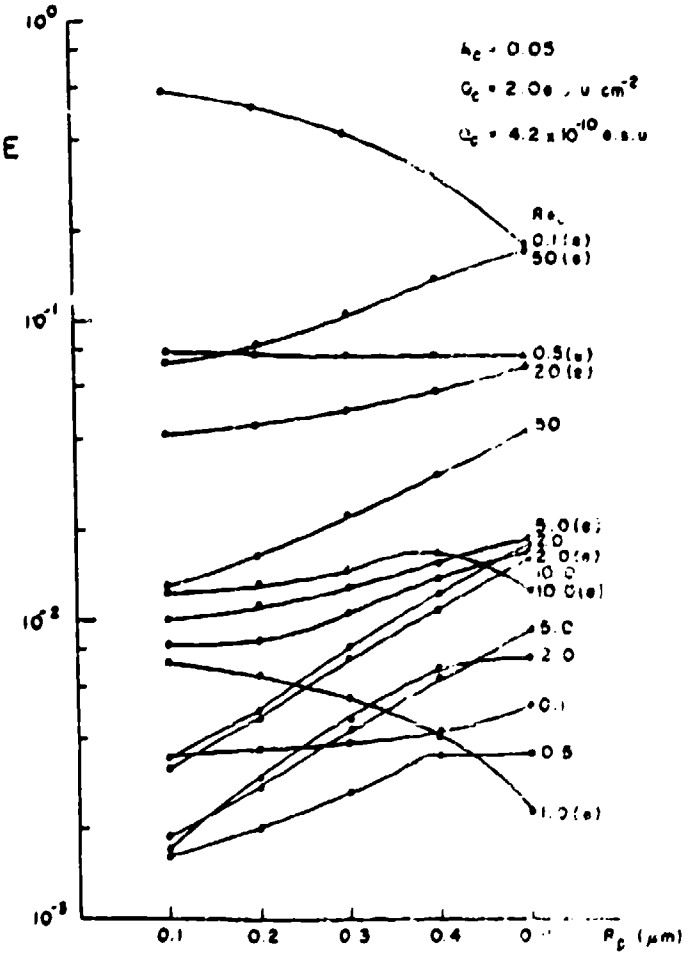


Fig. 3 Calculated collision efficiencies, E, of a charged spheroidal collector ($A_c$=0.05, $Q_c$=2.0 $R_c^2$ e.s.u.) with a charged spherical particle ($Q_p$=4.8x$10^{-10}$ e.s.u.)-marked with (e) as a function of, $Re_c$, and, $R_p$.

$0.5 < R_p < 2.5$ μm the collision efficiency is around 5% for $Re_c$ = 50, 2% for $Re_c$ = 20 and 1.5% for $Re_c$ = 10. The collision efficiency at $Re_c$ = 50 for particle radii between 0.5 μm and 3.0 μm bearing one elementary charge was increased three times by an electric surface charge of $Q_c$ = 2.0 esu $cm^{-2}$ on the collector.

The results of systematic study of the electric charge effect are plotted in Fig. 3. The collector charge was calculated according to the formula $Q_c = 2 a_c^2 \equiv 2R_c^2$ and particle charge was equal to one elementary charge ($4.803 \times 10^{-10}$ e.s.u.). The curve pattern in Fig. 3 reminds the complexity of the particle trajectories calculated for a charged spherical collector and for a charged particle by Zebel (1956). In the range of particle radii between 0.1 μm and 0.5 μm covering the considerable part of a Greenfield gap both the particle diffusion and inertial deposition are affecting the particle impaction on collector's surface. If the $Re_c$ were related to the steady settling of thin oblate spheroids ($C_D$ from Pruppacher and Klett, 1978) then for $Re_c$ > 20 the collision efficiency, E, for particle radii 0.1 μm was one order of magnitude larger for charged particles than for uncharged. For $Re_c$ > 20 and $R_p$ = 0.5 μm, E, was 3 to 4 times larger than the collision efficiency of uncharged particles.

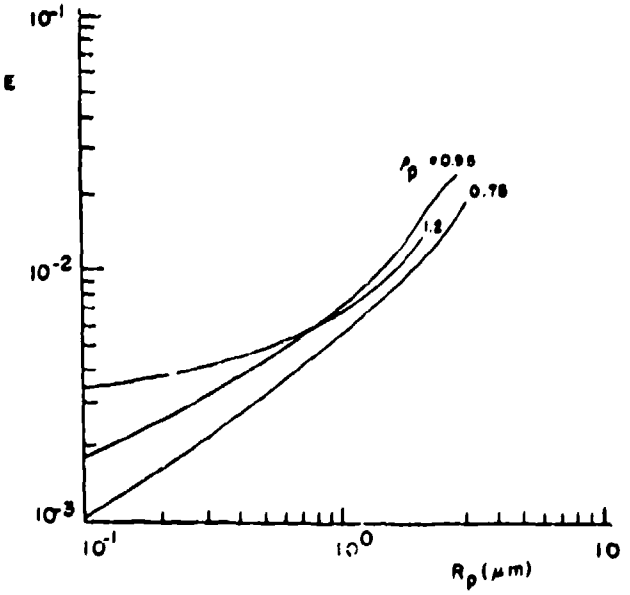


Fig. 4 The effect of different density of aerosol particles, $\rho_p$, on the collision efficiency for the main collector's semiaxis $A_c = R_c = 50.6$ μm.

Collector Reynolds numbers, $Re_c < 0.5$, were featured by two orders of magnitude difference in collision efficiencies for $R_p = 0.1$ μm and more than one order of magnitude difference if the cases of charged and uncharged particles were compared.

Finally, in Fig. 4 are plotted the results of the collision efficiency, E, calculations if different particle densities, $\rho_p$, and radii, $R_p$, are considered. The change in the density from 0.75 g $cm^{-3}$ to 1.20 g $cm^{-3}$ will influence the particle deposition in a significant way for particle radii, $R_p < 0.4$ μm. There is, however, not a dramatic change in E-curves for particles, $R_p > 0.8$ μm.

## 3. EXPERIMENTS WITH SCAVENGER MOTION AND PARTICLE DEPOSITION

### 3.1 Description of the Planar Scavenger Motion.

Only several experiments with falling planar scavengers were made in addition to those described in the Final Report on DAAG 29-79-C-0073 (Podzimek, 1981). They were aimed mainly to complete the relationship between the amplitude, $\delta$, of falling planar scavengers (disks, hexagons, squares, rectangles, etc.) and the corresponding scavenger Reynolds number, $Re_c$, and Wilmarth's stability number, I. Similar study was made for the frequency of motion of a falling scavenger, $f_\tau$.

In Fig. 5 are plotted together the data for planar scavengers falling in liquids (PD-1 to PD-6) and for disks falling in the air as a functional relationship between the scavenger's amplitude,

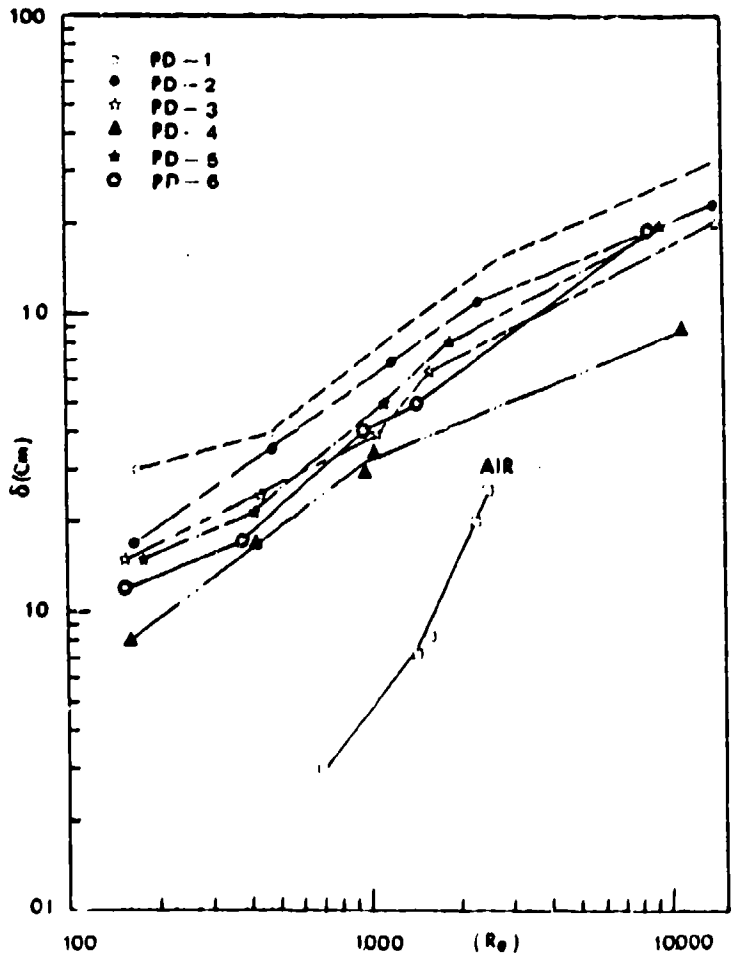


Fig. 5 The amplitude, $\delta$(cm), of the settling oscillatory motion of planar scavengers in a liquid (glycerol and water) and in the air as a function of Re.

[cm], and the mean $Re_c$ ($Re_c = \sqrt{Re_x^2 + Re_y^2}$). Pd-1 the curve is for a disk, PD-2 for a hexagon, PD-3 for a hexagon "ventilated" in the center, PD-4 hexagon ventilated at the rim, PD-5 and PD-6 for star-like models. All models (PD-1 to PD-6) were falling in the mixture of glycerol and water. The comparison supports the conclusions made earlier (Podzimek, 1981): one cannot compare the scavenger motion parameters deduced from observations made in liquid and in the air. The latter are featured by a smaller amplitude, $\delta$, for disks falling in the air at $700 < Re < 2{,}500$, and steeper increase of the curve $\delta = f(Re)$ in the air. There is, however, not a strong change in the wavelength of the oscillating planar models, $\lambda$[cm], falling in liquids (Fig. 6).

In the air, a falling paper disk is featured by a moderate change of the amplitude, $\delta$, and frequency, $f_c$, with $Re_c < 1{,}500$ and a dramatic change beyond this value (Fig. 7). The functional relationship for the frequency $f_c$ and amplitude, $\delta$, is reversed, i.e. with increasing $Re_c$ the amplitude increases and the frequency of oscillatory motion decreases. The same inverse dependence on the Wilmarth's stability parameter for a disk, I, was found for the frequency, $f_c$, and amplitude, $\delta$, of a falling paper disk (Fig. 8). the two curves for each dependence in Fig. 8 were obtained from two independent sets of measurement. That reveals a consistency in our findings in spite of a considerable scatter of the points.

In conclusion, the scavenger settling experiments performed in a large cylindrical settling chamber in quiescent air and in a horizontal wind tunnel at a side wind of about 0.7 m $s^{-1}$ [described in our previous report-Podzimek (1981)] and completed in this study] led to the following conclusions: the fall of symmetrical planar scavengers can be described by an "equivalent" disk model for $20 < Re_c < 200$ with the drag coefficient $C_D = \frac{2V_c(\rho_c - \rho_{air})g}{P_c \rho_{air} \bar{V}_c^2}$, where $\bar{V}_c$ is the volume of the scavenger, $P_c$ is the cross-section of the scavenger perpendicular to its trajectory and $V_c$ is the mean velocity of the falling scavenger (collector). The behavior of a falling disk can be sufficiently described by

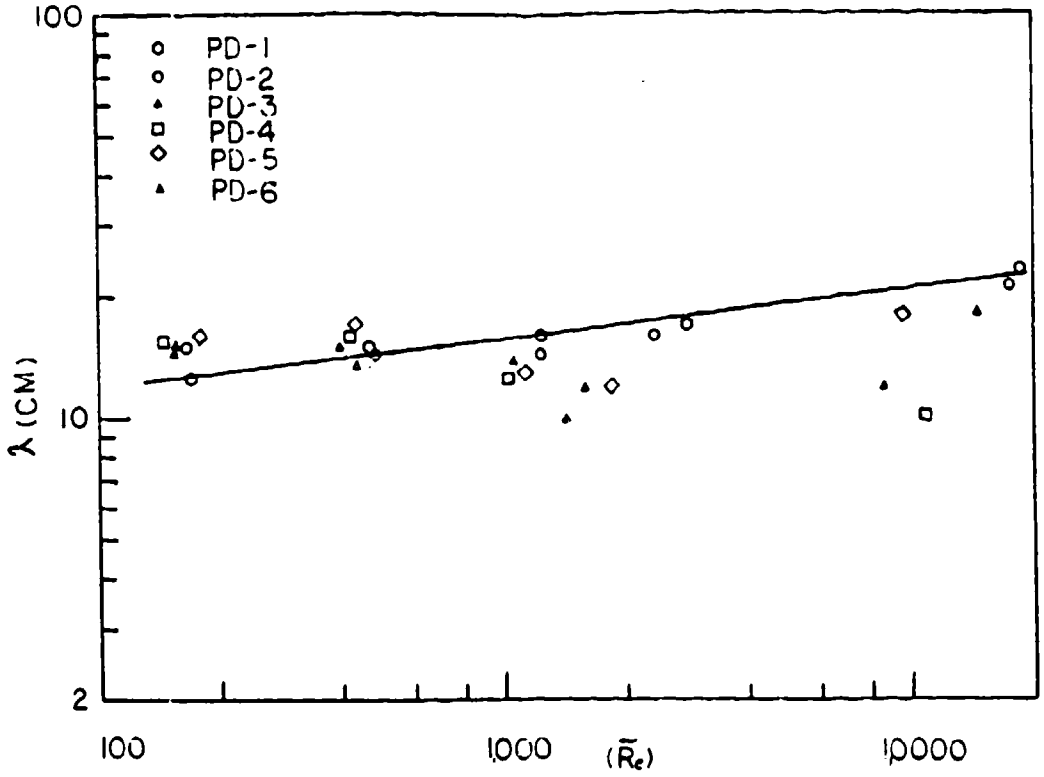


Fig. 6 The wavelength of the oscillatory motion, λ(cm), of the planar scavengers falling in the liquid as a function of Re.

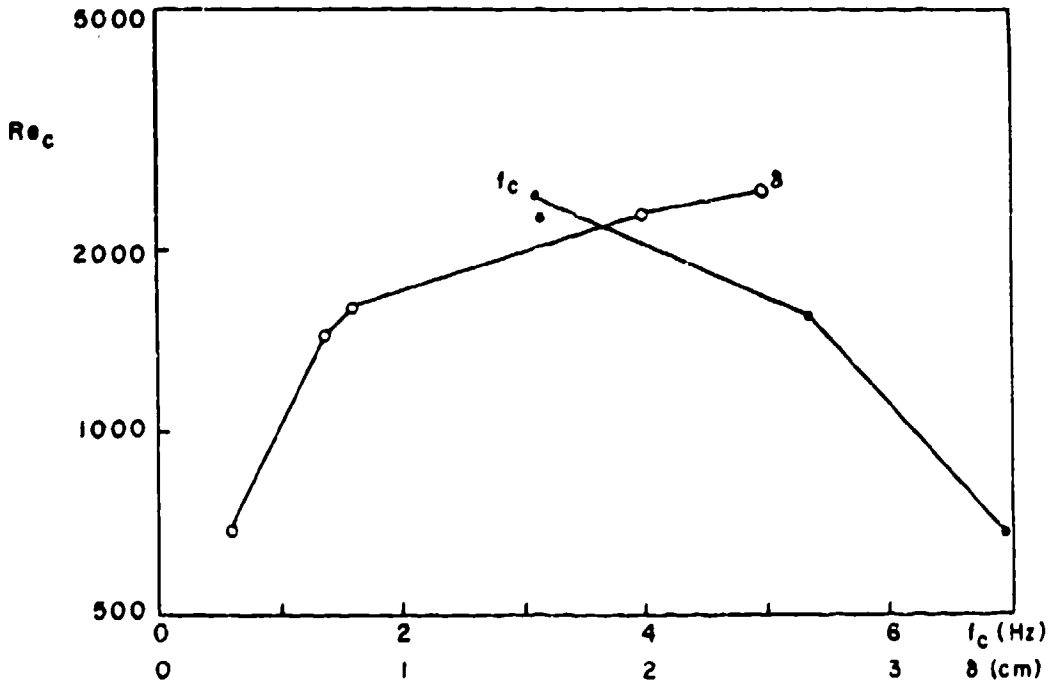


Fig. 7 The dependence of the amplitude, δ(cm), and frequency, f(Hz), of the paper disks falling in the air as a function of Re.

the curve $Re_c = f(Be_c)$, relating the Reynolds, $Re_c$, and Best ($Be_{c*} = C_D Re^2$ numbers. Slight side wind has a markable effect on the scavenger's behavior, when the scavenger starts to oscillate intensely ($Re_c > 90$). Then the amplitude, wavelength and frequency of motion are functions of $Re_c(Be_c)$ and of Wilmarth's stability parameter, I, (related to the moment of scavenger's inertia). Further was found that the frequency of oscillating disks can reach several units or tens of Hz and that a higher, $Re_c$, leads to the higher frequency, $f_c$, of oscillatory motion. This dependence cannot be, however, expressed by a simple monotone increasing function.

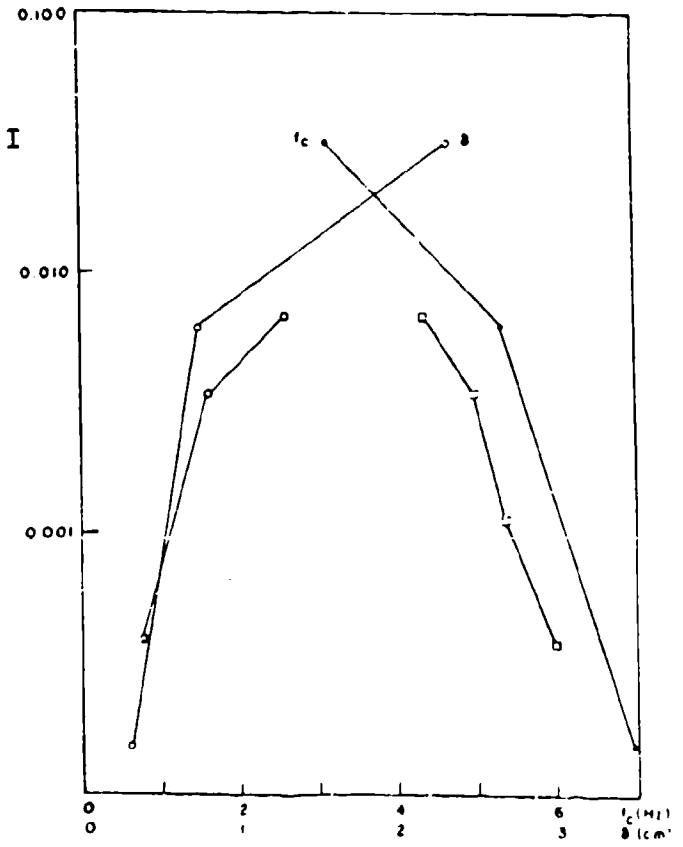


Fig. 8 The dependence of the amplitude, δ(cm), and frequency, f(Hz), of the paper disks falling in the air as a function of the Wilmarth's stability number, I.

## 3.2 Wind Tunnel Experiments with Smoke Particle Deposition on Model Scavengers.

### 3.2-1 Wind Tunnel.

After several modifications the current set up of the particle deposition experiments is presented in Fig. 9. The scavenger model is placed in the test section (15) of a low velocity wind tunnel (7) (Turbofan-Scott Engineering Science, Model 9005) with the measuring section diameter of 13.2 cm. The air velocity is regulated by a propeller (higher velocities), by the fume hood (8) and by the mixing chamber fan, where the clean outside air is mixed with a known aerosol flow (6). For most of the experiments titanium chloride aerosol was used. Only several experiments have been done with red phosphorus smoke. Titanium chloride ($TiCl_4$) aerosol was produced by the passage of the dry nitrogen gas from the container (1) through a humidifier (2) into a generating flash (3) where $TiCl_4$ reacted with water vapor. After removing the excess water from the aerosol-gas mixture, the droplets and particles came into the two electric furnace system (4 and 5) operated at temperatures around 700°C. The homogenized aerosol was vented further into the mixing chamber (6) where it was put in charge equilibrium in a cylindrical particle neutralizer with Kr-85 before entering the wind tunnel. The air-aerosol flow passed in the wind tunnel (made of plexi-glass) through two flow straighteners before reaching the test section and before entering into the fume hood (8). Measurement of air velocity profile in the test section has been done with the aid of a hot wire anemometer which was cross calibrated with the pressure transducer (16). This instrument was afterwards used for the mean velocity measurements based on pressure difference in two openings ahead and behind the test section. Relatively a wide section of almost constant velocity was reached in the middle of the test section (approximately 4 cm with the mean velocity error of $\pm$ 5% of the mean velocity). There the models were usually placed. The models fixed on a rigid wire were exposed to the aerosol flow in the center of a test section (15) in steady position or oscillating about the perpendicular direction or about an angle of

10° or 20° in reference to the main flow. The frequency of oscillation with a preselected amplitude (usually ± 10°) could be adjusted between several Hz and several tens of Hz with the aid of a vibrating mechanism (14) and its power generator (12).

The details of the device for model vibration and charging are seen in Fig. 10. The model (3) is suspended--approximately in the center of the test section--on wire fixed on a metallic rod which is set into oscillating motion (along its main axis) by a level (2) which is connected with an electromotor (1). Changing the position of the level (2) on the arm fixed on the rod with the model and varying the revolution rate of the motor (1), one can change the amplitude and frequency of the oscillatory motion at a preselected mean angle of attack of plate type model. The models of different material were "charged" to a chosen potential difference (1 kV, 2kV, 5kV, 8kV) by a generator (7) connected with the rod on which the model (3) is suspended. Electrical charging of the model has been done in two different ways: model was permanently connected with the generator during the experiment and the model was charged only for 3 sec at the beginning of the experiment. In order to obtain more uniform field and to avoid the effect of high polarized charges on the plexiglass wind tunnel walls (5) a grounded brass thin sheet was put around the test section (6). The neutralized aerosol samples for laser cavity aerosol spectrometer (ASAS 300A) are taken through a 10 cm long and 0.3 cm inner diameter metallic tube (4) connected by a 60 cm long and 0.6 cm inner diameter wide taygon tube.

Under normal conditions the tunnel was running at velocities between 0.25 $ms^{-1}$ and 3.00 $ms^{-1}$. Most of the measurements were performed at 1.0 $ms^{-1}$ for comparability reasons and because this velocity is very close to those measured with paper models freely falling in the settling chamber. The exposure (sampling) time was 2 min. Only exceptionally, a sampling time of 5 min. was selected for higher accuracy of particle counting and better reproducibility of measurements. During this time all effort has been done to keep the output of the aerosol generator constant.

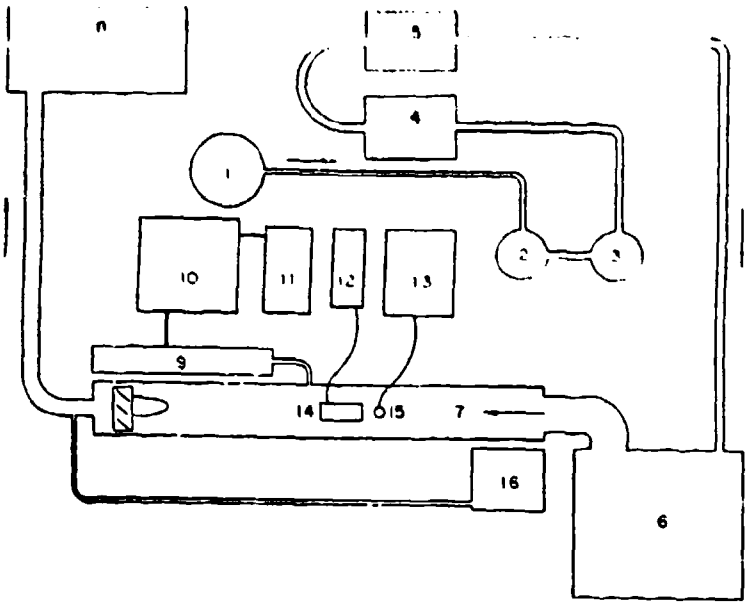


Fig. 9 Arrangement of the wind tunnel experiments: 1- nitrogen container; 2- humidifier; 3- $TiCl_4$ aerosol generating flask; 4 and 5- electrical furnaces; 6- air mixing chamber with Kr-85 neutralizer; 7- plexiglass wind tunnel with 13.2 cm; 8- fumehood; 9, 10 and 11- Laser Cavity Aerosol Spectrometer ASAS-300A (laser, electronic part, printer); 12 and 14- generator and model vibrating device; 13 and 15- electrostatic charge generator and model holder.

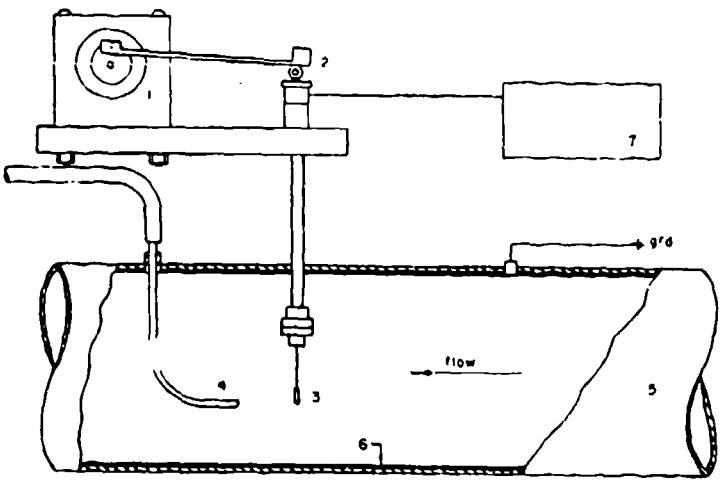


Fig. 10 Model Vibrating Device: 1-electromotor; 2- adjustable level for model vibration; 3- model; 4- aerosol sampling tube; 5- wind tunnel; 6- grounded metallic sheet; 7- electrostatic charge generator.

3.2-2 Aerosol Generation and Measurement.

The generation of smoke aerosol by reaction between $TiCl_4$ and water vapor and the production of red phosphorus smoke has been described earlier (Podzimek, 1981). However, the reproducibility of the experiments required to control well the state of the aerosol coming out of the generator (in Fig. 9: the generating flask, 3, with two stage furnace heating, 4 and 5 or the neutralizer, 6, with the diluting system). The aerosol, which was not sufficiently dried or shattered in the furnaces showed irregular spots and often on metallic plates the corrosion effects (Fig. 11). At a low incidence angle of the electron beam in the SEM the particles are clearly non-spherical in all particle sizes what is documented in the low magnification photograph (Fig. 12).

During the past two years a standard technique was elaborated, which enables to produce "dry" spherical particles (after the reactoin of $TiCl_4$ with water vapor). It consists essentially in removing the excess of water in the tubes and increasing the furnace temperature above 700°C. The second furnace (5 in Fig. 9) should have the temperature approximately 50°C higher for making the aerosol less polydisperse (probably through large particle shattering). The undiluted deposited aerosol has afterwards spherical shape (Fig. 13). After diluting the aerosol in the mixing chamber (6 in Fig. 9) with clean air (laboratory air cleaned in an absolute filter system) and sending the aerosol through electric charge neutralizer (Kr-85) the deposited particles had a spherical shape (Fig. 14). Finally we reached the mode of smoke aerosol production which remained steady for more than 30 min.

Practically all evaluations of the deposited aerosol have been done at a magnification of 1,000 x or in the optical or scanning electron microscope. For some special studies of particle deposition (e.g., along the rim) higher magnification was used combined often with coating of the specimen by gold. The standard procedure used for the evaluation in an optical microscope was to measure a strip in the middle of the disk's surface and to count all particulates with radii $R_p < 0.7; 1.4;$

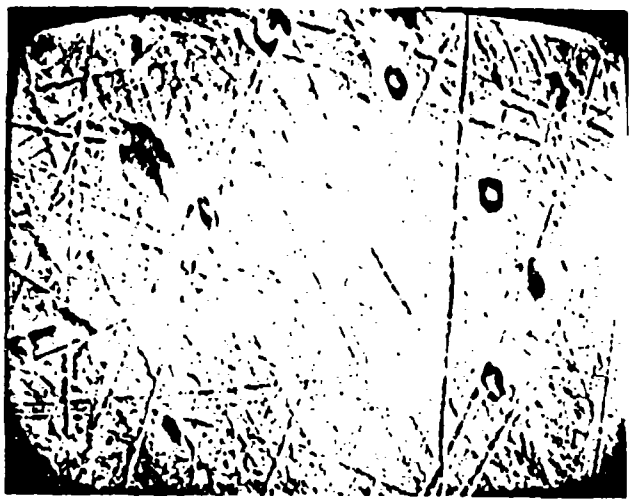

Fig. 11 $TiCl_4$ particles deposited on brass substrate (SEM, Mag 1850 x)

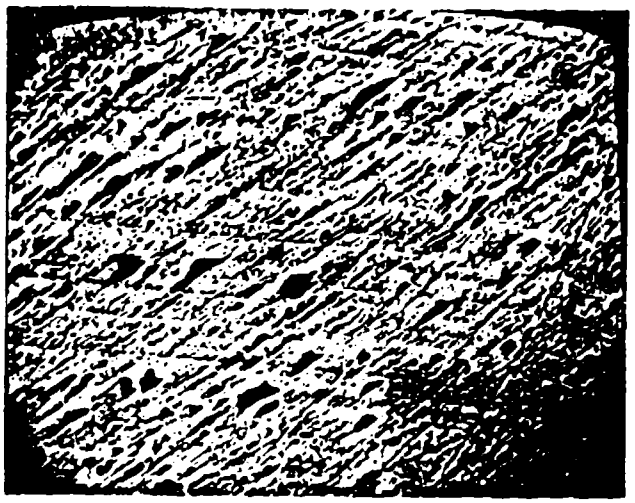

Fig 12 $TiCl_4$ particles deposited on brass substrate (SEM low beam incidence angle, Mag. 1100 x)

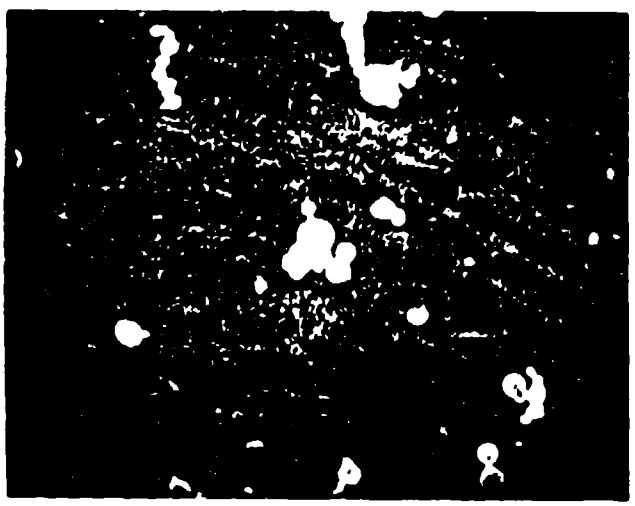

Fig. 13 $TiCl_4$ particles deposited on glass coated with gold (SEM, Mag. 3700 x)

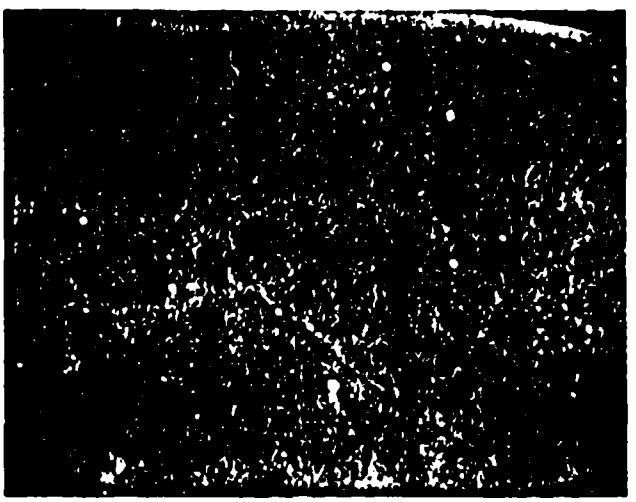

Fig. 14 $TiCl_4$ particles deposited on glass coated with gold (SEM, Mag. 740 x)

2.1 μm at a magnification of 1,000 x on both sides of the disks center. This enabled to judge the potential unsymmetry of the aerosol deposition and, if there was any, to correct it. For the calculation of the disk's collection efficiency it was assumed that the surface of the disk is covered uniformly with a central concentration symmetry by the deposited particles. The same procedure was applied for the particles deposited on the revese side of the disk. More detailed particle size distribution was used in the evaluation of scanning electron microscopical photographs, especially if large mgnification (e.g., 5,000 x) was used. Scanning electron microscope, combined with x-ray spectrum energy analyzer, was also used for checking the selected particle composition which was very important while checking if the stage of "dry" $TiCl_4$-$TiO_2$ particles was reached (large amount of Ti and little of Cl - Fig. 15).

Monitoring of the aerosol concentration and the size distribution has been done with the laser Cavity Aerosol Spectrometer ASAS-300A (Particle Measuring Systems, Boulder). The monitored volume in the instrument is 0.13 $cm^3$ $s^{-1}$ at a total sampling volumetric flow rate 5.0 $cm^3$ $s^{-1}$. After the new calibration the instrument covers the particle size ranges between 0.157 μm and 3.00 μm. This span is divided into four subranges (0.157 - 0.336 μm; 0.284 - 0.748 μm; 0.355 - 1.160 μm; 0.639 - 3.000 μm) each of them containing 15 size points on the distribution curve. Due to the different mean size intervals in different particle ranges it was necessary to normalize the data for obtaining a total particle size distribution monitored during each experiment on the four channels successively. In the final stage of developing the best way how to generate a steady concentration of $TiCl_4$ smoke aerosol the concentration of the aerosol fluctuated not more than $\pm$ 20% during one specific experiment. The size distribution of particulates in individual size ranges (referred to the total number of particulates in each range) is represented in Figs. 16, 17, 18 and 19 and the normalized integrated smoke particle size distribution is plotted in Fig. 20. It is clear that the individual size ranges do not

overlap well and that a considerable deviation of the total (normalized) distribution curve from the ideal log-normal distribution curve happens in the domain of the very small and large particulate sizes.

The aerosol size spectrum steadiness is well documented in Fig. 21 where during almost one hour the $TiCl_4$ aerosol was produced in the same way. At the beginning of the series mainly the small size ranges (III and IV) show considerable deviations from the log-normal distribution curve. After 15 minutes the samples (No. 2, 3 and 4) show a high stability and reproducibility of small particle fraction which includes about 70% of all particulates. After 40 minutes the large particle fraction starts to be unstable, probably due to the fact that additional water vapor was injected into the generating flask and aerosol became partly wet (curves 5a and 5b - for 5b the true size scale is plotted in μm).

```
COMMAND:IDENT 3

 QUALITATIVE ELEMENT IDENTIFICATION

SAMPLE ID:TiO2 ON AU

POSSIBLE IDENTIFICATION
   AU LA MA LB2
   CU KA
   AL KA
   TI KA
   ZN KA OR  RE LA
   SI KA
   ZR KA

          PEAK LISTING
      ENERGY    AREA  EL. AND LINE
   1   1.487    1440 AL KA
   2   1.751     605 SI KA
   3   2.166   10618 AU MA
   4   4.539     887 TI KA
   5   8.072    1491 CU KA
   6   8.674     791 ZN KA
   7   9.002     105 UNIDENTIFIED
   8   9.749    1324 AU LA
   9  11.578     350 AU LB2
  10  15.746      38 ZR KA

 COMMAND:
```

```
 X-RAY IDENT-SM/10

 QUALITATIVE ELEMENT IDENTIFICATION

SAMPLE ID:TiO2 ON AU

POSSIBLE IDENTIFICATION
   AU LA MA
   CU KA
   AL KA
   TI KA
   ZN KA OR  RE LA
   SI KA

          PEAK LISTING
      ENERGY    AREA  EL. AND LINE
   1   1.487    1440 AL KA
   2   1.751     605 SI KA
   3   2.166   10618 AU MA
   4   4.539     887 TI KA
   5   8.072    1491 CU KA
   6   8.674     791 ZN KA
   7   9.749    1324 AU LA
```

Fig. 15 Element identification of the substrate with the deposited $TiCl_4$ particles (no Cl was identified in this particular sample by the x-ray energy spectrum analyzer).

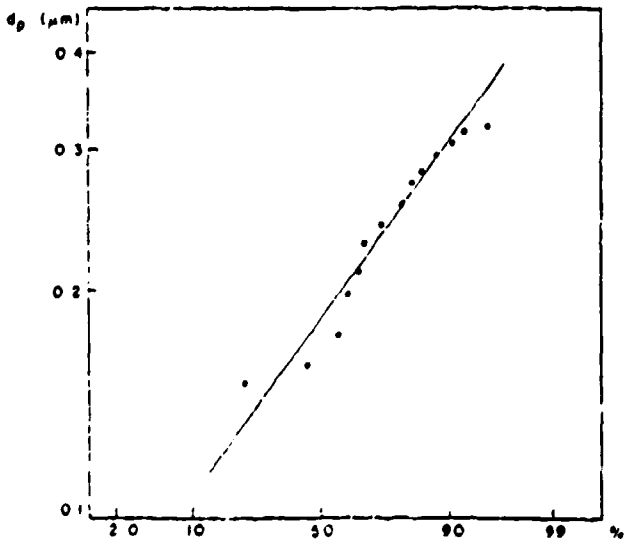


Fig. 16 $TiCl_4$ particle cumulative size distribution in the 4-th range of the ASAS-300A aerosol spectrometer.

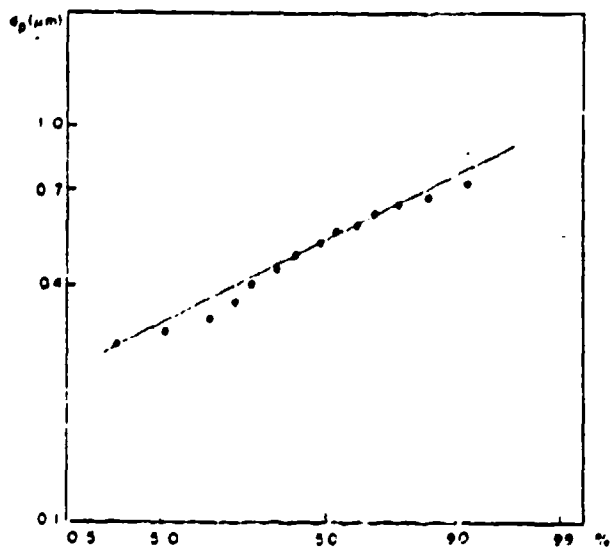


Fig. 17 $TiCl_4$ particle cumulative size distribution in the 3-rd range of the ASAS-300A aerosol spectrometer.

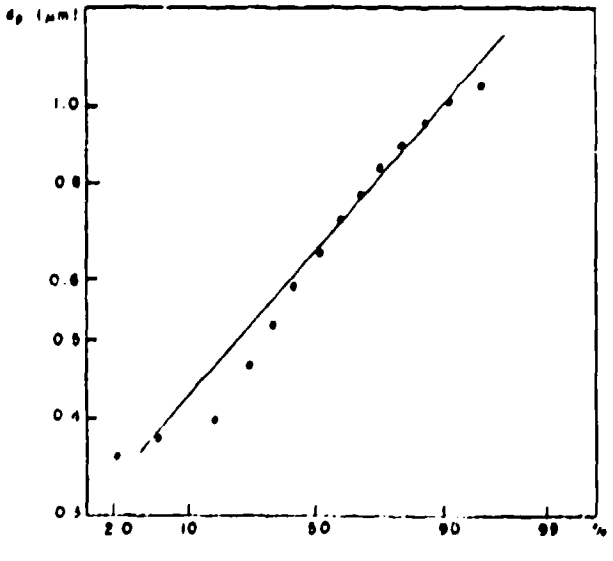


Fig. 18 $TiCl_4$ particle cumulative size distribution in the 2nd range of the ASAS-300A aerosol spectrometer.

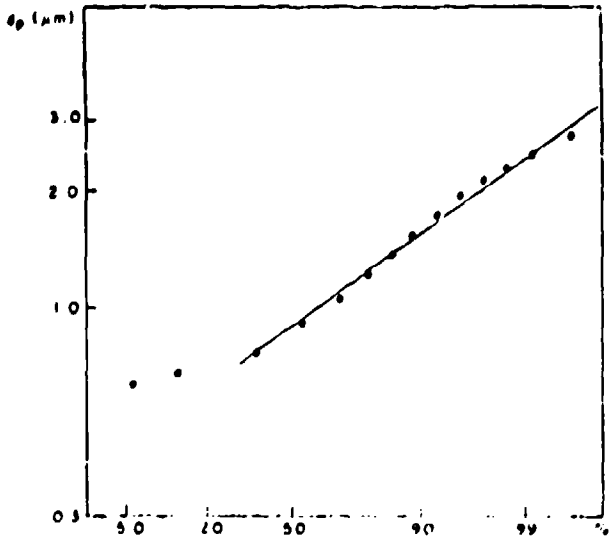


Fig. 19 $TiCl_4$ particle cumulative size distribution in the 1st range of the ASAS-300A aerosol spectrometer.

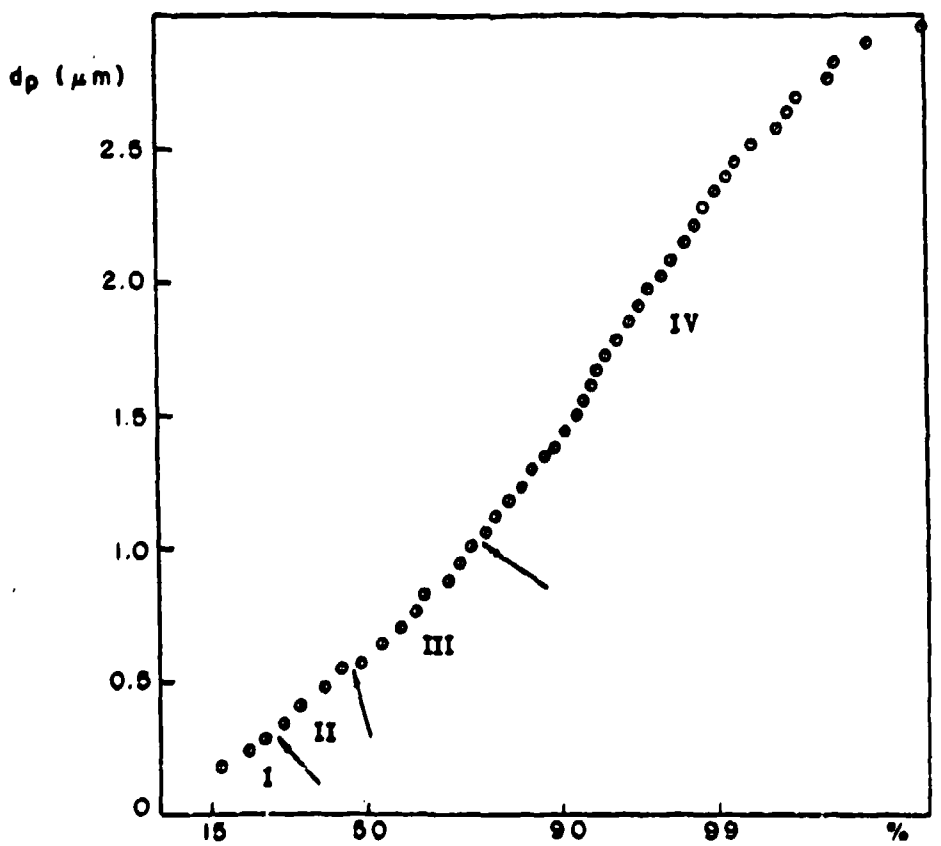


Fig. 20 Integrated $TiCl_4$ particle cumulative size distribution (ASAS-300A aerosol spectrometer).

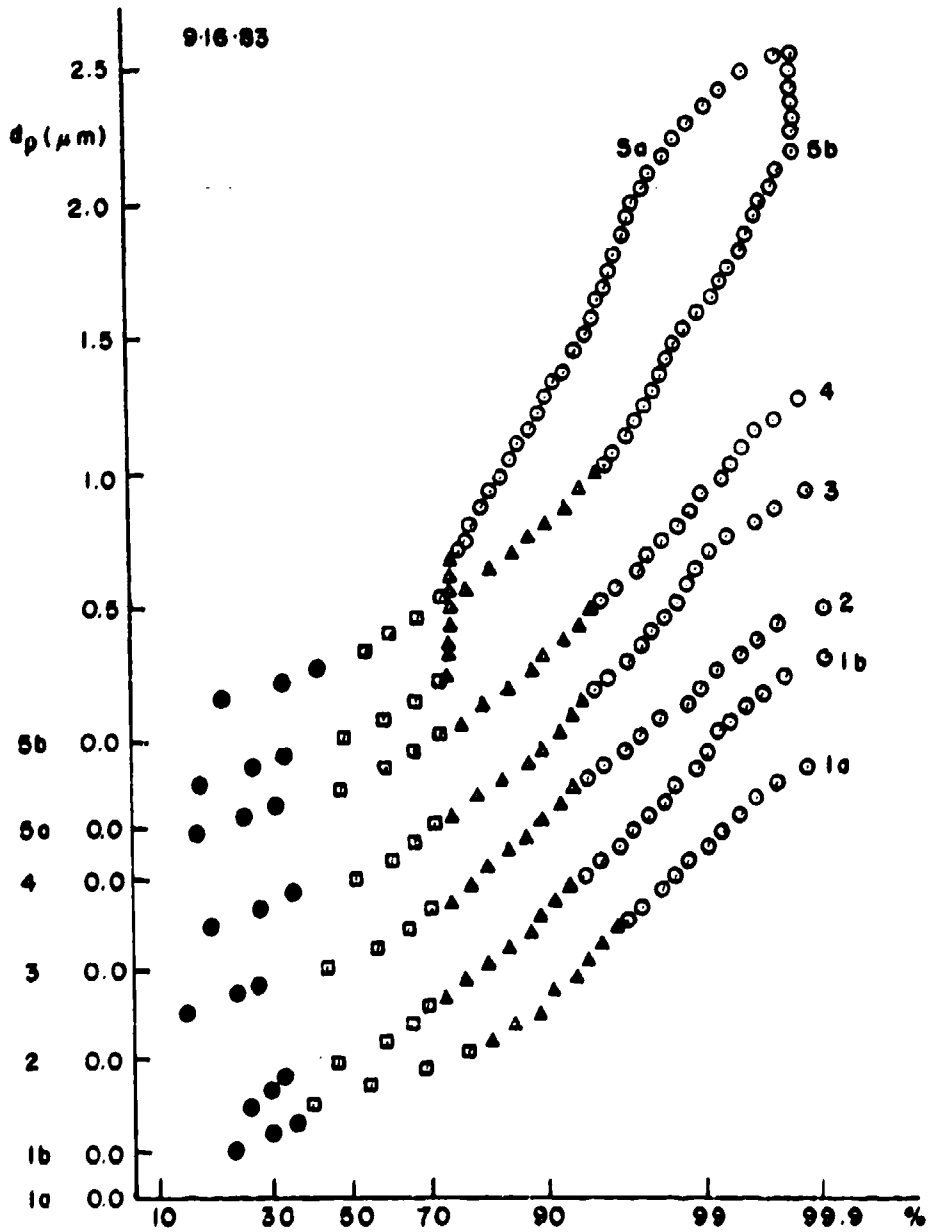


Fig. 21 Structural changes of the generated $TiCl_4$ aerosol. Time interval between 1a, 1b and 5a, 5b was 3 min. between 1-2, 2-3, 3-4 and 4-5 approximately 8 min.

3.2-3 Scavenger Model Preparation.

Models for free fall experiments and their production were described in the earlier reports (Podzimek, 1981). Wind tunnel experiments have been done with small disks, cylinders and grids of different materials.

Systematic measurements of deposited $TiCl_4$ particles have been performed with uncharged disks made of plexiglass or glass. Most of the plexiglass models had diameters of 0.50 cm and thickness of 0.05 cm. They were cemented to a wire which, together with a holding rod, could be set into an oscillatory motion in the center of the tunnel's test section. Glass disk (with especially sanded rim) had the diameter of 0.45 cm and the thickness of 0.10 cm. They were suspended in the same way like plexiglass models. For studies with charged models, their surface including the epoxide connection was coated by a thin layer of gold. Glass models were also used for the study of the effect of model oscillation on particle deposition.

Brass disks of 0.66 cm in diameter and 0.075 cm in thickness were used mainly for particle deposition on charged models. However, the deposited "wet" particles left very often irregular spots on their surface (Fig. 11) revealing a chemical reaction between $TiCl_4$ smoke particle and the substrate. For this reason the dielectric disks coated by gold were preferred for systematic measurements. Cylindrical models were made of wires or rods of different diameter and material (PVC, plexiglass, stainless steel, glass. During exposition there were attached to a specific holder in the wind tunnel's test section, which enabled their easy removal or fixing. Special holder was made for the study of two hydrodynamically interacting models.

The evaluation of deposited smoke particles in an optical microscope did not require special tools. In the scanning electron microscope, however, the exposed model had to be mounted on a special stage which enabled to scan with a simple manipulation the front and back side of a scavenger.

3.2-4 Deposition of Smoke Particles on Planar Scavengers .

Systematic measurements of the deposited smoke particulates concentrated on simple geometrical forms of collectors such as planar scavengers (disks), cylinders and grids. Planar scavengers were selected for the following reasons: referring to the same scavenger main cross-section thin oblate spheroid (disk) has much higher collection efficiency compared to a sphere (Martin and Podzimek, 1982). Referring to the unit of mass of the dispersed scavengers this advantage of planar scavengers is even more expressed. The hydrodynamic interaction of planar scavengers and their "falling scavenger zone effect" is more accentuated in the case of disks if compared with spheres. Finally, the theoretical models exist for the comparison of calculated and measured collection efficiencies of disks.

Experiments with falling scavengers in a cylindrical tank and in a horizontal wind tunnel (Podzimek, 1981) indicated that one should concentrate on paper disks (easy production, economic reasons) having approximate size of several mm to 1 cm. Their fall velocities ranged between 0.25 m $s^{-1}$ and 1.5 m $s^{-1}$. Several of them (the larger sizes) performed slight oscillatory motion (several Hz to 70 Hz) and few of them did tumble. For wind tunnel investigation, which was preferred for the longer exposure time and higher reproducibility of measurements, the disks were made of different material as described in 3.2-3. In total 36 systematic measurements were made with stationary disks, 17 with oscillating disks and 46 with electrically charged disks.

Deposition on stationary disks (Fig. 22) was featured by large scatter of data, probably due to the very difficult control of the state of generated smoke particles which passed through the Kr-85 neutralizer before reaching the tunnel's test section. In mean, the highest collection efficiency (around 1.2%) showed the plexiglass disks (0.5 cm in diameter) at 1 m $s^{-1}$, slightly lower efficiency (around 1.0%) had plexiglass disks at 0.25 m $s^{-1}$ and the lowest glass disks (0.5 cm in diameter) at 1 m $s^{-1}$. Always along scratched places or lines on a plexiglass surface was observed higher deposition of smoke particles and aggregate

formation. Considering the $Re_c$ of the disk (320 for 1 m $s^{-1}$ and 80 for 0.25 m $s^{-1}$), one can conclude from Fig. 22 that the calculated collision efficiencies (according to the model described in Section 2) are almost one order of magnitude higher than the measured data.

A typical particle number distribution along the disk's radius is presented in Fig. 23 (R = 1 is the rim and R = 15 is the center of the disk). On the obverse (front) side of the quiescent disk particles with the radius $R_p < 0.7$ μm have a very significant maximum close to the rim and almost half of this peak concentration in the center (particle numbers are plotted in relative units). Particles with $0.7 < R_p < 1.4$ μm had a significant peak close to the rim with an almost flat curve (number of deposited particles per unit of surface) toward the center of the disk. On the disk's reverse side the peak of the deposited particle curve was shifted a little from the rim towards the center and most of the samples showed a secondary maximum about the middle of the radius. This secondary maximum was comparable with the primary peak in 40% of samplings and in two cases it overrode the maximum at the rim. The mean ratio of the number of deposited particles on the front and back side of the stationary disk was 0.986 with the standard deviation from the mean value of $\sigma = 0.135$.

The oscillating disk (glass disk diameter 0.45 cm, $Re_c = 280$) with the amplitude of oscillatory motion $\pm$ 10° and frequency 10 Hz (Fig. 24) showed in mean a ratio between particles deposited at the obverse and reverse side 0.913. This ratio was 0.745 for a frequency of 60 Hz. In total, the oscillating disks were featured by a higher deposition of particulates on the reverse side of the model ($N_{ob}/N_{rev} = 0.846$ with a standard deviation of 0.065).

A typical particle deposition pattern for oscillating frequency 10 Hz is in Fig. 25. In spite of large deviation from this pattern in individual samplings, the highest deposition on the disk's front side was close to the rim (R = 1) for $R_p < 0.7$ μm. On the back side, however, the deposition was high and uniform on the whole surface. The deposition of particulates with $0.7 < R_p <$

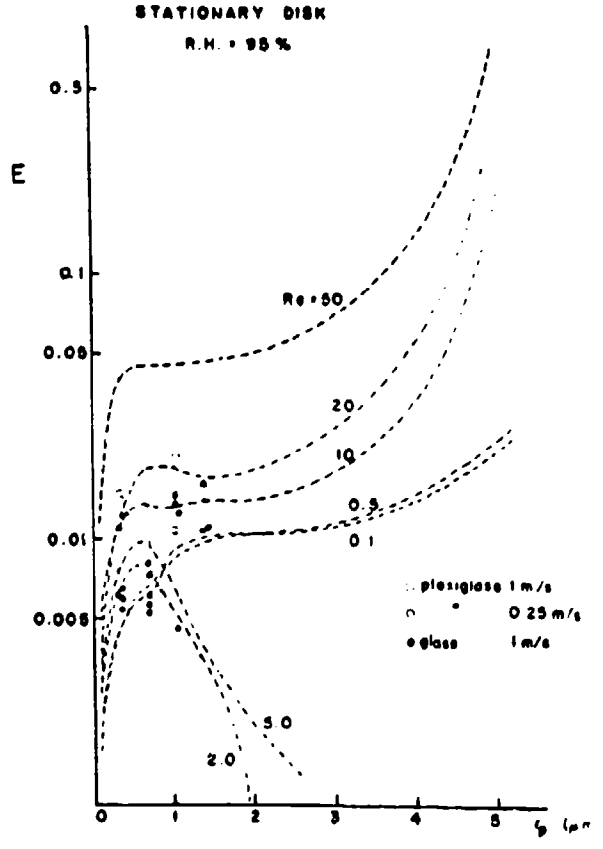


Fig. 22 Calculated collision efficiency (dashed lines) for an oblate spheroid ($Re_c$; $A_c$ = 0.05) and smoke particles of radius, $R_p$ [μm]. Measured data on a stationary disk in the wind tunnel are compared.

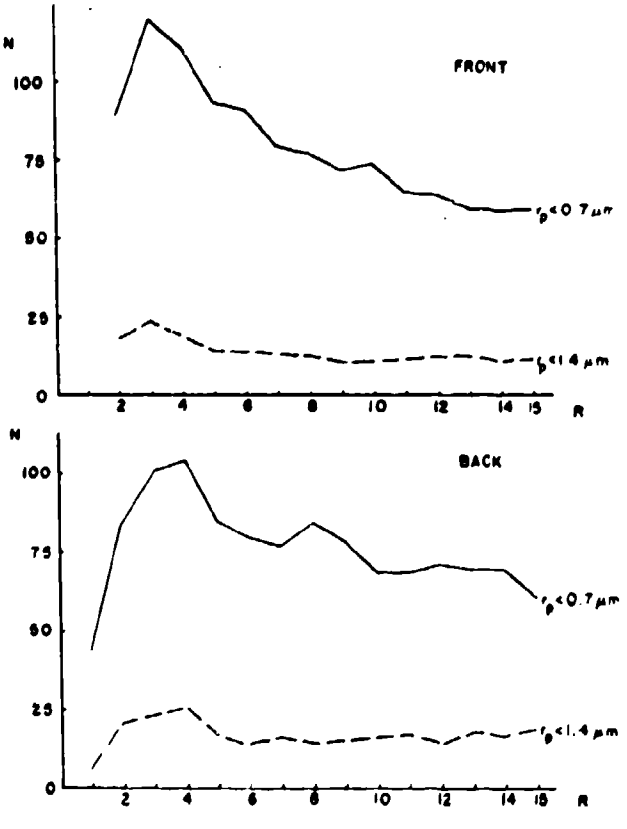


Fig. 23 Number of deposited particles in relative units counted along the radius of a quiescent glass disk (1 is the disk's rim), Langerge particles (dashed line), small particles (full line). $R_c$ = 0.25 cm, V = 0.25 m $s^{-1}$.

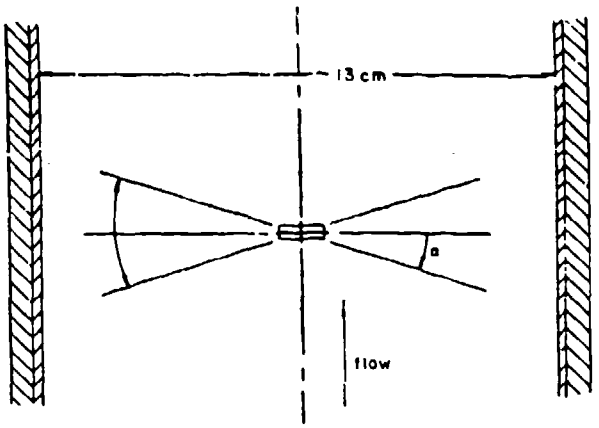


Fig. 24 Oscillating disk in the wind tunnel test section ($\alpha = \pm 17°$).

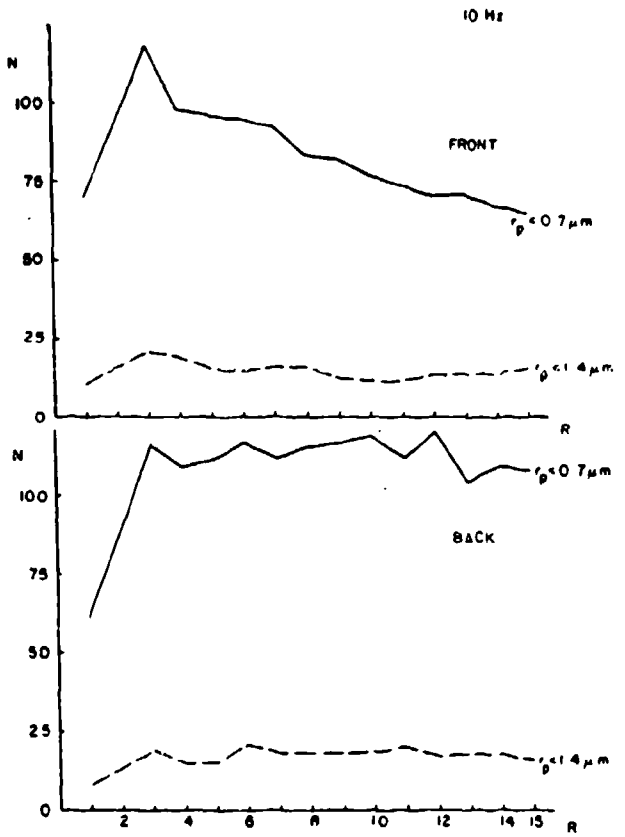


Fig. 25 Number of deposited particles in relative units counted along the radius of an oscillating disk (10 Hz, $\alpha = \pm 10°$). 1 is the disk's rim. $R_c$ = 0.25 cm, V = 0.25 m $s^{-1}$.

1.4 μm does not show any dramatic change across the whole front or back surface.

The comparison of the calculated collision efficiencies for a steady falling oblate spheroid (with the axis ratio of 0.05) with the measured collection efficiencies for an oscillating disk is made in Fig. 26. In spite of the higher measured total collection efficiency for oscillating disks, there is still a considerable difference between the calculated and measured efficiencies. The latter are usually several times lower than the calculated data.

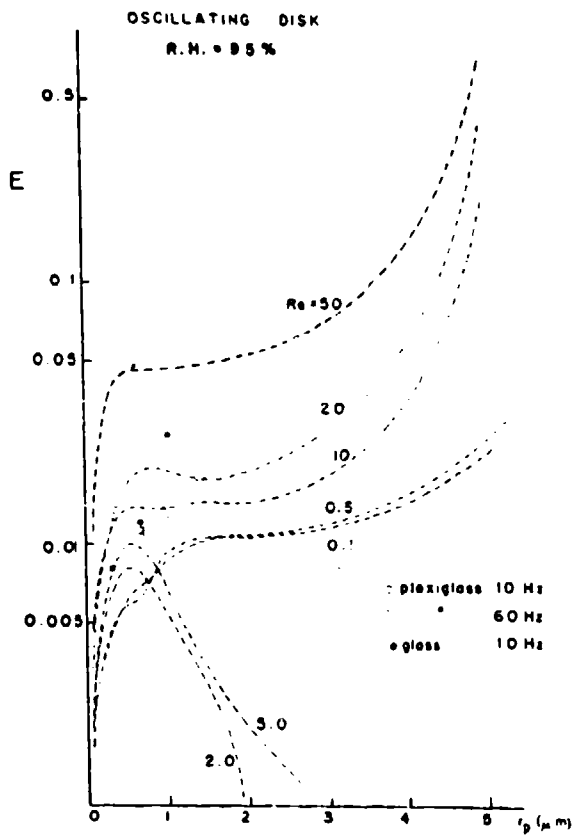


Fig. 26 Calculated collision efficiency (dashed lines) for an oblate spheroid ($Re_c$; $A_c$ = 0.05) and smoke particles of radius, $R_p$ [μm] in comparison with measured particle deposition on oscillating disks ($R_c$ = 0.25 cm, $Re_c$ = 80; α = ± 10°).

3.2-5 Deposition of Smoke Particles on Charged Disks.

The electric charges of the aerosol particles and/or of the collector affect strongly the particle deposition. In general, there is a very limited possibility to control the electric charging of smoke aerosol. Usually, a $TiCl_4$ particle concentration around $10^5$ $cm^{-3}$ exists at the outlet of the second furnace (No. 5 in Fig. 9). During several seconds of the aerosol passage through a 1.27 cm I.D. tygon tube, particles coagulate, deposit on the tube's wall and exchange their electric charges. One can assume that the aerosol is almost in charge equilibrium after passing into a Kr-85 neutralizer where clean air is used for aerosol dilution in the ratio 4:1 (nitrogen with aerosol). This explains the fact that neither the smoke aerosol size distribution nor the number of deposited particles on a scavenger were markably affected by the 10 mCi neutralizer before advancing into the wind tunnel. Several experiments with smoke particles not neutralized did not deviate much from the deposition of neutralized aerosol at flow speed 1.0 m $s^{-1}$.

Charging of dielectric or metallic collectors up to 8 kV has been done by an electrostatic generator connected with the model suspended in the central part of the tunnel's test section. Models were permanently connected with the generator during the sampling (usually 2 min.). The charge of 5 kV transferred to the model for 3 sec at the beginning of the experiment was neutralized soon so that the effect of electric charge on the aerosol deposition decreased markably after several tens of seconds (in Fig. 27 marked by circles) at a mean aerosol concentration of 16,000 $cm^{-3}$. In order to control better the electrostatic field around the collector and to avoid the effect of induced electrostatic charge on tunnel's wall, the wall in the test section was covered by a thin grounded brass foil. In this arrangement a potential difference of 1 kV imparted to the models corresponds to the potential gradient of 1360.48 V/cm (4.4896 esu/cm) at a distance of 0.25 cm from the disk's rim (a cylindrical model for field calculation was used), to 581.60 V/cm (1.9193 esu/cm) at a distance of 0.75 cm, 373.89 V/cm (1.2338

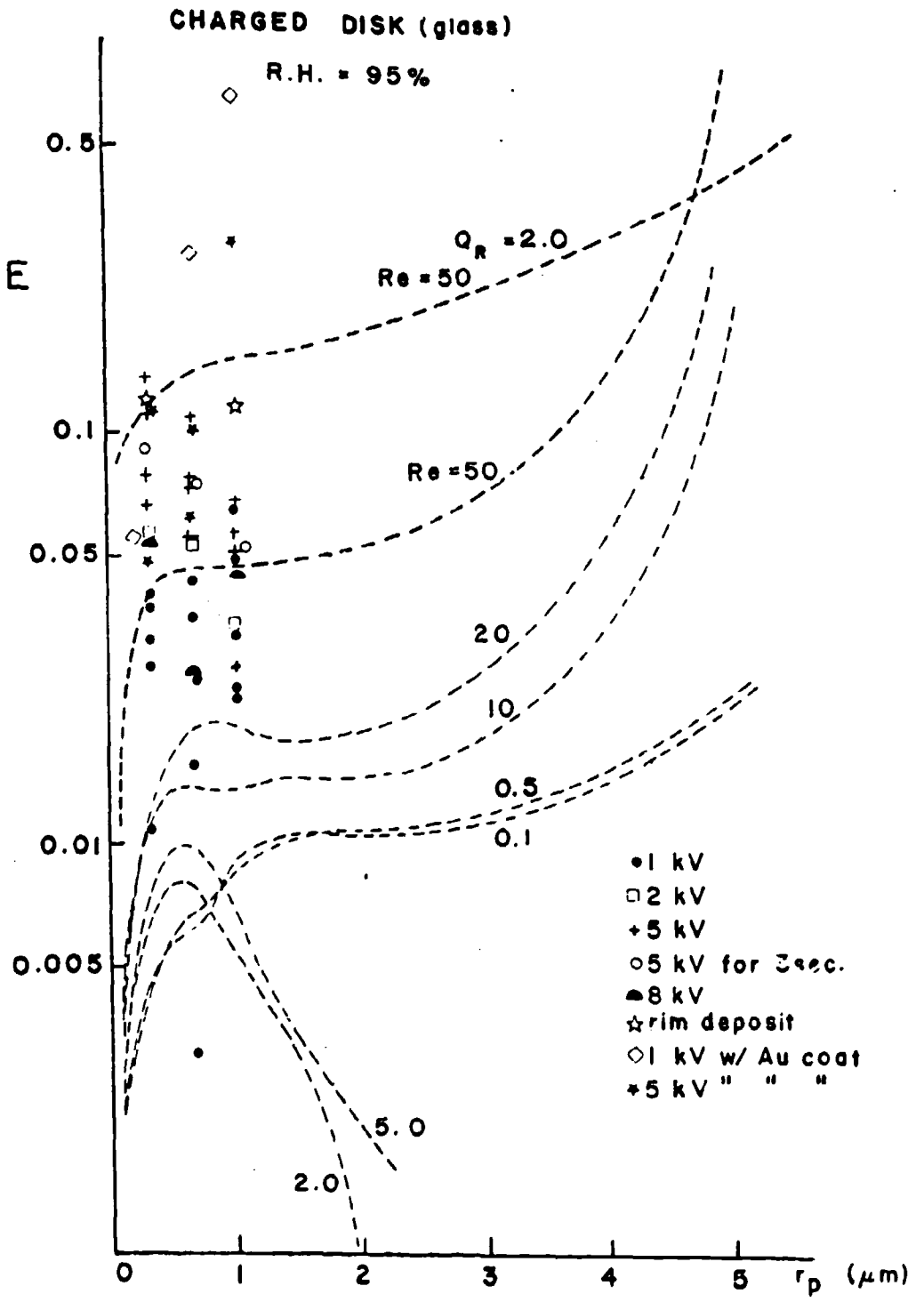


Fig. 27 Calculated collision efficiency (dashed lines) for a neutral oblate spheroid ($Re_c$; $A_c$ = 0.05) and for a charged spheroid ($Q_c$ = 2 esu $cm^{-2}$) in comparison with measured collection efficiency for smoke particles, $R_p$[μm]. $R_c$ = 0.225 cm; V = 0.25 or 1.0 m $s^{-1}$.

esu/cm) at 1.75 cm and 198.45 V/cm (0.6549 esu/cm) at 4.75 cm. At 5 kV one has a field gradient of 6852.4 V/cm (22.6129 esu/cm) in a distance of 0.25 cm from the disk's rim. These high potential gradients cause an anomalous-chain type-smoke particle deposition which will be discussed later.

Figure 27 summarizes the results of most of the experiments which have been performed with charged collectors. In the same diagram are plotted the calculated collision efficiencies (see Section 2) for oblate spheroids ($A_c$ = 0.05) with $Re_c$ ranging from 0.1 to 50. In addition, a curve for a spheroid with $Re_c$ = 50 and an electric charge of 2.0 esu $cm^{-2}$ is showing a potential effect of a charged collector on the aerosol particles bearing in their majority one elementary charge. Eighty percent of the 46 experiments have been done with glass disks 0.45 to 0.50 cm in diameter and 0.10 cm in thickness. Nine glass disks were coated by gold which ensured electric conductivity of their surface. Several experiments have been done also with plexiglass disks and brass disks (which, unfortunately, showed often chemical reaction between $TiCl_4$ particles and the surface). The measured mean collection efficiencies from the Fig. 27 for three main sizes of smoke particulates are plotted for different voltage differences in Fig. 28. It is apparent that the 5 kV voltage difference shows a markable effect on small particle ($d_p$ < 1.4 μm) deposition and almost no effect on the deposition of particles with $d_p$ > 1.4 μm. The collection efficiency for particles with $d_p$ < 0.7 μm increases from its value of 2.5% for 1 kV potential difference to 10.8% for 5 kV and then drops to 5.5% for 8 kV. The number of particulates (counted on both sides of a disk) can be easily underestimated in the case of the potential difference of 8 kV. As was mentioned earlier, the very high potential gradients close to the disk's surface cause the aggregation of particulates, which are very difficult to count individually. Low airflow velocity of 0.25 m $s^{-1}$ does not change dramatically the dependence found for the velocity of 1.0 m $s^{-1}$. This supports the hypothesis that inertial deposition does not play a dominant role in the mechanism of small particle ($d_p$ < 1.4 μm) removal for similar conditions.

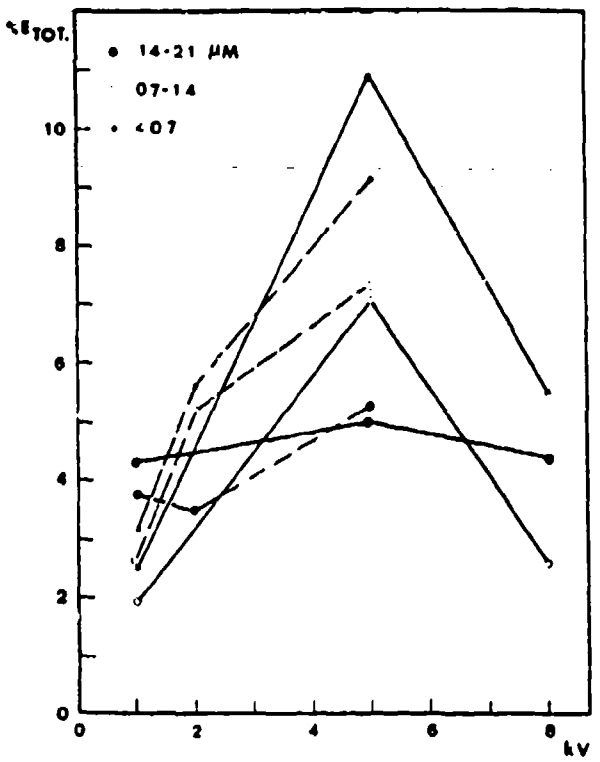


Fig. 28 Measured collection efficiencies of a charged disk in dependence of scavenger "charge" (1 to 8 kV) and smoke particle size ($d_p$ in µm).

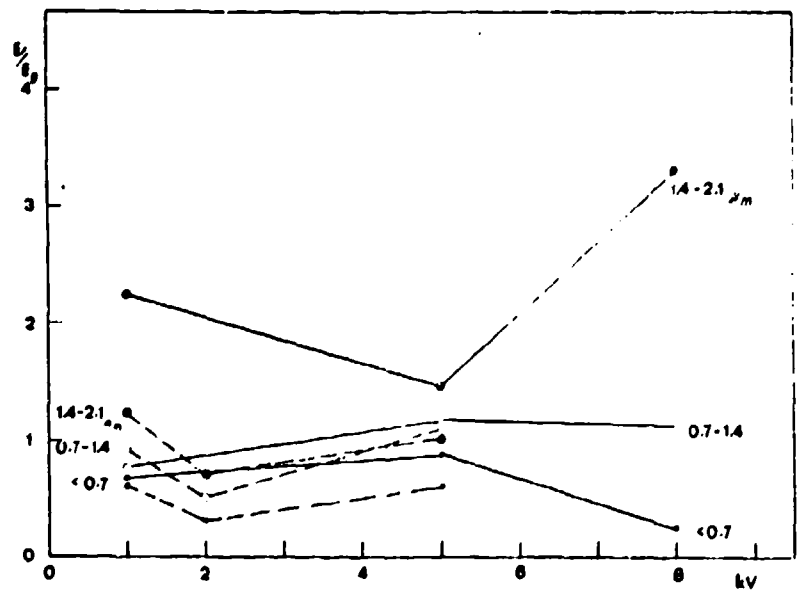


Fig. 29 Ratios of the measured collection efficiencies for a front and backside of a charged disk in dependence of scavenger "charge" and particle size.

Another important parameter is the ratio of the disk's collection efficiency on the front and back side (Fig. 29). Bearing in mind that each point in Figs. 28 and 29 is a mean only of three pairs of measurements with ± 20% of data scatter, we can conclude that only in the case of particles larger than 1.4 μm there is an apparent effect of inertial forces on the particle deposition on the obverse side of a disk at a velocity of 1 m $s^{-1}$. The number of particles deposited along the disk's radius, R, (R = 1 refers to the rim and R = 12 to the center) shows the prevailing deposition (in relative numbers) close to the rim, especially at a velocity of 0.25 m $s^{-1}$ for very small particles (Figs. 30 and 31). There is also some evidence that in mean the small particle ($d_p$ < 1.4 μm) deposition on the disk's reverse side prevails.

The evaluation of the number of deposited particles on the obverse and reverse side of a disk--especially at high voltage differences--is hampered by the large clusters of particulates and by the deposition of particulates at the rim. Occasionally was found more than 50 individual particles in a large cluster at $\Delta V \geq$ 5 kV. Because there was some evidence that the large clusters are released from the dielectric (plexiglass) tunnel wall, care was taken to check its cleanness before each set of experiments. In spite of that, one was able to observe often chain-like structures on the disk's surface (Figs. 13, 32, 33). An attempt was made to evaluate the individual particles forming chains of more than five particles. Due to this counting uncertainty, one can expect in mean deviations of -20% from the real counts.

The deposition of particles at the rim was investigated in a series of measurements in the electron microscope. Because of the inhomogeneous particle deposition and oriented chain formation along the rim of dielectric models, the experiments included only the glass models (with well-defined edge) coated by gold. In Fig. 34 are shown the deposited $TiCl_4$ particles at the edge of a charged disk with diameter of 0.45 cm. The particle numbers are plotted in counts per 45 x 17.5 $\mu m^2$ area so that 22 pictures were taken in the SELM at a magnification of 5,000 x across the edge of 1 mm thickness. The highest particle deposition is in the middle

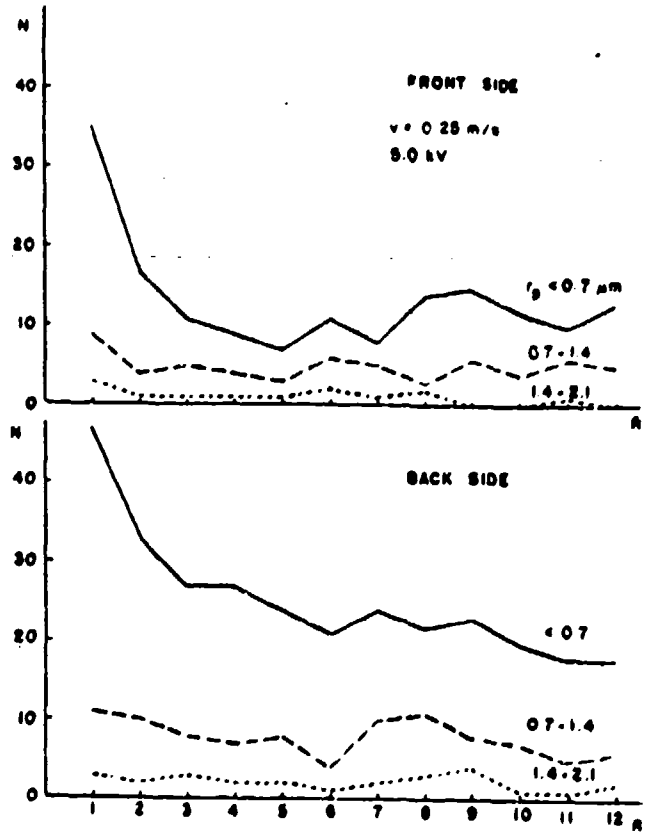


Fig. 30 Number of deposited particles in relative units measured along the radius of a charged glass disk ($R_c$ = 0.225 cm). 1 is the disk's rim. Small particles (full line), large particle (dashed line). V = 0.25 m $s^{-1}$; 5.0 kV.

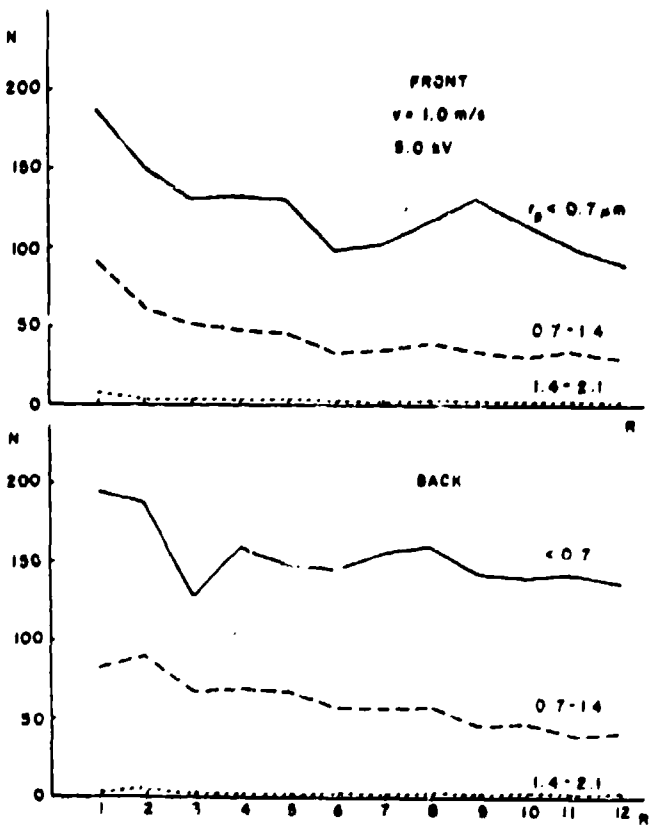


Fig. 31 Number of deposited particles in relative units measured along the radius of a charged glass disk ($R_c$ = 0.225 cm). 1 is the disk's rim. V = 1.0 m $s^{-1}$; 5.0 kV.

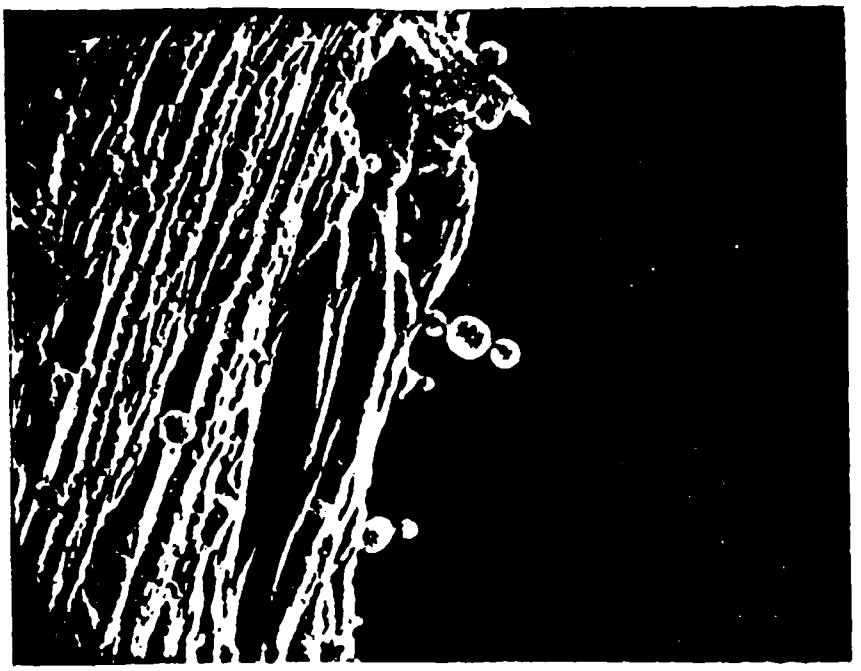

Fig. 32 Chain-like aggregates of $TiCl_4$ particles at the rim of a glass disk coated with gold (5.0 kV, Magn. 3200 x).

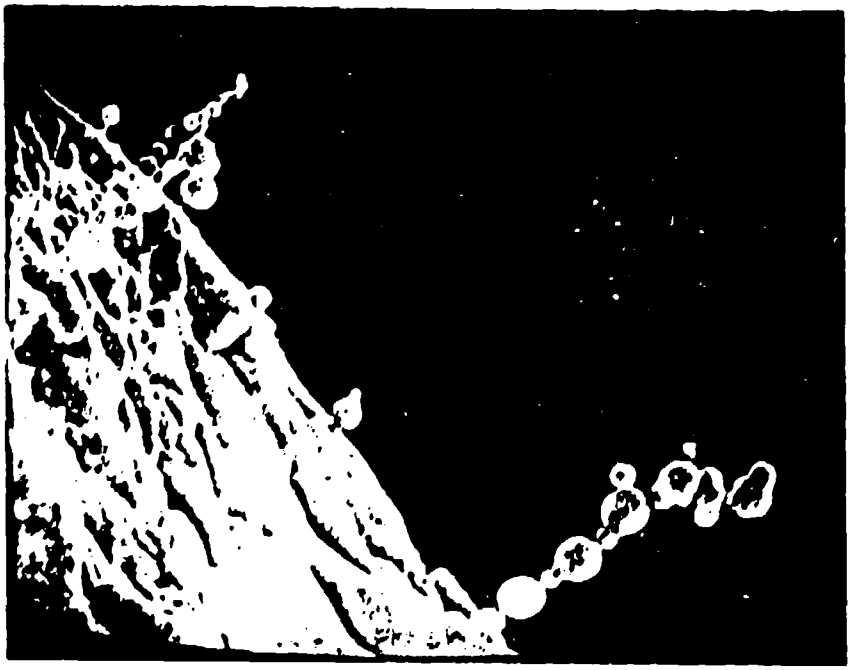

Fig. 33 Chain-like aggregates of $TiCl_4$ particles at the rim of a glass disk ($R_c$ = 0.225 cm) coated with gold (8 kV, Magn. 4000 x).

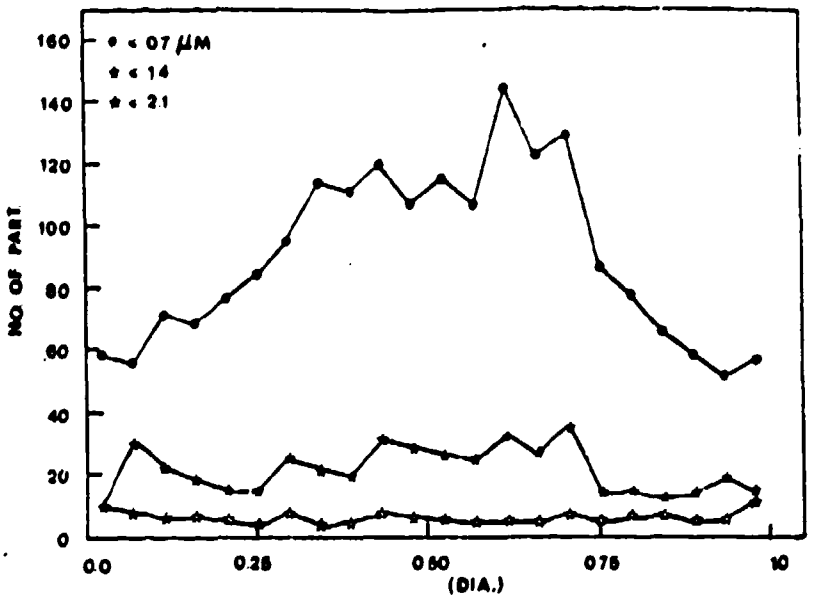


Fig. 34 Number of deposited $TiCl_4$ particles at the rim of a glass disk coated by gold. Each point corresponds to an area of 45 x 17.5 $\mu m^2$ ($R_c$ = 0.225 cm; 5 kV, V = 1.0 m $s^{-1}$).

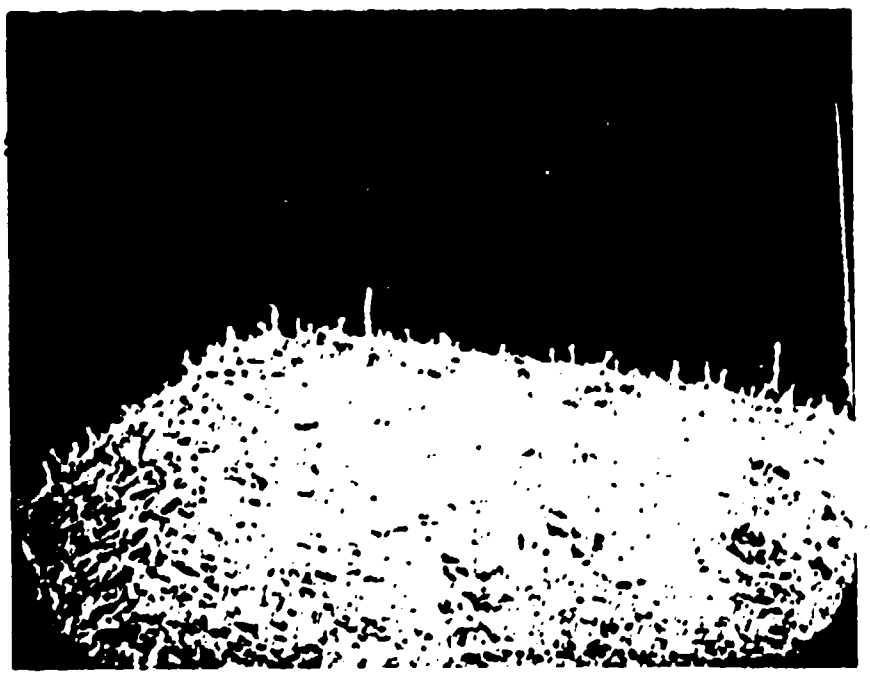

Fig. 35 The edge of a glass disk coated by gold and "charged" to 5 kV after being exposed for 2 min. to $TiCl_4$ aerosol.

of the edge. If all particles found in the chain-like aggregates at the side of a rim of a disk "charged" with 5 kV (Fig. 35) were counted as individual particles, the total number of deposited aerosol increased almost 100%. These facts must be considered if one confronts the results of the numerical models for smoke particle deposition with the measurement, or if one tries to increase the scavenging efficiency of planar scavengers.

Another set of experiments was aimed to determine whether the dielectric charged models (glass) coated by a metal (gold) have in mean higher collection efficiency than models of pure glass. The models were glass disks (of 0.45 cm in diameter) divided into one half which was coated by gold and the other half which was left untreated. Both halves were "charged" in different experiments with 1 kV, 5 kV and 8 kV. Unfortunately, the particle evaluation in the SELM was much more reproducible in the case of the coated half than on the glass surface. Nevertheless, the number of particulates in different positions on the disk's surface shows that a "charge" of 1 kV does not change much the pattern of deposited particles on both compared halves. "Charging" the disk with 5 kV and 8 kV led to the preliminary conclusion that larger particle counts were found in mean at the rim of the uncoated half than on the coated one ($N_{un}/N_{co} = 1.133$). On the plain disk's surface this relationship was reversed ($N_{un}/N_{co} = -0.594$, so that in mean no dramatic change due to the induced charges on dielectric disks was found. The experiments of this kind will continue.

3.2-6 Deposition of Smoke Particles on Cylinders.

In total, twenty-one experiments have been done with $TiCl_4$ particle deposition on dielectric and metallic cylinders in the domain of $Re_c$ ranging from 3.4 to 44.0. Two of the series had to be rejected for the high contamination of the PVC materials by the unknown compound of Ti as was demonstrated clearly by the x-ray spectrum energy analyzer. Practically all evaluations are referred to charged models because for uncharged models the estimated collection efficiencies were below 0.1% in the domain of $Re_c$ used. Also, the applied technique of photographing the deposits on five different sites around the cylinder did not enable to obtain statistically significant results in case of uncharged cylinders. One series with a systematic investigation of particles deposited on two uncharged glass cylinders (3.63 mm in diameter) which were hydrodynamically interacting was made, however, with a long exposure time (5 min.).

The cylinders were attached in a horizontal position to the rod, which was used for the exposure of planar models, and exposed for 2 minutes at flow speed of 1 m $s^{-1}$ in the central part of the tunnel's test section to the smoke. The number of deposited particles in the size ranges $d_p$ smaller than 0.35; 0.70; 1.05; 1.40; 1.75; 2.10; 2.45 and 2.80 μm were evaluated from the scanning electron microscope photographs. Usually, five pictures (magnification 1000 x) around the half circumference of the cylinder were taken and the assumption was made that the aerosol is continuously distributed around the cylinder and that the deposit is symmetrical with respect to the horizontal plane. In the case of cylinders with diameters larger than 3.0 mm several more pictures were taken. However, the system of taking the photographs at angles 0°, 45°, 90°, 135° and 180° with reference to the direction of the undisturbed airflow was maintained.

Smoke particle deposition on charged metallic cylinders (brass cylinders with diameters from 0.051 cm to 0.3937 cm) which were permanently connected with the generator supplying voltages between 1.0 kV and 8.0 kV can be summarized in the following way: the collection efficiency of a brass cylinder 0.2362 cm in

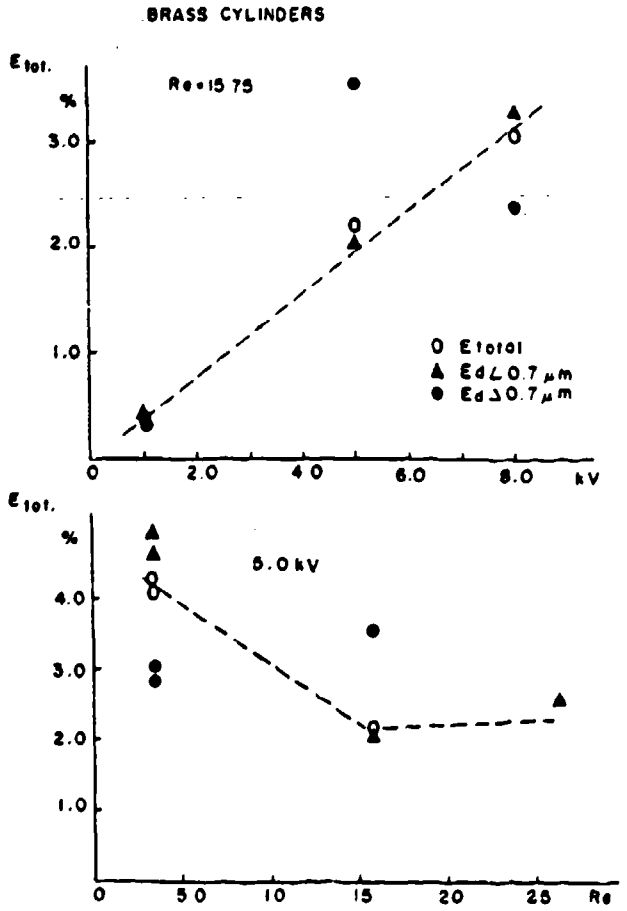


Fig. 36 Total collection efficiency, E, of a brass cylinder at $Re_c$ = 15.75 and V = 1.0 m $s^{-1}$ as a function of electric "charge" (upper figure). Total collection efficiency, E, as a function of $Re_c$ for constant "charge" of 5.0 kV and smoke particles smaller and larger than 0.7 µm.

diameter for $TiCl_4$ aerosol with parameters described in paragraph 3.2-2, increased with increasing electric charge (Fig. 36). This dependence was linear for particles with $d_p$ < 0.7 µm. Considerable deviations were found for large particles ($d_p$ > 0.7 µm). In the lower diagram in Fig. 36 is represented the collection efficiency of the same brass cylinder ("charged" to 5 kV) in dependence on the $Re_c$ of the cylinder. For small particles there is a decrease in collection efficiency from a value of more than 4.0 for (Re = 3.4) to 2.5 (for Re = 3.40). Large particles are again deviating from this rule. That can be explained by a statistical error of particle counting. Usually several hundred of particles were counted on the five photographs taken around the cylinder's circumference in comparison to only several tens of large particles. In spite of these uncertainties some specific

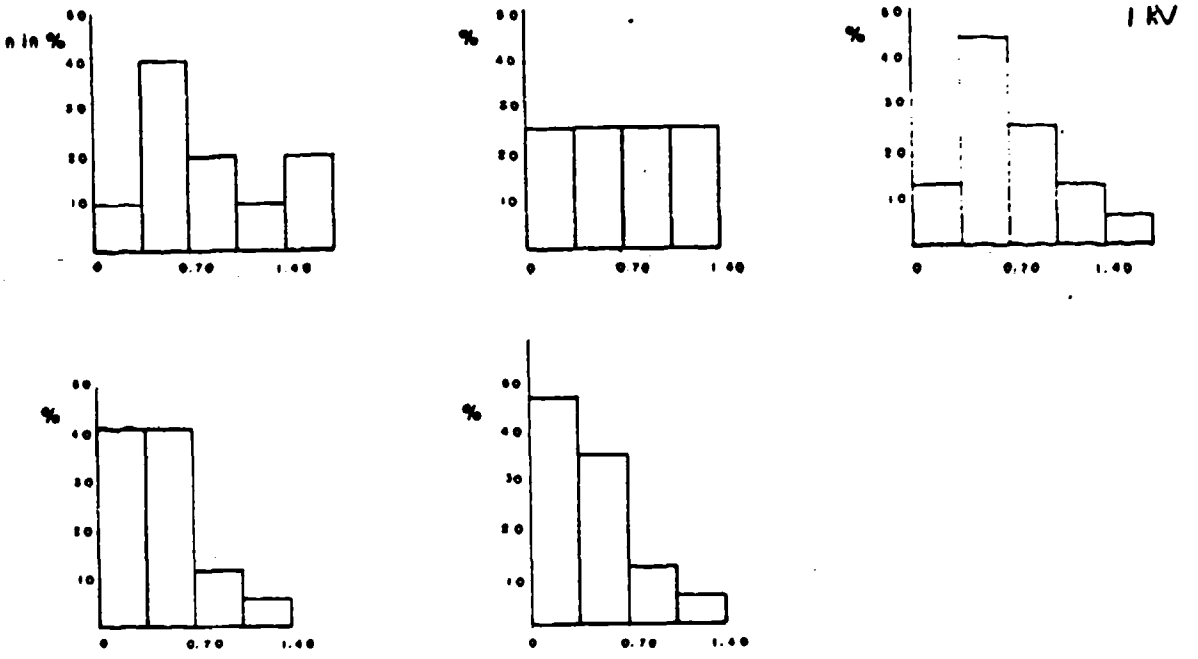


Fig. 37 Deposition of $TiCl_4$ particles, ($R_p$) around a brass cylinder ($R_c$ = 0.118 cm, $Re_c$ = 15.75). Pictures were taken at 0°, 45°, 90°, 135°, and 180° angles. Cylinder "charge" 1 kV.

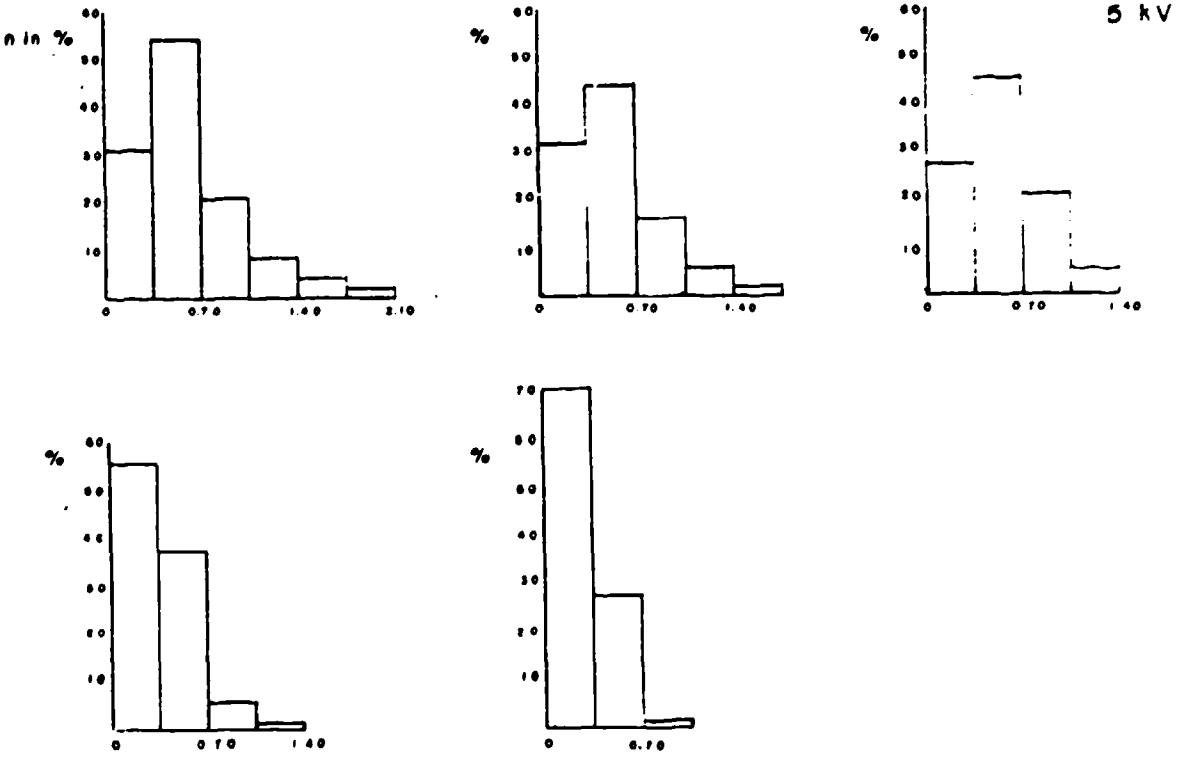


Fig. 38 Deposition of $TiCl_4$ particles, ($R_p$), around a brass cylinder ($R_c$ = 0.118 cm, $Re_c$ = 15.75). Pictures were taken at 0°, 45°, 90°, 135°, and 180° angles. Cylinder "charge" 5 kV.

features of the particles deposited on the brass cylinder 0.236 cm in diameter "charged" to different potentials can be found. The front surface at 1 kV around the stagnation point is characterized by a high deposition of particles with diameters $d_p$ > 1.05 μm (Fig. 37) and low concentration of very small particulates. Just the opposite situation is found on the back of the cylinder. The samples taken at the "charge" of 5 kV and 8 kV strongly accentuate this dependence (Figs. 38 and 39). 98% of all

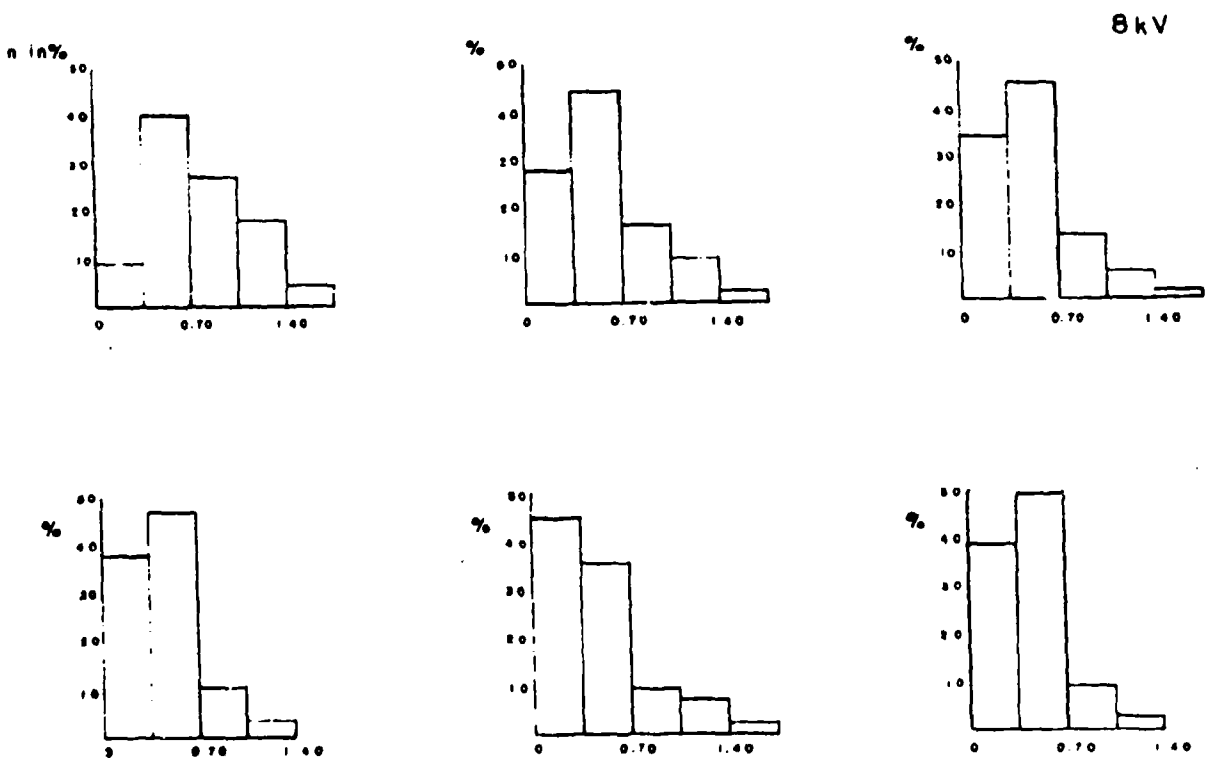


Fig. 39 Deposition of $TiCl_4$ particles, ($R_p$), around a brass cylinder ($R_c$ = 0.118 cm, $Re_c$ = 15.75). Pictures were taken at 0°, 45°, 90°, 135°, 180°, and 315° angles. Cylinder "charge" 8 kV.

particulates which deposited at 5 kV around the back stagnation point (and 81% at 8 kV) have diameters $d_p < 0.7$ μm. There is, however, an indication that at a very high "charge" (8 kV) the deposition of very large particulates ($d_p > 1.40$ μm) is increasing. At the extreme tangential points of a cylinder with the flowfield in all evaluated seven cases there was a dominating peak (around 45% of all particulates) corresponding to the particle size $0.35 < d_p < 0.70$ μm.

The data will be completed by more measurements in the domain of low "charges" and will include also the systematic measurements with dielectric cylinders. With the data now available, one can only make some qualitative estimates and speculate about the relationship to several models describing the particle deposition on charged cylinders (e.g., Zebel, 1956). However, the effect seems to be significant although less important if compared with charged disks. The most spectacular is the interaction of inertial and electrical forces in particle deposition on the front and back side of the cylinder.

Several measurements have been made with <u>dielectric charged cylinders</u> (glass tube, $d_c$ = 0.359 cm; glass rod, $d_c$ = 0.315 cm; ceramic rod, $d_c$ = 0.396 cm; plastic rod-PVC, $d_c$ = 0.660 cm and plastic rod-unknown composition but contaminated with Ti containing substances, $d_c$ = 0.318 cm). The results of these few measurements are contained in Table I.

TABLE I

| Material | $d_c$ [cm] | Re | $E_{tot}$ [%] | $E_d$<0.7 m | $E_d$>0.7 m |
|---|---|---|---|---|---|
| Glass tube | 0.359 | 23.93 | 2.567 | 2.372 | 3.442 |
| Glass rod | 0.315 | 21.00 | 3.878 | 4.448 | 1.870 |
| Ceramic rod | 0.396 | 46.40 | 5.628 | 6.176 | 3.552 |
| Plastic rod-PVC | 0.660 | 44.00 | 9.202 | 8.430 | 11.817 |
| Plastic rod-white | 0.318 | 21.20 | 5.590 | 9.003 | 0.867 |

As was mentioned earlier, the results of the deposition measurement on the plastic white rods are rather questionable due to the Ti contamination. Because all cylinders were exposed in 1 m $s^{-1}$ aerosol flow and "charged" with 5 kV the collection efficiencies, E(%), can be compared. The maximal efficiency showed PVC rod, in spite of its lowest Stokes number. Small and large $TiCl_4$ particles were collected well especially on the microscopical unevenesses and hair-like structure of its surface. The same effect one observed on the ceramic rod, where many of the smoke spherical particles were deposited among the microscopical grains on the rod surface. Apparently an induced charge effect on the uneven surface plays an important role in particle scavenging. The number of deposited particles on glass tube and rod did override slightly the efficiency of a brass cylinder (for 5 kV and $d_c$ = 0.394 cm it was E = 2.364). Few measurements do not permit to explain the difference between the collection efficiency of a glass rod ($E_{tot}$ = 3.878%) and glass tube ($E_{tct}$ = 2.567%) with almost the same diameter.

3.2-7 Deposition of Smoke Particles on Grids.

The deposition of micron and submicron smoke particles on mesh type models and fine fibers has been suggested in our previous report (Podzimek, 1981). Ultrafine particles might be scavenged in this way very effectively due to the large surface exposed to Brownian diffusion and larger particles by inertial deposition due to the high Stokes number if the scavengers would fall sufficiently fast. In the domain of Greenfield gap ($0.2 < d_p < 1.0$ μm) where most of $TiCl_4$ particles exist, the potentially most effective mechanism seems to be the deposition in electrostatic fields. Therefore several pilot experiments have been performed with charged metallic scavengers (electron-microscopical grids, mesh 300, diameter of 0.3 cm and thickness of 0.00127 cm) which were exposed to 1 m $s^{-1}$ aerosol flow in the wind tunnel. The disk's main plane was perpendicular to the airflow and its charge was selected from 1 to 8 kV.

In Figs. 40 and 41 are plotted some preliminary results of particle counting on the rim (wider ring around the grid. The numbers correspond to the counted particles of a specific size in one photograph the surface of which corresponds to an area of the grid's rim of 92.1 x 67.7 μm. Position 1 is the outer, and 4 or 5 the inner edge of the rim. The evaluation was performed only for the frontal side of the grid. For 1 kV charge there is a high deposit on the outer edge of the rim where 43 individual particles with $d_p < 0.7$ μm were found in picture No. 1. However, in Fig. 40 were not plotted the particles forming chains perpendicularly oriented towards the surface along the edge. A rough estimate of the number of particulates in these chain-like aggregates reveals that they are composed of more than 137 particles whereas in the five pictures across the grid's rim were found 107 particles. Due to the electrostatic field around and inside the grid with respect to the grounded shielding at the wall, not many aggregates are found on the inner edge of the rim and on the grid inside. Similar picture of deposited particles was found for 5 kV (Fig. 41) with the only difference that the aggregates found at the outer edge were numerous, however, shorter if compared to those at

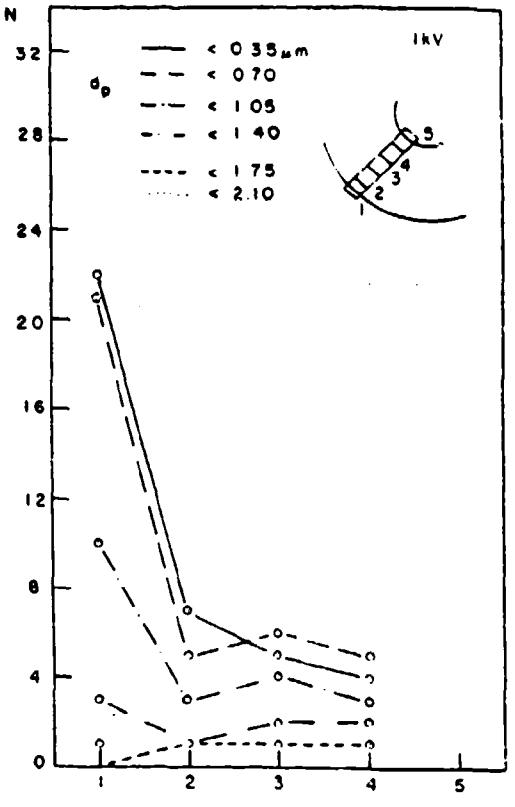


Fig. 40 Number of deposited smoke particles across the rim of an ELM grid charged to 1 kV.

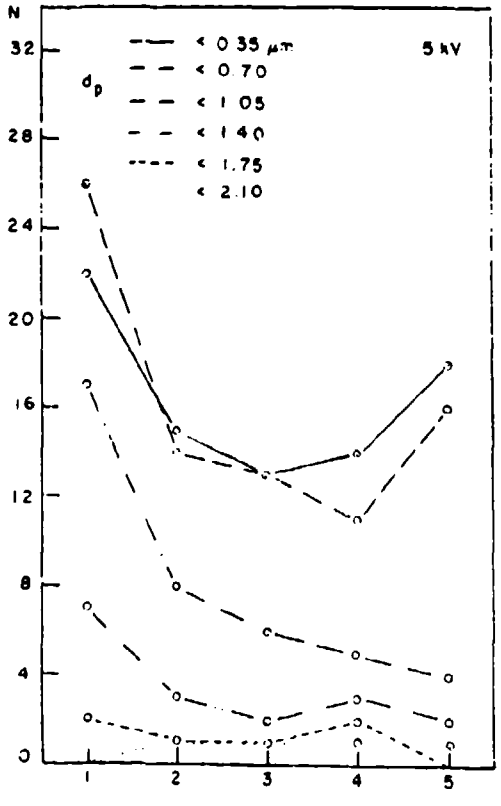


Fig. 41 Number of deposited smoke particles across the rim of an ELM grid charged to 5 kV.

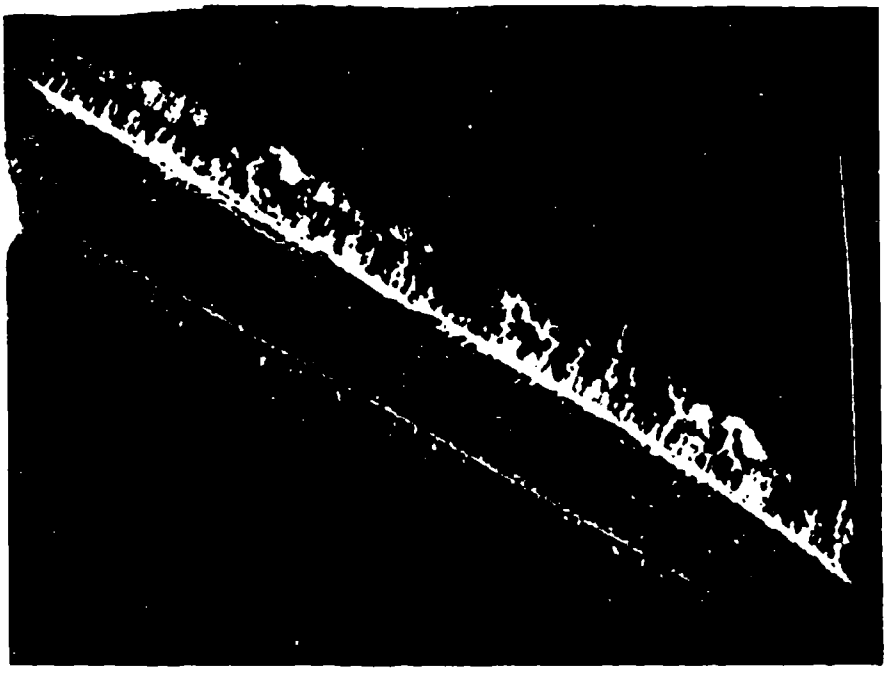

Fig. 42 Deposited $TiCl_4$ particles at the edge of an ELM grid "charged" with 5 kV (Magn. 1000 x).

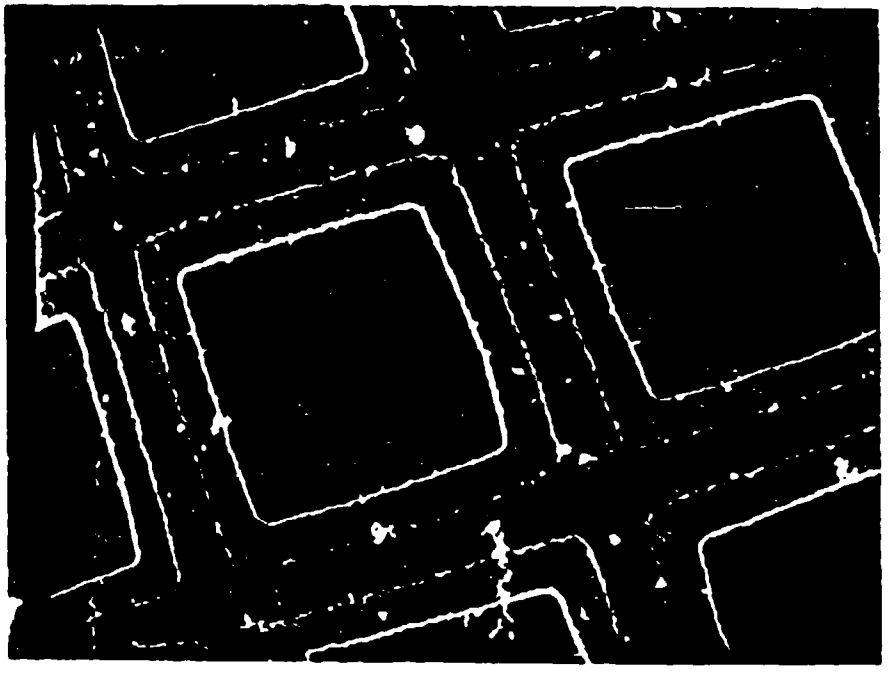

Fig. 43 Deposited $TiCl_4$ particles and aggregates on the ELM grid "charged" with 5 kV (Magn. 500 x).

1 kV (Fig. 42). More little aggregates were also found along the inner edge of the rim in comparison to the sample of 1 kV (Fig. 43).

An attempt was made to calculate the scavenging efficiency of a grid type model using the same procedure as described in paragraph 3.2-4 and 3.2-5 except the reference cross-section of the grid. That was obtained by subtracting from the circle's area (with $\pi R^2 = 0.0707\ cm^2$) the "empty" ventilated area (approximately $0.0451\ cm^2$). The total collection efficiency of a grid charged to 1 kV was 5.21% for smoke particles with $d_p < 0.7\ \mu m$, 1.97% for $0.7 < d_p < 1.40\ \mu m$ and 0.41% for $1.40 < d_p < 2.10\ \mu m$. For the same particle size ranges and for a "charge" of 5 kV the efficiencies were 5.64%, 2.83% and 1.18%. Compared to the values of E for a charged dielectric disk (5 kV) with $R_c = 0.225$ cm (Fig. 26), one finds the collection efficiency of the grid charged to 5 kV very alike if very small particles are considered. For particles with $d_p > 0.7\ \mu m$ the collection efficiency of a charged grid (5 kV) is lower that of a charged disk. A potential difference of 1 kV makes the collection efficiency of a grid superior to that of a dielectric disk. This opens a new avenue of research with the final goal to find grid type scavengers (made of cheaper material than ELM grids) which could be easily charged and bear the electric charge for sufficiently long time.

# 4. POTENTIAL EFFECT OF THE FALLING SCAVENGER ZONE

## 4.1 Effect on the Smoke Cloud Dynamics.

The effect of falling scavengers on the smoke cloud is explained by the drag exerted by the scavengers on the air with smoke particles. This drag, which many authors consider as equivalent to the scavenger weight, creates an air motion inside of the smoke cloud, which affects like a feedback the scavenger settling and smoke particle deposition. Most of our thoughts on this line are based on several articles and reports published mainly in cloud physics literature (e.g., Clark and List, 1971; List and Clark, 1973; Girard and List, 1974; Girard and List, 1975).

The "first approach" system of equations can be based on the following assumptions and scenario of a model experiment:
a) A homogeneous and monodisperse smoke cloud is confined to a space of 1200 x 1200 x 200 $m^3$ with a "frictionless wall" on the top and at the side (Fig. 44). Smoke particles are assumed to

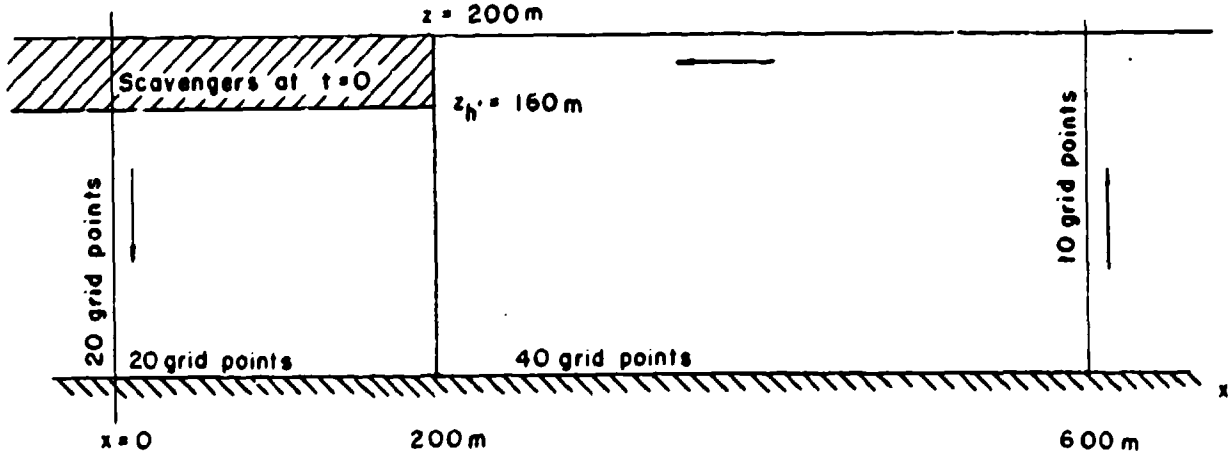


Fig. 44 Scheme for the modeling of falling scavenger zone effect.

travel with the air due to their small size ($d_p$ = 0.6 μm; $\rho_p$ = 1.0 g $cm^{-3}$, or $\rho_p$ = 2.0 g $cm^{-3}$). As pilot study a two-dimensional model with 1200 grid points seems to be very useful.

b) Above the 200 m high smoke layer is temperature inversion. $\frac{dT}{dz}$ = - 10°C/100 m or -0.6°C/100 m in the smoke layer prevails.

c) Planar scavengers are assumed to be of the same size and mass and will be released in a uniform way just above the smoke layer and will settle in quiescent atmosphere (no horizontal wind). The main parameters of some paper scavengers selected from our previous experiments are presented in Table II.

TABLE II

| Type of Scavenger | Material | Diameter [cm] | Thickness [cm] | Cross Section [$cm^2$] | Mass [g] | Settling Velocity [$cms^{-1}$] | $C_D$ | Re |
|---|---|---|---|---|---|---|---|---|
| disk | paper | 0.86 | 0.018 | 0.584 | 0.0056 | 125.0 | 0.950 | 672 |
| disk | paper | 1.90 | 0.018 | 2.840 | 0.0286 | 134.0 | 0.876 | 1,612 |
| square | paper | 0.90 | 0.018 | 0.810 | 0.0082 | 131.0 | 0.915 | 736 |
| square | paper | 1.40 | 0.018 | 1.960 | 0.0193 | 132.0 | 0.896 | 1,475 |
| hexagon | paper | 0.87 | 0.018 | 0.583 | 0.0054 | 129.0 | 0.922 | 723 |
| hexagon | paper | 1.72 | 0.018 | 2.750 | 0.0277 | 130.0 | 0.923 | 1,410 |

Selecting the first type of scavenger (paper disk with $d_c$ = 0.86 cm), one would assume the scavenger mixing ratios e.g., $q_1$ = 0.01; $q_2$ = 0.03; $q_3$ = 0.07; and; $q^4$ = 0.15, what corresponds to the scavenger concentration 1.786 scav/1 g air, 5.357 scav/1 g air, 12.500 scav/1 g air, and 26.786 scav/1 g air (1 g air ≅ 0.773 liter). For different types of scavengers in Table II were calculated from a simple momentum equation the relaxation times to show after what time the released scavengers will resume a steady settling velocity, $V_{CT}$. One can assume that all of the mentioned models will settle in 1 second at a velocity within 0.95 $V_{CT}$ and $V_{CT}$ if the scavengers will not intereact hydronamically.

d) The basic system of equations have to include the momentum equation which for the case of constant mixing ratio of smoke mass and scavenger mass can be expressed in accordance with Girard and

List (1975) in the form

$$\frac{\partial \vec{V}}{\partial t} + \nabla \cdot \vec{V}\vec{v} = - \rho_o \nabla P - g(B - \rho_{cp}) + \nabla \cdot \mu_t \nabla \vec{V} \quad . \quad (11)$$

$\vec{v}$ is the velocity vector, $\vec{V}$ is the momentum vector (e.g., $\rho_o \vec{v}$); $\rho_o$ is the air density in the isentropic base state (with the potential temperature $\theta_o$ = const.); $P = p'/\rho_o$, with $p'$ the pressure deviation of the perturbed state; $B = \rho_o \theta_v'/\theta_o$, with $\theta_v'$ the virtued potential temperature deviation; $\rho_{cp} = \rho_{ac} + \rho_{ap}$, is the total density of scavengers, $\rho_{ac}$, and of smoke particles, $\rho_{ap}$, expressed as [g/cm$^3$ air]; $\mu_t$ is the dynamic eddy viscosity featuring the main state of the turbulent atmosphere ($\mu_t = C^2 \Delta^2 \cdot |Def|^{1/2}$; $0.2 < c < 0.4$; $\Delta$ = grid interval; $|Def|$ is the momentum deformation tensor.

The thermodynamic equation can be simplified in comparison with Girard and List (1975) model which is considering the phase transition of water. Therefore, assuming no physico-chemical intereactions between smoke and scavenger, an isentropic basic state, the entropy transport equation may be written as

$$\frac{\partial s}{\partial t} + \nabla \cdot s\vec{v} = \nabla \cdot (K_s \nabla s) \quad . \quad (12)$$

$s = B + \alpha \rho_{ap}$ with $\alpha$ being a factor describing the heat released or absorbed per unit smoke particle density in the air and temperature. The eddy entropy exchange coefficient, $K_s$, is assumed to be proportional to $\mu_t$.

The transport equation for smoke and scavenger substance is based on the following equation for smoke particles

$$\frac{\partial \rho_{ap}}{\partial t} + \nabla \cdot \rho_{ap} \vec{v} = \nabla \cdot K_{ap} \nabla \rho_{ap} + K(R_c, R_p) \frac{\rho_{ap}}{m_p} \frac{\rho_{ac}}{m_c} \quad (13)$$

In eq. (13) $m_p$, $\rho_{ap}$, are the mass and the density of a smoke particle in the air, $m_c$ is the mass of a scavenger and $K_{ap}$ is a turbulent exchange coefficient for the smoke particles in the air. It is further assumed that the smoke particles are moving with the air, are not evaporating, and their deposition on the ground is

not influenced by the substrate. The scavenging term is not included in any of the previous studies of falling precipitation zones and requires a more detailed analysis: the simple form of the collection kernel $K(R_c, R_p)$ is

$$K(R_c,R_p) = E\pi (R_c + R_p)^2 (V_{\infty c} - V_{\infty p}) \qquad (14)$$

if the smoke aerosol is monodisperse and all scavengers of the same size. The collection kernel will resume, however, a very complicated form if the side wind will affect the motion of a scavenger.

For the scavengers one assumes that scavengers do not interact among themselves. Their position in space, $\vec{r}$, and their mass per unit volume, $M_c$ are changing according to the equations

$$\frac{D\vec{r}}{Dt} = \vec{v}(\vec{r},t) - \vec{w}_c \ , \qquad (15)$$

$$\frac{DM_c}{Dt} = \frac{D(N_c m_c)}{Dt} (\vec{r},t) \ . \qquad (16)$$

$\frac{D}{Dt}$ is the substantial derivative, $\vec{v}$ is the vector of the flow field, $\vec{w}_c$ represents the settling scavenger velocity vector, $N_c$, is the total number of scavengers per unit volume of air and $m_c$ is the changing mass of the collector. The basic assumption is that the initial position, $\vec{r}_o$, and the mass $M_{co} = N_{co} m_o$ are known at the time $t_o$.

The last equation which completes the system of equations (11) to (16) is the continuity equation

$$\nabla \cdot \vec{V} = 0 \ . \qquad (17)$$

Following the suggestion by Girard and List (1975), (17) is for numerical solution replaced by a combination of eq. (11) and (17)-special type of Poisson equation

$$\nabla \cdot \rho_o \Delta P = -g\frac{\partial}{\partial z}(B-\rho_{cp}) + \nabla \cdot [-\nabla \cdot \vec{V}\vec{v} + \nabla \cdot \mu_t \nabla \vec{V}] \ . \qquad (18)$$

Numerical solution to the system of equations (11) to (18) for a two-dimensional case is discussed in detail by Girard and List (1975) and by Clark and List (1971) for a simplified model. There are, however, two basic differences in the suggested model: our model includes the coagulation term in eq. (13) which affects all equations of the mixed Lagrangean-Eulerian system. On the other hand, it does not include the evaporation-condensation terms of the Girard-List model.

e) Several parameters in the system of equations will require a special investigation such as the turbulent exchange coefficients. The kinematic eddy viscosity of 500 $m^2$ $sec^{-1}$ would be a suitable value for starting the study of its relationship to the eddy entropy exchange coefficient, $K_s$, and to the smoke particle turbulent exchange coefficient, $K_{ap}$. An open question remains the turbulent dispersion of the settling scavengers. Girard and List (1975) assume for instance a smooth settling path of drops of 0.78 mm radius. However, this assumption must not be necessarily valid for non-spherical scavengers, such as disks, which are much more sensitive to turbulent flow fluctuation. Also, largely unknown is the interaction of smoke particulates in the down draft with the substrate of a specific roughness and the potential re-entrainment of particulates once deposited on the ground.

## 4.2 Estimates of the Potential Effects of the Falling Scavenger Zone on the Scavenging of Smoke Particulates.

Because of the limited time available for the whole program and lack of financial sypport of the expensive program of a numerical solution to the sustem of equations in paragraph 4.1, only an estimate of the potential effect of the falling scavenger zone was attempted. For this aim the available articles, mainly by Clark and List (1971) and Girard and List (1975), were used. The main difference between the Clark-List and Girard-List two-dimensional models is the neglection of the complex thermodynamic process, as has been described earlier in the Girard-List model, and substituting the corresponding equations by the conservation of energy equation

$$\frac{\partial}{\partial t} \iint [\tfrac{1}{2}(u^2+w^2) + gqz]dxdz = -\iint gqV_c \, dxdt -$$

$$-\nu_t \iint [(\frac{\partial u}{\partial x})^2 + (\frac{\partial u}{\partial z})^2 + (\frac{\partial w}{\partial x})^2 + (\frac{\partial w}{\partial z})^2] \, dxdz \, . \qquad (19)$$

q is the mixing ratio of smoke particles and scavengers in dry air [kg/kg] and $\nu_t$ the air kinematic viscosity in the energy dissipation term.

In spite of different geometry of their two-dimensional model (40 km x 10 km, collectors confined to 3 km x 3 km space were released at 8 km altitude) and dimensions of the spherical scavengers (e.g. $R_c$ = 0.078 cm with $V_c \cong 6$ m $s^{-1}$), several important conclusions are made.

From the study by Clark and List (1971) one learns that the convective velocity of the scavenger zone (equal to the excess of the observed air velocity over the scavenger terminal velocity) depends not only on scavenger loading (mixing ratio) but also on the terminal velocity of scavengers. The importance of loading decreases with increasing scavenger velocity. The difference in convective velocity surpasses 1 m $s^{-1}$ for q = 0.01 and q = 0.08

and $V_c = 4\ m\ s^{-1}$. For $V_c = 1.5\ m\ s^{-1}$ the convective velocity difference for q = 0.01 and q = 0.03 is comparable with the scavenger settling velocity. The internal circulation in the falling zone redistributes the scavengers in such a way that for times larger than 200 sec (not applicable to our case) a double minimum in the horizontal profile of the air's vertical velocity forms. At the same time the horizontal advection of the falling scavengers affects the scavenger distribution and leads, after a long time to the scavenger deficiency near the axis of symmetry. Girard and List (1975) found a very interesting coupling between the positions of the updraft centers and warm air regions (amplitude of the centers are out of phase).

In conclusion, it seems that the investigation of falling scavenger zone is a very important subject which might change considerably the calculated and measured collection efficiency of scavengers. Due to the relatively low altitude (200 m) of the smoke layer, the scavenger dispersion will not be very significant, and for the same reason, the thermodynamic effect can be probably neglected.

## 5. DISCUSSION OF THE RESULTS

Theoretical studies concentrated mainly on the following points: are the planar scavengers (collectors) more efficient than the spherical collectors if the same mixing ratio (g or kg of collectors per 1 g or 1 kg of air) is taken as a basis for the comparison? What is the mean total collision efficiency of neutral thin oblate spheroids colliding with neutral aerosol particles in dependence of particle size and Reynolds number, $Re_c$ (referred to oblate spheroid)? What is the mean total collision efficiency of a charged planar collector with a charged aerosol particle?

The first question is answered positively in this report and documented in a special article by Martin and Podzimek (1982). In the latter work was also shown that the Brownian diffusion dominates the capture of smoke particles with $R_p \leq 0.01$ μm and the inertial deposition prevails at $R_p \geq 0.1$ μm. The oblate spheroid has an axis ratio of 0.05 and $Re_c$ ranging from 0.1 to 50.0. Fig. 1 clearly demonstrates how for the same $Re_c$ (referred or to the main semi-axis of a prolate ellipsoid or to the radius of a sphere) and uniform aerosol ($R_p$ = 0.6 μm and $\rho_p$ = 0.95 g $cm^{-3}$) the deposition on planar scavenger dominates. However, for a specific $K^* = \pi R^2_c V_\infty$ (the geometric volume swept out per unit time) the ratio will reverse. These findings are supported by many field observations (e.g., Itagaki and Koenuma, 1962; Podzimek, 1965; Carnuth, 1967; Reiter and Carnuth, 1969; Podzimek, 1970; Magono, et al., 1974; Magono, et al., 1975; Graedel and Francy, 1975) and by laboratory studies (e.g., Sood and Jackson, 1969; Sasyo 1971; Knutson, et al., 1976; Yue and Podzimek, 1976; Prodi, 1976).

The mean values of the collision efficiencies plotted in Fig. 2 represent only the contribution of the smoke particles transported about an oblate spheroid ($\Lambda_c$ = 0.05) under the influence of outer forces and at the given geometry of particle interaction. The model includes the field on both sides of the scavenger. The collision efficiency curves are featured by a competetion between the settling rate of the oblate spheroid, its hydrodynamic effect and the smoke particle size. This leads to a

saddle shape of the collision efficiency line for $Re_c > 10$. The steep increase of the collision efficiency for the small particle sizes in the Greenfield gap ($0.1 < R_p < 0.5$ μm) is caused mainly by phoretical forces which are surpassed by inertial forces for $R_p > 2.0$ μm. One cannot compare this dependence with the "classical" diagram of theoretical collision efficiencies calculated for a micron-size droplet colliding with a spherical collector (e.g., Pruppacher and Klett, 1980, p. 481). For the purpose of this study-scavenging of smoke particulates with median sizes between 0.4 and 1.5 μm - essential is the fact that planar scavengers are attaining the high collision efficiency (saddle of the curve) in this size range.

There are, however, several important problems which have to be studied before one could be satisfied with the existing numerical models for the determination of collision and collection efficiencies of planar models. One of them was successfully investigated in this study: the effect of smoke particle density on the collision efficiency of a planar collector with a tiny spherical particle (Fig. 4). This effect, which is the result of particle inertia and flow field about the collector, can represent an increase in collision efficiency of 28% if one compares the particle ($R_p = 0.3$ μm) with a density of $\rho_1 = 1.20$ g cm$^{-3}$ with another particle of $\rho_2 = 0.95$ g cm$^{-3}$ and considers an oblate spheroid with $A_c = 0.05$ and $R_c = 50.6$ μm. This result supports and extends the earlier study by Martin, et al. (1980). Another important problem seems to be the improvement of the current procedures for calculating the collision efficiencies, which are based on several not sufficiently investigated assumptions. Among them belong the use of the ventilation coefficient, the superposition scheme in calculating the total effect of different outer forces on the particle deposition and the very general question of the justification of the use of particle continuity equation--discussed partly by Volschuk (1971)--for the particle impaction and removal. Finally, applicability of creeping flow equation for $Re_c > 10$ should be investigated.

The electric charge effect was investigated under the

assumption that only Coulomb type forces are effective between collector and smoke particle. In Fig. 27 the calculated collision efficiency curve is plotted for an oblate spheroid with $A_c = 0.05$ and $Re_c = 50$ bearing an electric charge of 2.0 esu $cm^{-2}$ colliding with aerosol particles charged with one elementary charge. The collision efficiencies are several times higher if compared to neutral particles and--in the range of particles with $R_p = 0.1$ μm--the difference makes almost one order of magnitude. There are no theoretical studies in the literature which would deal with a model similar to that presented in this study except those which were published in co-authorship of investigators participating in this project (Martin, et al., 1981; Martin and Podzimek, 1982). Due to the lack of comparison with other investigations one can conclude that--based on this study--the electric charge will be one of the dominating parameters in smoke particle scavenging by planar collectors if one will be able to put a high charge on the collector and maintain it for sufficiently long time.

Experimental investigation of the planar-scavenger motion focussed in this study on the comparison of the data on oscillatory motion of planar bodies in liquids and in the air, on the parameters featuring the fall of paper planar models in the air and on the hydrodynamic intereaction of several planar scavengers falling close to each other. The detailed evaluation of all the measurements with falling paper models in the air complete the previous study by Podzimek (1981). This study stresses the original conclusion about the comparability of observations made in liquids and in the air, provided that the corresponding $Re_c$ will not surpass 700 (Podzimek, 1982; Podzimek and Martin, 1982) and that the main parameters of similarity (Re,Be) are the same. The obtained settling velocities e.g., for disk are in good agreement with Schiller (1932), Willmarth, et al. (1964), Podzimek (1969), Jayaweera and Cottis (1969), List and Schemenauer (1971). Beyond the value of Re = 700, when the disks start to oscillate markably, it is impossible to use any measurements in liquids for an observation in the air.

In this study was related the amplitude and frequency of the

oscillating paper disks to Reynolds numbers ($Re_c$) and Wilmarth's stability numbers (I). Below $Re_c$ = 1500 the amplitude of the disk's motion moderately increased and the frequency of the disk's swinging decreased with increasing $Re_c$ (Fig. 7). For $Re_c$ > 1500 the same dependence was markably magnified. A similar picture was obtained for the relationship between the amplitude and frequency of the disk's oscillatory motion in the air and the Wilmarth's stability number. In a perfect analogy to the $Re_c$ = 1500 we found that at I > 0.005 starts the dramatic change in the investigated relationship. These results are not in disagreement with a recently published study on the motion of free falling ellipsoides (Stewart and List, 1980). With regard to the relatively insignificant increase of collection efficiency by swinging disk-like scavengers and the optimum scavenger size between 2 mm and 10 mm, one will try rather to seek other means of effective scavenging than enhancing the oscillatory motion of a scavenger (electric charge, grid type models, etc.).

The hydrodynamic interaction of several scavengers released simultaneously was limited to the analysis of 15 pairs of planar scavengers released simultaneously and photographed at stroboscopic illumination (Podzimek, 1981). Some of the important conclusions are: symmetrical scavengers (disks, squares, hexagons, stars) of the same size start to interact hydrodynamically on a distance less than three diameters (for 1500 < $Re_c$ < 3700) if one of the scavengers is in the wake of its precursor, and on a distance less than one diameter if the scavenger is at the side of the other. The effect of this interaction is the amplification of the swinging motion, and usually, the change of the direction of the mean trajectory of just touching scavengers of several degrees. From the 15 evaluated pairs of settling scavengers it was hard to establish a picture of a general validity because of the large scatter of data. This observation does not support the hypothesis pronounced earlier (Podzimek, 1969) that planar models of the same size can interact during their fall and form a stable configuration. Similar aggregates of the planar models (disks, hexagons) formed

only in liquids and usually the stable "butterfly" aggregates were observed on unequal plates (Podzimek, 1965).

The experimental study of the smoke particle deposition on disks in the wind tunnel was featured by a better stability of $TiCl_4$ aerosol parameters (not changing considerably almost for 30 min.), by a good control of electrical properties of the aerosol and scavengers and an improved evaluation in an optical and SELM microscope if compared with the technique described in the previous report (Podzimek, 1981). Deposition on stationary disk models at airflow velocities of 0.25 m $s^{-1}$ or 1.0 m $s^{-1}$ and $Re_c$ between 80 and 320 showed that in mean the total collection efficiencies of disks ($A_c$ = 0.05, $R_c$ = 2.25 to 2.50 mm) for the smoke aerosol ($R_p$ = 0.3 μm) ranged from 0.70 to 1.20%. Higher collection efficiencies were found in mean on plexiglass models, lower values featured glass and metallic models. The deposition of small particulates ($R_p$ < 0.35 μm) on the back side of the models overrides or is comparable with the deposition on the front side [$(\overline{N_{ob}/N_{rev}})$ = 0.986 with a standard deviation of 0.1351. The peak in particle number curve close to the rim of the front side is shifted towards the center on the back side. Often a secondary maximum in the particle distribution curve on the back side was observed in agreement with the earlier findings (Podzimek, 1970). Particles with $R_p$ > 0.35 μm are collected more on the disk's front side due to their greater inertial mass. This pattern of deposited particles is rather insensitive to the increase of $Re_c$ from 80 to 320.

Swinging models were investigated at 10 Hz and 60 Hz frequencies and at the amplitude of ± 10°. Several trials were made with models oscillating around the mean angle of attack of 10° or 20°. Most of the experiments done at $Re_c$ 80 or 320 with dielectric disks showed that on the front side is lower particle deposition in comparison to the back side. From the evaluation of 5 sets of measurements the ratio of $(\overline{N_{ob}/N_{rev}})$ = 0.846 with a standard deviation of 0.065 for small particulates. There is a noticeable effect of the higher frequency on this mean ratio. It decreased from 0.913 for 10 Hz to 0.745 for 60 Hz. Figure 25

shows also the markable difference in particle deposition on the front and back (reverse) side. The more uniform and high deposition on the back side contributes mainly to the higher scavenging (collection) efficiency of the oscillating disks if compared to the stationary scavengers. For a glass disk 4.5 mm in diameter the mean total collection efficiency, E, was slightly over 0.7% for quiescent models, 1.09% for scavengers oscillating at 10 Hz and 1.42% for 60 Hz.

The electric charge effect was studied with disk cylinder and grid type models. Models of scavengers were made of electric conductive and dielectric materials and most of the experiments with disks (Fig. 27) have been done at a flow speed of 1.0 m $s^{-1}$ and charging electrode permanently connected with the model. The charge imparted to the scavenger was high and corresponded to the potential difference of 1; 2; 5 and 8 kV referred to the grounded brass sheet around the tunnel wall. To the potential difference of 1 kV (5 kV) corresponds to a charge of 0.568 esu (2.863 esu) on the glass disk of 4.5 mm in diameter.

Mean collection efficiency of glass disks, on which particles with $R_p < 0.7$ μm were deposited, was 2.69 for 1 kV potential difference, 5.45 for 2 kV and 9.53 for 5 kV. These values represent a mean of four individual measurements at least. They are much higher than for neutral scavengers and are comparable with the calculated collision efficiencies of a charged spheroid with an aerosol particle bearing one elementary charge. The model, however, is based on several idealized assumptions, such as the constant charge of the scavenger and coulombic force between a charged particle and a collector. Other forces, such as electrical image force between a charged particle and neutral collector (and vice versa), the influence of an outer uniform electric field and the electric dipole interaction force between neutral particles, both being polarized in a uniform external field, are not considered yet. A systematic measurement in the near future will include also the measurement of electric charges on individual particles. The assumption of one elementary charge on each particle which passes through a neutralizer is probably

unrealistic. A simple model of particle charging in a bipolar atmosphere (e.g. Keefe et al., 1959) assumes that 13.3% of the aerosol with $R_p$ = 0.5 µm will be neutral, 25.3% will bear one elementary charge (e), 21.4% will have 2e, 16.2% 3e and 10.9% 4e etc. Future research should include some of the mentioned processes discussed in detail by Kraemer and Johnstone (1955), Zebel (1965, 1969), Davies (1973) and Nielsen and Hill (1976a, 1976b).

This research calls attention to the particle depositoin at the charged disk's rim which, especially for rough surfaces, represents an extremely effective scavenging site. There is some evidence that long chain aggregates of smoke particles form preferentially at 1 kV and 8 kV, while at 5 kV (on a glass disk) were observed many, but shorter aggregates. The analysis and explanation of the bizarre structure of the chain-like aggregates (large sphere connected with another by a tiny spherical particle) and the task to control the aggregate formation represent one of the most challenging fields of this investigation. Most of the aggregates are formed at the rim and on the front side of a charged scavenger, while the majority of particles smaller than 0.7 µm is deposited on the back side (Fig. 29).

Cylindrical models have been electrically "charged" to the same potential differences like the disks. The collection efficiencies increase with the cylinder's charge and decrease with cylinder's $Re_c$ (Fig. 36). For $Re_c$ = 3.5 the mean collection efficiency for a brass cylinder exposed at an air velocity of 1.0 m $s^{-1}$ was 4.0%. Particle deposition around the cylinder's circumference (Figs. 37, 38, 39) follows the scheme predicted by a numerical model developed e.g., by Zebel (1969) if one bears in mind that the cylinder is directly charged (Zebel assumed that dielectric cylinder had a surface charge distribution according to the polarizing field parallel to the main airflow). The surface charge on a metallic cylinder of 0.8593 esu/$cm^2$ (corresponds to 1 kV in Fig. 37) caused a substantial difference of deposited particle pattern on the front (windward) side of the cylinder and on its back side. The former is featured by small numbers of

smoke particles ($R_p < 0.35$ μm), by a maximum for $0.35 < R_p < 0.70$ μm and by relatively high counts of particles with $R_p > 1.05$ μm. Around the line of symmetry on the back side, the relationship is just reversed. One finds a similar situation at a potential difference of 5 kV (which corresponds to the surface charge of 4.3281 esu/cm$^2$): only the ratios are magnified (Fig. 38).

The results of the experiments with smoke particle deposition on grid type scavengers indicate one of the most promising lines of research in the future. Grid type scavengers, which were modeled by ELM grids, represent very effective collectors for all particle sizes. Electric charge contributes favorably to the particle capturing mainly around the scavenger's rim and also inside on the grid (Figs. 40 and 41). The scavenging efficiencies are comparable or higher than those of solid planar models (several percent for 1 kV and more than 5% for 5 kV). Another favorable factor for increasing the collection efficiency of the grid type scavengers is the potential use of grids made of charged fibers (e.g., Davies, 1973, p. 106-110) or fibers which consist of dielectrics (usually polymers) carrying a strong positive and negative electric charge (Filtrete$^R$; J. vanTurnhout, et al., 1978). Currently tests are prepared with these materials together with another "self-charging" filter material names Poly-Mag 80 (Piper Industries, Inc., Clarendon, Ark.).

Due to the relatively shallow layer of smoke cloud above the ground in our scenario of the application of scavenger technique, the falling scavenger zone effect can be considerably simplified if compared to the model by Clark and List (1971) or Girard and List (1975). One can probably neglect the large scale dynamics and thermodynamics, which was used for the explanation of the precipitation distribution and its effect on the air circulation, and concentrate on the dynamics of the scavenger zone. This has an utmost importance for calculating the scavenger motion and interaction with the smoke particles. The change in scavenger relative velocity might affect strongly the scavenging effect, actually lowering the collection efficiency of scavengers. Rough estimates made in this preliminary study indicate that the effect

is not negligible at assumed parameters and that more effective scavenging can be attained if the scavengers will be dropped subsequently in smaller quantities.

## 6. CONCLUSION

The two year effort of investigating the clearing of military smoke cloud with scavenging technique concentrated on the numerical modeling of the scavenging of smoke particulates by a planar scavenger (neutral or charged oblate spheroid) and on the analysis of the free falling model motion for the suitable simulation of the scavenging in a laboratory wind tunnel. Laboratory wind tunnel experiments included the deposition of $TiCl_4$ particles on stationary, oscillating and electrically charged models. Systematic measurements were performed with disks, which were compared with the calculated deposition on oblate spheroids, cylinders (rods) of different material, and on grids. The study of the falling scavenger zone effect was limited to the analysis of the equations governing the impact of the falling scavengers on the air motion and to the assessment of how this induced air motion might affect the scavenging efficiency. Our independent program, which should include in addition particle coagulation terms, was not started for two reasons: it would be too expensive and the results of a complex program would be probably insignificant with regard to the limited depth of a smoke layer and the assessments made in this report.

The most important findings of the two year program can be summarized as follows:

1) Theoretical analysis and numerical program which included the effect of inertial, phoretical and electrical forces showed that a planar scavenger is more efficient than a sphere (referred to the same swept out air volume and particle sizes typical for a military smoke cloud).

2) Numerical calculation predicts the mean collection efficiency of a thin oblate spheroid colliding with smoke particles ($R_p$ = 0.3 μm) to be between 0.5 and 1.5% for scavenger Reynolds number $2.0 < Re_c < 20.0$ and around 4.0% for $Re_c$ = 50.

3) Numerical calculation predicts the mean collection efficiency of a charged thin oblate spheroid colliding with smoke particles ($R_p$ = 0.3 μm) to be around 14% for $Re_c$ = 50.

4) Numerical calculation stresses the importance of smoke

particle density (which is not sufficiently known) for the calculation of collection efficiency.

5) Analysis of stroboscopic records of falling paper disks leads to the conclusion that around $Re_c$ = 700 the disks start to oscillate with a frequency between 7 and 10 Hz. At higher $Re_c$ a superimposed frequency greater than 50 Hz was occasionally observed.

6) Amplitude and frequency in the domain of $Re_c$ for disk's oscillatory motion are related to the $Re_c$ and to the Wilmarth's stability number (I). Amplitude increases with increasing parameters $Re_c$ and I, and frequency decreases.

7) Scavengers (disk, square, hexagon, triangle, star) interact effectively on a distance of less than one diameter while falling in the air. The result of the interaction is the accelerated motion and change in the scavenger trajectory. Stable configuration of joined scavengers after the contact--as observed often in liquids--has not been found in the air.

8) Collection efficiencies of stationary disks deduced from the measurements of smoke particle deposition in a wind tunnel are in the range of 0.5 and 2.0% for $80 < Re_c < 320$ and particles typical for smoke cloud. The deposition of particles with $R_p <$ 0.7 μm on the back side of the disk overrides in mean that on the front side.

9) Collection efficiencies of oscillating disks (10 Hz, 60 Hz) for $Re_c > 300$ surpass slightly those for stationary disks. Smoke particle deposition pattern is featured by lower deposition on the front side and higher and more uniform counts on the back side.

10) Collection efficiencies of electrically charged disks were around 3% for a potential difference of 1 kV and more than 5% for 5 kV and 8 kV at $80 < Re_c < 320$. Exceptionally metal coated glass disk showed collection efficiency larger than 20% for a typical smoke aerosol. There was no large difference in collection efficiency between disks made of dielectric or metallic material.

11) Large number of particles is deposited along the rim of

charged models. Rough surface, especially of dielectric materials, represents the site of maximal particle deposition. Particles form both long chains and large aggregates contain--at potential differences larger than 5 kV--often more than 50 individual particles.

12) Deposition of smoke particles on charged cylinders made of different material was featured in mean by lower collection efficieny if compared with the same volume of air swept out by a charged disk. Experiments with charged brass cylinders for $Re_c$ = 15.75 showed a clear dependence of the collection efficiency on the electric charge. For 5.0 kV potential difference was demonstrated how with increasing $Re_c$ the total collision efficiency is decreasing. High deposition was found on charged cylinders made of plastic materials (e.g, PVC), especially those with a rough surface.

13) High collection efficiencies were found during experiments with charged grids. Surprising enough was the fact that for 1 kV on an ELM grid the collection of smoke particles was comparable in mean with that of 5 kV. One can speculate about the effect of the electric field around the grid and inside at the effectively ventilated sites.

This research report represents a sincere effort of two investigators and their students to find the most effective way to remove the particulates from the smoke cloud and transport them in a short time to the ground. The most significant results mentioned above are directly related to the specific points in the "Statement of Work: (DAAK11-81-C-0075): Our points 1 and 5 to 13 are referring to point (1) of the Statement; our points 6 and 7 concentrate on points (2) and (3) of the Statement; our point 13 refers to point (4); our points 1 to 4 comply with point (5) of the Statement; points 7 and 8 to 12 are related to (6); our paragraphs 4.1 and 4.2 concentrate on points (7), (8) and (9) of the Statement (with the limitation of the effort mentioned above); our points 1 to 3 and 5 to 13 cover the task under point (10) and our progress reports, publications and papers presented at the CSL* Scientific Conferenceon Obscuration and Aerosol Research comply with point (11) of the Statement.

*Known as the U.S. Army Chemical Research and Development Center (CRDC) in July 1983 and the U.S. Army Chemical Research, Development and Engineering Center (CRDEC) in March 1986.

## LIST OF ALL PUBLICATIONS

Martin, J.J., and J. Podzimek, 1982: Scavenging of smoke particles by planar collectors, Proc. CSL Conference on Obscuration and Aerosol Research, Aberdeen, August.

Podzimek, J., 1982: Study of the motion of bodies simulating the fall of ice crystals, Prepr. Conf. on Cloud Physics, Chicago, AMS-Boston, November, 103-106.

Podzimek, J., and J.J. Martin, 1982: Deposition of submicron particulates on model scavengers, Precipitation Scavenging, Dry Deposition, and Resuspension, Elsevier Sci. Publ., New York, 493-503.

Podzimek, J., 1983: Deposition of smoke particles on stationary and oscillating scavengers, Ext. Abstract in Aerosol Sci. Technol. 2, 266.

Podzimek, J., and J.J. Martin, 1983: Progress in the clearing or modifying aerosol clouds by scavenging technique, Proc. CSL Conference on Obscuration and Aerosol Research, Aberdeen, June.

## LIST OF PARTICIPATING SCIENTIFIC PERSONNEL

Dr. Josef Podzimek, Prof. Mechanical and Aerospace Engineering, and Senior Investigator in the Graduate Center for Cloud Physics Research, UMR-Rolla - approx. 35% of his capacity on this project.

Dr. J.J. Martin, Assist. Prof., Dept. of Physics and Investigator in the Graduate Center for Cloud Physics Research, UMR-Rolla - approx. 20% of his capacity on this project.

No Ph.D. or M.S. Thesis related to this project were defended during the contract period.

## LITERATURE CITED

Carnuth, W. (1967), Arch. Meteor., Geophys., Bioklim., Ser. A16, 321.

Carstens, J.C., and Martin, J.J. (1982), J. Atmos. Sci. 39, 1124.

Clark, T.L., and List, R. (1971), J. Atmos. Sci. 28, 718.

Davies, C.N. (1973), Air Filtration, Acad. Press, London.

deAlmeida, F.C. (1976), J. Atmos. Sci. 33, 571.

deAlmeida, F.C. (1977), J. Atmos. Sci. 34, 1286.

Girard, C., and List, R. (1974), The fall of precipitation particle zones, Prepr. Conf. on Cloud Physics, Tucson, October; AMS, Boston, 223.

Girard, C., and List, R. (1975), Pageoph, 113, 1036.

Graedel, T.E., and Franey, J.P. (1975), Geophys. Res. Lett. 2, 325.

Hall, W.D., and Pruppacher, H.R. (1976), J. Atmos. Sci. 33, 1995.

Happel, J., and Brenner, H. (1965), Low Reynolds Number Hydrodynamics, Prentice-Hall, Englewood-Cliffs.

Itagaki, K., and Koenuma, S. (1962), J. Geophys. Sci. 67, 3927.

Jayaweera, K.O.L., and Cottis, R.E. (1969), Quart. J. Roy. Met. Soc. 95, 703.

Keefe, D., Nolan, P.J., and Rich, T.A. (1959), Proc. Roy. Irish Acad. 60, 27.

Knutson, E.O., Sood, S.K., and Stockham, J.D. (1976), Atmos. Environ. 10, 395.

Kraemer, H.F., and Johnstone, H.F. (1955), Ind. Engin. Chem. 47, 2426.

List, R., and Clark, T.L. (1973), Atmosphere, 11, 179.

List, R., and Schememauer, R.S. (1971), J. Atmos. Sci. 28, 110.

Magono, C., Endoh, T., Hariyama, T., and Kuboda, S. (1974), J. Meteor. Soc., Japan, 52, 407.

Magono, C., Endoh, T., and Itasaka, M. (1975), J. Fac. Sci., Hokkaido Univ., 4, 103.

Martin, J.J. (1979), A numerical study of the efficiency with which aerosol particles collide with simple planar ice crystals, Ph.D. Thesis, Dept. of Meteorology, Univ. of California, Los Angeles.

Martin, J.J., and Podzimek, J. (1982), Scavenging of smoke particles by planar collectors, Proc. CSL Conference on Obscuration and Aerosol Research, Aberdeen, August.

Martin, J.J., Wang, P.K., and Pruppacher, H.R. (1980a), J. Atmos. Sci. 37, 1628.

Martin, J.J., Wang, P.K., and Pruppacher, H.R. (1980b), J. Colloid Interfacial Sci. 78, 44.

Martin, J.J., Wang, P.K., Pruppacher, H.R., and Hamiele, C.A.E., (1980c), Pageoph. 118, 1109.

Martin, J.J., Wang, P.K., Pruppacher, H.R., and Pitter, R.L. (1981) J. Atmos. Sci., 38, 2462.

Nielsen, K.A., and Hill, J.C. (1976a), Ind. Engin. Chem. Fundam., 15, 149.

Nielsen, K.A., and Hill, J.C. (1976b), Ind. Engin. chem. Fundam. 15, 157.

Pitter, R.L. (1973), An experimental and numerical investigation of the evolution of ice particles in Atmospheric clouds, Ph.D. Thesis, Dept.of Meteorology, Univ.of California, Los Angeles.

Pitter, R.L. (1977), J. Atmos. Sci. 34, 1797.

Pitter, R.L., and Pruppacher, H.R. (1974), J. Atmos. Sci. 31, 551.

Podzimek, J. (1965), J. Rech. Atmos. 1, 19.
Podzimek, J. (1969), The growth of an ice crystal in a mixed cloud (in Czech), Part I. pp. 183, Part II, pp. 137, D.S. Thesis, Charles University, Prague.

Podzimek, J. (1970), Contribution to the problem of the collection efficiency of falling ice crystals, Prepr. Conf. on Cloud Physics, Fort Collins, August; AMS, Boston, 13.

Podzimek, J. (1981), Clearing of military smoke cloud with scavenging technique, Final Report, DAAG-29-79-C-0073, Univ. of Missouri-Rolla, June.

Podzimek, J. (1982), Study of the motion of bodies simulating the fall of ice crystals, Prepr. Conf. on Cloud Physics, Chicago, November; AMS, Boston, 103.

Prodi, F. (1976), Scavenging of aerosol particles by growing ice crystals, Prepr. Int. Conf. on Cloud Physics, Boulder, July; AMS, Boston, 70.

Pruppacher, H.R., and Klett, J.D. (1978 and 1980), Microphysics of Clouds, D. Reidell Publ. Co., Dordrecht.

Reiter, R., and Carnuth, W. (1969), Arch. Meteor. Geophys., Bioklim., Ser. A18, 111.

Russell, J. (1962), Aeron. Res. Counc. Rep. & Mem., No. 3331, London.

Sasyo, Y. (1971), Papers in Meteor. and Geophys. 22, 69.

Slinn, W.G.N. and Hales, J.M. (1971), J. Atmos. Sci. 28, 1465.

Sood, S.K., and Jackson, M.R. (1969), Scavenging of atmospheric particulate matter by falling hydrometeors, Proc. 7th Int. Conf. on Cond. and Ice Nuclei, Sept., Prague-Vienna, NCSAV, 299.

Stewart, R.E., and List, R. (1980), The aerodynamics of freely falling disks and implications for understanding the free fall motions of atmospheric particles, Proc. 8th Int. Conf. on Cloud Physics, Clermont-Ferrand, July, I-st Vol., 299.

van Turnhout, J., Albers, J.H.J., Adamse, J.W.C., Hoeneveld, W.J., and Vischer, J. (1978), Paper pres. to Inst. of Physics, Meeting on Electrostatic Filters and Precipitation, London, December.

Voloschuk, V.M. (1971), Vvedenie v gidrodynamiku grubo-dispersnykh aerozolie, Gidrometeoizdat, Leningrad.
Woo, S. (1971), Simultaneous free and forced convection around submerged cylinders and spheres Ph.D. Thesis, McMaster Univ., Hamilton, Ontario.

Yue, P., and Podzimek, J. (1976), New technique for studying the deposition of droplets on the ice crystal surface, Prepr. Int. Conf. on Cloud Physics, Boulder, July; AMS, Boston, 180.

Zebel, G. (1965), J. coll. Interf. Sci. 20, 522.

Zebel, G. (1969), Staub-Reinhalt. Luft, 29, 62.

# APPENDIX 1

## CREEPING VISCOUS FLOW EQUATIONS FOR AN OBLATE SPHEROID

According to Happel and Brenner (1965) the flow around an oblate spheroid can be best described in oblate spheroidal coordinate system which transforms the cylindrical coordinates, x, y, into spheroidal coordinate system, $\xi$, $\eta$. Because of the axial symmetry one can handle the problem like a two-dimensional transformation in a complex plane (Fig. A1)

$$z + iy = c \sinh (\xi + i\eta) \qquad (1.A)$$

with the azimuthal coordinate in both systems $\phi$. $c > o$ is a parameter which has to be selected so that $\xi$ will remain constant on the surface of the spheroid ($\xi = \xi_o$). Bearing in mind the ranges of spheroidal coordinates ($0 \leq \xi < \infty$; $0 \leq \eta \leq \pi$; $0 \leq \phi \leq 2\pi$) one can write

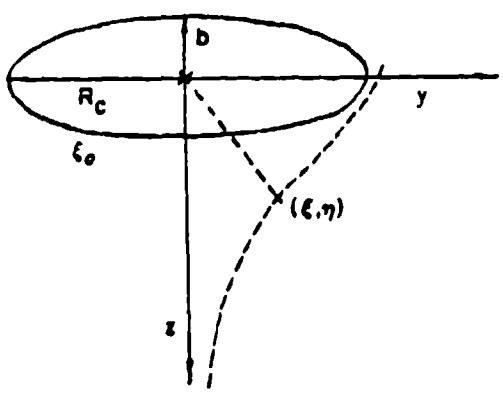


$$z = c \sinh \xi \cos \eta; \quad y = c \cosh \xi \sin \eta$$

and

$$\frac{z^2}{c^2 \sinh^2 \xi} + \frac{y^2}{c^2 \cosh^2 \xi} = 1 \qquad (2.A)$$

At the spheroid surfaces the axes ratio $\Lambda_c = \frac{b}{R_c} = \tanh \xi_o$ and for the equator ($\xi = \xi_o$, $\eta = \frac{\pi}{2}$), $c = R_c \operatorname{sech} \xi_o$.

The further procedure is based on Pitter's (1973) interpretation

of Happel and Brenner's (1965) transformation with the metric coefficients

$$h_\xi = h_\eta = [c^2(\sinh^2 \xi + \cos^2 \eta)]^{-1/2} \equiv h$$
$$h_\phi = 1/(c \cosh \xi \sin \eta) \equiv \frac{1}{y} \quad . \tag{3.A}$$

Using the standard approach of vector field analysis for the new coordinate system with the unit vectors, $\vec{e}_\xi$, $\vec{e}_\eta$, $\vec{e}_\phi$, one deduced the following relationships:

Equation of continuity [for an incompressible flow and $i = \xi(1), \eta(2), \psi(3)$]

$$\nabla \cdot \vec{V} = h_\xi h_\eta h_\phi \sum_{i=1}^{3} \frac{\partial}{\partial x_i} \left(\frac{h_i V_i}{h_\xi h_\eta h_\phi}\right) = 0 \tag{4.A}$$

with the stream function $\psi$ defined as

$$\vec{V} = \frac{\vec{e}_\phi}{y} \times \nabla\psi \quad . \tag{5.A}$$

From the last relationship the velocity components can be defined as

$$V_\xi = -\frac{h}{y}\frac{\partial\psi}{\partial\eta} \; , \; V_\eta = \frac{h}{y}\frac{\partial\psi}{\partial\xi} \quad . \tag{6.A}$$

Equation of the vorticity of the flow is defined as

$$\vec{\omega} = \nabla \times \vec{V} = h_\xi h_\eta h_\phi \begin{vmatrix} \vec{e}_\xi/h_\xi & \vec{e}_\eta/h_\eta & \vec{e}_\phi/h_\phi \\ \frac{\partial}{\partial\xi} & \frac{\partial}{\partial\eta} & \frac{\partial}{\partial\phi} \\ V_\xi/h_\xi & V_\eta/h_\eta & V_\phi/h_\phi \end{vmatrix} \tag{7.A}$$

If one considers the form of an operator $E^2$ in oblate spheroidal coordinates

APPENDIX 1

$$E^2\psi = \frac{1}{c^2(\sinh^2\xi + \cos^2\eta)}\left[\frac{\partial^2}{\partial\xi^2} + \frac{\partial^2}{\partial\eta^2} - \tanh\xi\,\frac{\partial}{\partial\xi} - \cot\eta\,\frac{\partial}{\partial\eta}\right]\psi \qquad (8.A)$$

the eq. (7.A) can be written in the form

$$\vec{\omega} = \vec{e}_\phi\,\frac{E^2\psi}{y} \qquad (9.A)$$

With the aid of the introduced parameters and operators the Navier-Stokes equation can be arranged for the steady state, viscous, inconpressible and axisymmetric flow from its original form

$$\vec{V}\cdot\nabla\vec{V} = -\frac{1}{\rho}\nabla p + \nu\nabla^2\vec{V} \qquad (10.A)$$

into an equation more suitable for numerical solution. Using the operator $\nabla\times$ twice on the eq. (10.A), one obtains

$$\nabla\times(\vec{V}\times\vec{\omega}) = \nu\nabla\times(\nabla\times\vec{\omega}) \qquad (11.A)$$

Because

$$\nabla\times\vec{\omega} = \vec{e}_\xi\left(\frac{h}{y}\,\frac{\partial E^2\psi}{\partial\eta}\right) - \vec{e}_\eta\left(\frac{h}{y}\,\frac{\partial E^2\psi}{\partial\xi}\right)$$

the right hand side of eq. (11.A) can be written in the form

$$\nabla\times(\nabla\times\vec{\omega}) = \vec{e}_\phi\,\frac{E^2(E^2\psi)}{y} = -\vec{e}_\phi\,\frac{E^4\psi}{y} \qquad (12.A)$$

The left hand side of eq. (11.A) can be rearranged, considering

$$\vec{V}\times\vec{\omega} = \vec{e}_\xi\left(h\frac{\partial\psi}{\partial\xi}\,\frac{E^2\psi}{y^2}\right) + \vec{e}_\eta\left(h\frac{\partial\psi}{\partial\eta}\,\frac{E^2\psi}{y^2}\right)$$

in the form

$$\nabla \times (\vec{V} \times \vec{\omega}) = \vec{e}_\phi h^2 \left[\frac{\partial}{\partial \xi}\left(\frac{\partial \psi}{\partial \eta}\frac{E^2\psi}{y^2}\right) - \frac{\partial}{\partial \eta}\left(\frac{\partial \psi}{\partial \xi}\frac{E^2\psi}{y^2}\right)\right] \quad . \quad (13.A)$$

With the aid of the Jacobian operator

$$J_{\xi,\eta}(\psi,F) = \frac{\partial \psi}{\partial \xi}\frac{\partial F}{\partial \eta} - \frac{\partial \psi}{\partial \eta}\frac{\partial F}{\partial \xi}$$

and the scalar vorticity from eq. (9.A) $\zeta = \vec{e}_\phi \vec{\omega} = \frac{E^2\psi}{y}$
the eq. (11.4) will take the final form

$$E^2(\zeta,y) = \frac{yh^2}{\nu} J_{\xi,\eta}(\psi,\xi/y) \quad . \quad (14.A)$$

Equation (14.A) is usually solved in nondimensional form. The transformation is done by means of ratios to semi-major axis length, ($R_c$), the velocity of fluid at infinity, $U_\infty$, and the kinematic viscosity, $\nu$. Then

$$\psi^* = \frac{\psi}{R_c^2 U_\infty} \quad ; \quad \zeta^* = \frac{R_c \zeta}{U_\infty}$$

$$C^* = \frac{C}{R_c} = \operatorname{sech}\xi_o \quad ; \quad Re^* = \frac{2R_c U_\infty}{\nu}$$

$$y^* = \frac{y}{R_c} = \operatorname{sech}\xi_o \cosh\xi \sin\eta \quad .$$

In this way the eq. (14.A) will be rewritten in the form

$$E^2(\zeta^* y^*) = \frac{Re^*}{2} \frac{\cosh\xi \sin\eta}{\operatorname{sech}\xi_o(\sinh^2\xi + \cos^2\eta)} J_{\xi,\eta}(\psi^*, \zeta^*/y^*) \quad (15.A)$$

Another arrangement of eq. (15.A) can be done by introducing two modified (nondimensional) vorticities, $F^* = \zeta^*/y^*$, $G^* = \zeta^* y^*$, what yields for $E^2\psi^* = G^*$

$$E^2 G^* = \frac{Re^*}{2} \frac{\cosh\xi \sin\eta}{\operatorname{sech}\xi_o(\sinh^2\xi + \cos^2\eta)} J_{\xi,\eta}(\psi^*, F^*) \quad . \quad (16.A)$$

APPENDIX 1

# APPENDIX 2
## NUMERICAL SOLUTION OF NAVIER-STOKES EQUATION FOR AIRFLOW PAST AN OBLATE SPHEROID

The procedure adapted in this work is that of Pitter (1973) with some slight modification for Re > 20 or for differently shaped rim of the disk.

In essence, finite-difference technique with a grid in oblate spheroidal coordinates was used. The two dimensional grid (symmetrical along the axis in the direction of the flow) has a finer mesh near the spheroid. The normal step was set at 0.1 for $\Delta\xi$ (labeled in the numerical program as A), 6° for $\Delta\eta$ (labeled as B) ($0 < \eta < \pi$). The index I was used for the polar angle, $\eta$, and J for the radial coordinate, $\xi$. J = 1 was set for $\xi = \xi_o$, the surface of the spheroid.

Several examples of the partial derivations and of the operators are taken from the Pitter's study (1973):

$$\left.\frac{\partial\psi}{\partial\xi}\right|_{(I,J)} = \frac{\psi(I,J+1) - \psi(I,J-1)}{2A} \qquad (17.A)$$

$$\left.\frac{\partial^2 G}{\partial\eta 2}\right|_{(I,J)} = \frac{G(I+1,J) - 2G(I,J) + G(I-1,J)}{B^2} \quad . \qquad (18.A)$$

From the eq. $E^2\psi = G$ and solution for $\psi(I,J)$ was obtained

$$\psi^{n+1}(IJ) = [\tfrac{1}{2} A^2B^2/(A^2+B^2)]\Big\{\psi^n(I,J+1)[1-\tfrac{1}{2} A \tanh\xi(J)/A^2] + ,$$

$$+ \psi^n(I,J-1)[(1+\tfrac{1}{2} A \tanh\xi(J)/A^2] + \psi^n(I+1,J)[(1-\tfrac{1}{2} B \cot\eta(I)/B^2] + \qquad (19.A)$$

$$+ \psi^n(I-1,J)[(1+\tfrac{1}{2} B \cot\eta(I)/B^2]) - \operatorname{sech}^2\xi_o(\sinh^2\xi(J) + \cosh^2\eta(I)G^n(I,J)\Big\} .$$

The superscripts, n + 1, n, are introduced for describing the iteration steps. Eq. (16.A) (the asterisks are omitted) was used for deducing G(I,J)

$$G^{n+1}(I,J) = [\tfrac{1}{2}A^2B^2/(A^2+B^2)]\left\{ G^n(I,J+1)[1-\tfrac{1}{2}A\ \tanh\xi(J)/A^2] + \right.$$

$$+ G^n(I,J-1)[(1+\tfrac{1}{2}A\ \tanh\xi(J)/A^2] = G^n(I+1,J)\ [1-\tfrac{1}{2}B\ \cot\eta(I)/B^2] +$$

(20.A)

$$\left. + G^n(I-1,J)[1+\tfrac{1}{2}B\ \cot\eta(I)/B^2] - [Re\ \mathrm{sech}\xi_o \cosh\xi(J)\ \sin\eta(I)/(8AB)]\ x \right.$$

$$x\left[[\psi^n(I,J+1)-\psi^n(I,J-1)][F^n(I+1,J)-F^n(I-1,J)]-[\psi^n(I+1,J)\ -\right.$$

$$\left.\left. - \psi^n(I-1,J)]\ [F^n(I,J+1)-F^n(I,J-1)]\right]\right\} .$$

The eq. (20.A) serves for the deduction of F because of the relationship $F = G/y^2$.

One assumed that along the main axis of symmetry and at the spheroid surface the stream function is constant (zero) i.e., $\psi = 0$ for $\eta = 0$ and $\eta = \pi$ and for $\xi = \xi_o$. Outside of the spheroid's boundary, there was a free flow velocity, i.e. $\psi = 1/2\ \mathrm{sech}^2\xi_o \cosh^2\xi_\infty \sin^2\eta(I)$ for $\xi = \xi_\infty$, what implies no vorticity ($G = 0$). Also, along the main axis of symmetry there is $G = 0$. The conditions on the spheroid surface (no flow through the surface, no slip) led to the equation of vorticity at the spheroid's surface

$$G(I,1) = \frac{\cosh^2\xi_o}{\sinh^2\xi_o + \cos^2\eta(I)}\ \frac{\partial^2\psi}{\partial\xi^2}\bigg|_{\xi=\xi_o} \qquad (21.A)$$

$$\frac{\partial^2\psi}{\partial\xi^2}\bigg|_{(J=1)} = \frac{8\psi(1,2)\ -\ \psi(1,3)}{2A^2}$$

Because of the variability of the vorticity on the spheroid sur-

APPENDIX 2

face, the G is re-evaluated before every iteration.

Relaxation of stream ($\psi$) and vorticity (G) fields is based on Pitter's detailed analysis (1973) and Woo's (1971) studies of the stability and the speed of convergence of the solution to similar equations. The approach is based on some kind of "first approach" analytical solution (e.g., Oberbeck) for a specific Re. Trials for convergence have been done for a similar Re in a numerical model using the scheme for residual calculation

$$\psi^R(I,J) = [\psi^{n+1}(I,J) - \psi^n(I,J)/\psi^{n+1}(I,J)$$

$$G^R(I,J) = [G^{n+1}(I,J) - G^n(I,J)]/G^{n+1}(I,J) \quad . \tag{22.A}$$

The data was plotted into two field regions and from the first checkboard region, with the data updated according to

$$\psi^{n+1}(I,J) = \psi^n(I,J) + \alpha(I,J)\psi^R(I,J)$$

$$G^{n+1}(I,J) = G^n(I,J) + \gamma(I,J)G^R(I,J) \tag{23.A}$$

were determined the data for the second region by an iterative procedure.

Parameters $\alpha$, $\gamma$ are essential for stability, speed and convergence of solution. They have been discussed in detail by Woo (1971) using a scheme developed by Russell (1962). Finally, when the residuals were within a certain limit (0.01%), the fields were considered convergent for this specific numerical procedure, Russell's (1962) analysis justified for $\alpha$ a value of 1.3036, however, for $\gamma$ - due to the difficulties related to the relaxation of vorticity - it varied considerably following the relationship

$$\gamma(I,J) = \frac{\Gamma}{1+[\frac{1}{2}(P^2+Q^2)]^{1/2}} \tag{24.A}$$

where $0.001 < \Gamma < 2.0$ and

APPENDIX 2

$$P = -\frac{\partial \psi}{\partial \eta}\frac{Re}{2y} \; ; \; Q = \frac{\partial \psi}{\partial \xi}\frac{Re}{2y} \quad .$$

Pitter (1973) used also several other techniques for checking the steep convergence of solution. One of the techniques was suggested by Woo (1971) which was based on creating some artificial instabilities (multiplying the relaxation factors $\alpha$ and $\gamma$ by 20th iterations) and investigating the convergency or divergency of the solution. This was accompanied by the study of the accuracy of the converged solution, for which Pitter (1973) used the pressure distribution and the determination of the pressure drag and friction drag coefficients.

Attached is the computer program for the viscous incompressible flow past a thin oblate spheroid flow chart.

**APPENDIX 2**

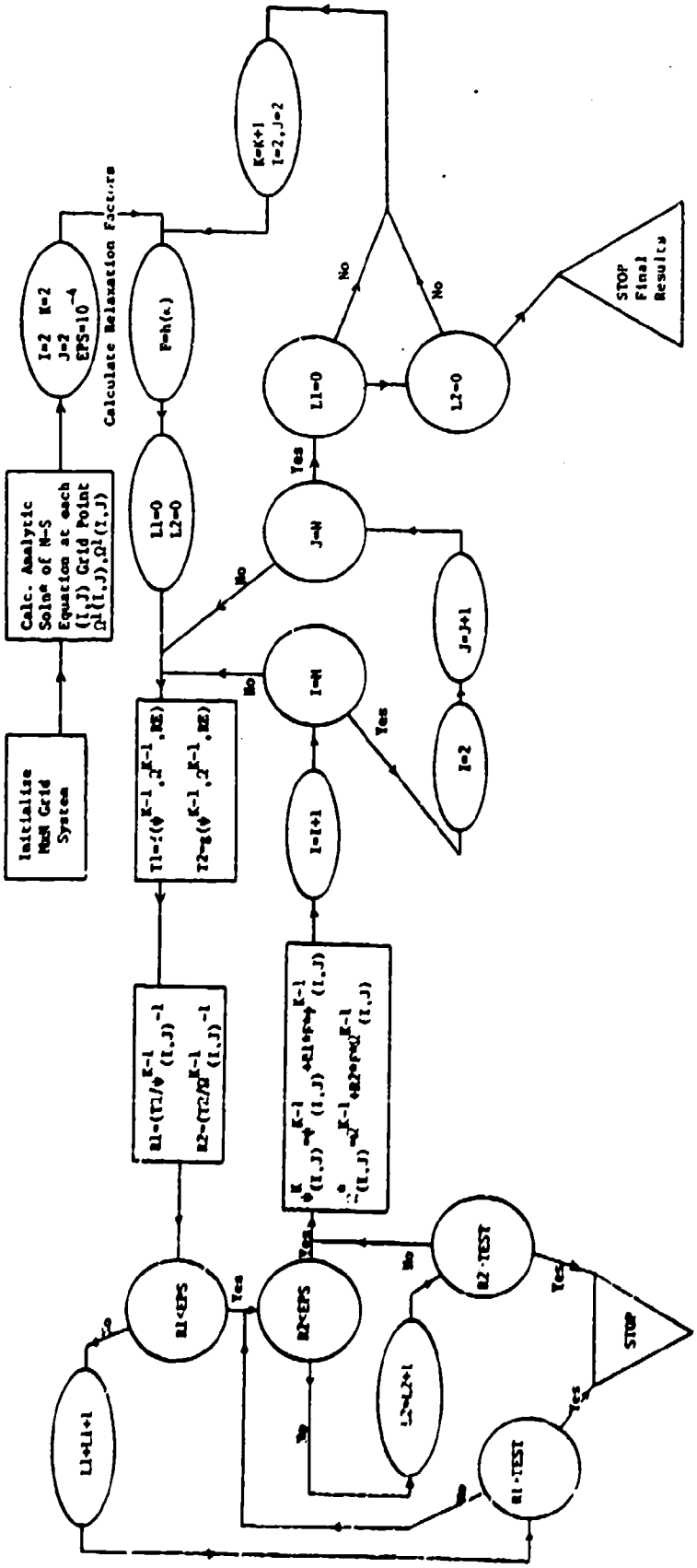


COMPUTER PROGRAM FOR THE VISCOUS INCOMPRESSIBLE FLOW PAST AN OBLATE SPHEROID

Flow Field Program Flow Chart

APPENDIX 2

Blank

# APPENDIX 3

## CALCULATION OF SMOKE PARTICLE MOTION AROUND AN OBLATE SPHEROID AND THE DETERMINATION OF THE COLLISION EFFICIENCY

If the collector and the spherical smoke particle are settling in the quiescent air, their motion--under the assumption of a very slow acceleration--can be deduced from the following basic equations

$$m_c \frac{d\vec{V}_c}{dt} = m_c \vec{g}\left(1-\frac{\rho_{air}}{\rho_c}\right) - \frac{\pi}{4} C_{DC} Re_c R_c \mu (\vec{V}_c - \vec{U}_p) \qquad (25.A)$$

$$m_p \frac{d\vec{V}_p}{dt} = m_p \vec{g}\left(1-\frac{\rho_{air}}{\rho_p}\right) - \frac{\pi}{4} C_{Dp} Re_p R_p \mu (\vec{V}_p - \vec{U}_c) \; . \qquad (26.A)$$

$\vec{V}_c, \vec{V}_p$ and $\vec{U}_c, \vec{U}_p$ are the velocities of the collector (oblate spheroid) and of the particle and the velocities of the air induced by the collector and by the particle. $R_c, m_c$ are the radius (main half axis) and the mass of the collector; $R_p, m_p$ the radius and mass of the smoke particle and, $C_{DC}, Re_c$, and, $C_{DP}, Re_p$, are the corresponding drag coefficients and Reynolds numbers. $\vec{g}$ is the acceleration in the gravitational field; $\rho_{air}$, $\rho_c$, $\rho_p$ are the air, collector and particle densities. $\mu$ is the coefficient of air dynamic viscosity.

Choosing for reference quantities $V_{c\infty} = |\vec{V}_{c\infty}|$, $R_c$ and for time $t^*$ the time corresponding to the passage of the air (particle) with the velocity $V_{c\infty}$ the distance $R_c$ one can write the eq. (25.A) in the nondimensional forms as

$$\frac{dV_c^*}{dt^*} = \vec{g}^*\left(1-\frac{\rho_{air}}{\rho_c}\right) - \frac{\pi}{4} C_{DC} Re_c \mu^* (\vec{V}_c - \vec{U}_p^*) \; . \qquad (27.A)$$

In eq. (27.A) $\vec{V}_c^* = \vec{V}/V_{c\infty}$; $\vec{U}p^* = \vec{U}/V_{c\infty}$; $\vec{g}^* = \vec{g}\ R_c/V_{c\infty}^2$; $t^* = t\ V_{c\infty}/R_c$; $\mu^* = \mu R_c^2/(m_c V_{c\infty})$.

Equation similar to (27.A) can be deduced for acceleration of the smoke particle. With the addition of two vector equations for velocities of the collector and smoke particle a complete set of eight equations (for x- and y- components) describing the forces acting on the bodies and their velocities is established. This number can be, however, reduced if one considers the following relationships:

$$\frac{dV_{cz}}{dt} = C_1 - C_2(V_{cz}-U_{pz}) \cong 0 \qquad (28.A)$$

$$\frac{dV_{cy}}{dt} = - C_2(V_{cy}-U_{py}) \cong 0 \quad ,$$

where $C_1 = \vec{g}(1- \frac{\rho_{air}}{\rho_c})$ and $C_2 = \pi C_{DC}\ Re_c\ \mu$. The asterisks for dimensionless quantities (as in eq. 27.A) were omitted. Further, one can assume that the much larger collector (scavenger) steadily falling down (in the z-direction) will not deviate much from the z axis ($\frac{dr_{cy}}{dt} \cong 0$; $r_{cy}$ is the y-component of a radius vector $\vec{r}_c$). Therefore, the five following equations will describe the scavenger and smoke particle behavior:

$$\frac{dz_{pz}}{dt} = V_{pz} \qquad (29.A)$$

$$\frac{dV_{pz}}{dt} = C_3 - C_4(V_{pz}-U_{cz}) \qquad (30.A)$$

**APPENDIX 3**

$$\frac{dr_{py}}{dt} = V_{py} \tag{31.A}$$

$$\frac{dV_{py}}{dt} = - C_4 (V_{py} - U_{cy}) \tag{32.A}$$

$$\frac{dr_{cz}}{dt} = 1 \quad , \tag{33.A}$$

where $C_3 = \vec{g}(1 - \frac{\rho_{air}}{\rho_p})$; $C_4 = \pi C_{DP} Re_c \mu$. The vertical and horizontal distance between the centers of oblate spheroid and spherical smoke particle is

$$\Delta z = r_{pz} - r_{cz} \; ; \; \Delta y = r_{py} - r_{cy} \cong r_{py} \tag{34.A}$$

The air flow field velocities are calculated in accordance with formulas deduced in Appendix 1 and 2.

$$U_\xi = - \frac{h}{y} \frac{\partial \psi}{\partial \eta} = \frac{\psi(I-1,J) - \psi(I+1,J)}{2B \; \text{sech}^2 \xi_o \cosh\xi \; \sin\eta (\sinh^2 \xi + \cos^2 \eta)^{1/2}} \tag{35.A}$$

$$U_\eta = \frac{h}{y} \frac{\partial \psi}{\partial \xi} = \frac{\psi(I,J+1) - \psi(I+1,J)}{2A \; \text{sech}^2 \xi_o \cosh\xi \; \sin\eta (\sinh^2 \xi + \cos^2 \eta)^{1/2}} \tag{36.A}$$

The not abbreviated system of eight equations would, however, require a knowledge of the velocities around spherical smoke particles, $u_{pz}$, $u_{py}$. According to Pitter (1973) a cylindrical

APPENDIX 3

coordinate system was preferred for the calculation of $u_{pz}$, $u_{py}$ in that case. This required the transformation of oblate sphercidal components to cylindrical coordinates following the equations

$$U_z = \frac{U_\xi \cosh\xi \cos\eta - U_\eta \sinh\xi \sin\eta}{(\sinh^2\xi + \cos^2\eta)^{1/2}} \quad , \qquad (37.A)$$

$$U_y = \frac{U_\xi \sinh\xi \sin\eta + U_\eta \cosh\xi \cos\eta}{(\sinh^2\xi + \cos^2\eta)^{1/2}} \quad . \qquad (38.A)$$

The transformation between the two coordinate systems has been done according to the general relationship

$$U_\xi = U_z \frac{\partial z}{\partial \xi} + U_y \frac{\partial y}{\partial \xi}$$

$$U_\eta = U_z \frac{\partial z}{\partial \eta} + U_y \frac{\partial y}{\partial \eta} \quad . \qquad (39.A)$$

The integration scheme outlined in this section required several checking of the accuracy and stability--which strongly affect the calculation of particle trajectory and collision efficiency of the scavenger (Pitter, 1973; deAlmeida, 1976, 1977). For most of these calculations Hamming's predictor-corrector-modifier method with Runge-Kutta method (for starting the integration) was used. The integration subroutine used is named HPCG (IBM Manual H20-02053, System/360 Scientific Subroutine Package).

Other procedures were necessary for terminating the trajectory of particles which hit or miss the collector. In essence, the spherical particle did hit the spheroid at the moment when the distance, D, between the collector's surface and the center of the

particle was equal to the particle radius. This required to solve the equation (Pitter, 1973)

$$\frac{dD}{d\theta} = \frac{1}{D} [\sin\theta \cos\theta(1-A_c^2) + A_c y \sin\theta - x \cos ] \equiv 0 \quad .$$

Equally, the calculation of particle trajectory was terminated one semi-major axis length behind the collector. No wake capture was found for large smoke particles.

Collision efficiencies were determined by a trial method. Two offset positions, $y_{low}$ and $Y_{high}$ were selected (initially 0.0 and 1.0) and according to hit or miss situation new positions were finally found, $y_c$ for a specific size of particle.

The collision efficiency, E, for a specific smoke particle with the radius, $R_p$, which was deposited on a thin ($A_c = 0.05$) oblate spheroid of, $R_c$, is

$$E = \frac{\pi y_{cr}^2}{\pi(R_c+R_p)^2} = \frac{y_{cr}^{*2}}{(1+p)^2} \quad . \qquad (40.A)$$

Usually the offset critical distance, $y^*_{cr}$ is nondimensional ($y^*_{cr} = \frac{y_c}{R_c}$) and the ratio of particle radius to collector semi-axis ($p = \frac{R_p}{R_c}$) as well.

In our calculations following data were assumed: collector radius from $R_c = 50.6$ μm to $R_c = 639.2$ μm collector density $\rho_c = 0.90$ g cm$^{-3}$, particle size $0.1 < R_p < 5.0$ μm), particle density from, $\rho_p = 0.75$ g cm$^{-3}$ to $\rho_p = 1.20$ g cm$^{-3}$, air density $\rho_{air} = 1.23 \times 10^{-3}$ g cm$^{-3}$ and dynamic viscosity of air $\mu = 1.667 \times 10^{-4}$ poise. Usually the calculation started at a position of 50 collector semi-major axis lengths upstream from the oblate spheroid.

The computer program for the calculation of the smoke particle deposition on a thin oblate spheroid is attached.

APPENDIX 3

# COMPUTER PROGRAM FOR THE CALCULATION OF THE SMOKE PARTICLE DEPOSITION ON A THIN OBLATE SPHEROID

## Collision Efficiency Program Flow Chart

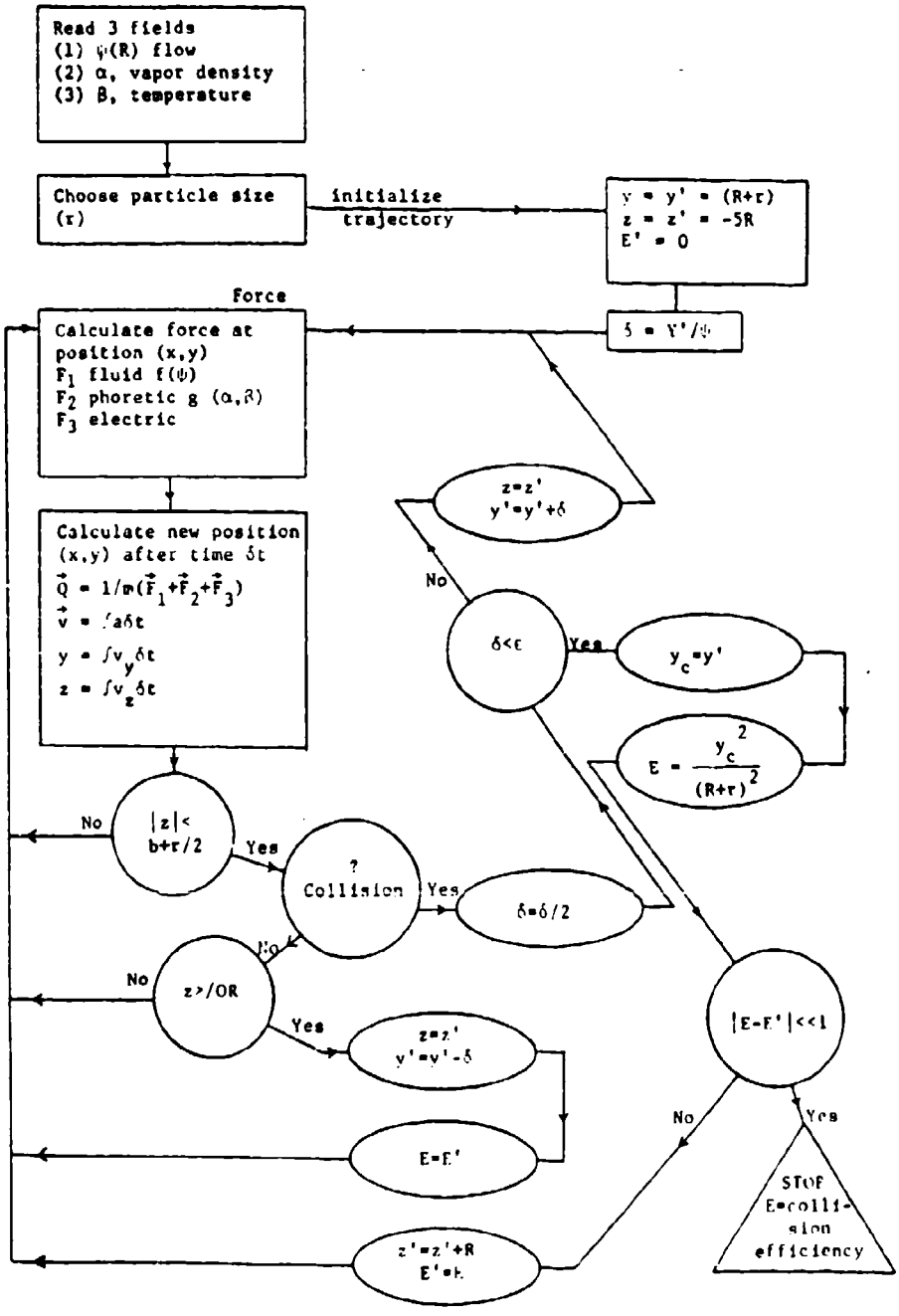


APPENDIX 3